SAPIENZA
UNIVERSITÀ DI ROMA

Faculty of Mathematics, Physics and Natural Sciences

Department of Earth Sciences

Ph.D. in Earth Sciences

XXX cycle

Passive seismic investigations for landslide hazard study in rock masses

Roberto Iannucci

Tutor
Prof. Salvatore Martino

Co-tutors
Ph.D. Luca Lenti (IFSTTAR-Paris)
Ph.D. Sebastiano D'Amico (University of Malta)

December 2017

Index

Abstract

Assessment of landslide hazard and managing the related risk have always been widely studied topics in the scientific community due to the presence of populated settlements as well as tourist and cultural heritage sites threated by slope instability processes. In the last decade, geophysical techniques have been integrated in multidisciplinary approaches to study gravity-induced slope instability processes as well as to design monitoring systems devoted to infrastructure management.

In the here-presented Ph.D. thesis, an experimental methodology was tested in two case studies of rock masses involved in landslide processes for evaluating as passive seismic approaches can be applied to: i) study the landslide susceptibility and produce a landslide hazard zonation; ii) assess the landslide hazard (in terms of probability of occurrence); iii) manage the landslide risk. For the two case studies, the gravity-induced slope instability processes occur at different scale and in a different natural environment: i) one rock cliff slope in coastal environment on the island of Malta (Selmun case study); ii) one rock slope in mountainous area in Central Italy (Peschiera case study). The experimental methodology applied in this work employed two passive seismic approaches: i) seismic ambient noise analysis carried out by single-station measurements; ii) seismic monitoring operated through seismic array/network (permanent or temporary) of sensors.

The Selmun Promontory, located in the North Western coast of Malta (Central Mediterranean Sea), is involved in a landslide process due to the geological setting of the area: the over-position of a limestone (i.e. stiff rock) on a plastic clay induces a lateral spreading phenomenon associated to falls, slides and/or topples of different-size rock blocks from the limestone plateau edge. The seismic ambient noise measurement analysis allowed to obtain remarkable outputs in terms of stability level of the several unstable zones and, therefore, to evaluate their different landslide susceptibility in the framework of a landslide hazard zonation. In addition, the main eigenmode frequency of an unstable large rock block was obtained and a preliminary study of specific parameters was carried out in the time domain on long seismic noise measurements carried out in stable and unstable zones. On the other hand, the installation of an array having the SNS geometry allowed to detect and locate few microseismic events produced by the unstable limestone plateau edge.

The Peschiera Spring Slope, located in Central Apennines (Central Italy) at about 70 km North East from Rome, is involved in a rock mass creep phenomenon associated to a deep karst dissolution. The seismic ambient noise measurements evidenced the different seismic response of the different zones of the slope involved in the complex landslide process. Since the Peschiera Spring Slope hosts an important drainage plant that provides water to the city of Rome, an accelerometric network was installed in 2008 and a nanoseismic SNS array was added in 2014. The SNS array recorded hundreds of microseismic events originated within the slope and related to its instability process. Such events were distinguished in two different types: i) failures related to rock mass fracturing, with a duration from 1 to few seconds; ii) collapses, with a duration less than 1 s and a typical waveform of impact. In this Ph.D. thesis, 397 events (i.e. 16 failures and 381 collapses) were characterised by NanoseismicSuite software in terms of local magnitude M_L and hypocentre. While the failures resulted distributed into the whole slope, the collapses focused in two different spatial clusters below the groundwater level, at a depth in which karst processes produce cavities. The clusters were treated as two distinct microseismic sources and a frequency-magnitude curve of events was produced for each one, for describing the attitude to produce events having different values of magnitude. Then, an automated procedure for quickly analysing events recorded by the accelerometric network was developed.

Finally, a landslide hazard matrix was implemented for the both case studies based on the statistic frequency of the occurred events (i.e. values of long seismic noise for the Selmun case study and M_L values of collapses for the Peschiera case study) and their probability of exceedance in a fixed period, giving an useful contribution for managing the related landslide risk.

In conclusion, the here-presented Ph.D. thesis evidences as passive seismic can be considered as a useful tool for investigating and monitoring gravity-induced slope instability processes since it allows to achieve the different initial objectives, i.e. evaluate the landslide susceptibility, assess its hazard and, finally, implement a tool for contributing to manage the related risk.

Riassunto

La valutazione della pericolosità da frana e la gestione del relativo rischio sono sempre stati temi ampiamente studiati nella comunità scientifica data la presenza di insediamenti popolati così come siti turistici e di interesse culturale minacciati da processi di frana. Nell'ultimo decennio, le tecniche geofisiche sono state integrate in approcci multidisciplinari per studiare processi di instabilità gravitativa e progettare sistemi di monitoraggio dedicati alla gestione di infrastrutture.

Nella presente tesi di Dottorato di Ricerca, una metodologia sperimentale è stata testata in due casi di ammassi rocciosi coinvolti in fenomeni di frana per valutare quanto gli approcci di sismica passiva possano essere applicati a: i) studiare la suscettibilità da frana e produrre una zonazione della pericolosità da frana; ii) valutare la pericolosità da frana (in termini di probabilità di occorrenza); iii) gestire il rischio da frana. I processi di instabilità gravitativa avvengono a differente scala e in un diverso ambiente naturale nei due casi di studio scelti: i) una falesia rocciosa in ambiente costiero sull'isola di Malta (caso di studio Selmun); ii) un versante roccioso in area montuosa nel Centro Italia (caso di studio Peschiera). La metodologia sperimentale applicata in questa tesi di Dottorato di Ricerca impiega due differenti approcci di sismica passiva: i) analisi di rumore sismico ambientale effettuate con misure a stazione singola; ii) monitoraggio sismometrico operato attraverso sensori in configurazione di *array*/rete (permanente o temporanea).

Il Promontorio di Selmun, situato nella costa Nord-Ovest di Malta (Mar Mediterraneo Centrale), è coinvolto in un processo di frana legato alla successione geologica dell'area: la sovrapposizione di un calcare (roccia rigida) su un'argilla plastica induce un *lateral spreading* associato a caduta, scivolamento e/o ribaltamento di blocchi rocciosi di varie dimensioni dal bordo della placca di calcare. L'analisi delle misure di rumore sismico ambientale ha permesso di ottenere notevoli risultati riguardo il livello di stabilità delle diverse zone instabili e, quindi, di valutare la loro differente suscettibilità da frana nel quadro di una zonazione di pericolosità da frana. In aggiunta, è stato ottenuto il principale moto proprio di un ampio blocco di roccia instabile ed è stato effettuato nel dominio del tempo uno studio preliminare di specifici parametri di misure di rumore sismico ambientale di lunga durata effettuate in zone stabili e instabili. D'altra parte, l'installazione di un *array* a geometria SNS ha permesso di individuare e localizzare alcuni eventi microsismici originati dal margine instabile della placca calcarea.

Il Versante delle Sorgenti del Peschiera, localizzato nell'Appennino Centrale (Italia Centrale) a circa 70 km a Nord-Est di Roma, è coinvolto in un fenomeno di *creep* in ammasso roccioso associato ad una dissoluzione carsica profonda. Le misure di rumore sismico ambientale hanno evidenziato la diversa risposta sismica delle varie zone del versante interessato dal complesso processo di frana. Dato che il versante delle Sorgenti del Peschiera ospita un importante impianto di drenaggio di approvvigionamento di acqua per la città di Roma, una rete accelerometrica è stata installata nel 2008 ed un *array* SNS è stato aggiunto nel 2014. L'*array* SNS ha registrato centinaia di eventi microsismici originati nel versante e legati al suo processo di instabilità. Tali eventi sono stati distinti in due diversi tipi: i) rotture legate alla fratturazione dell'ammasso roccioso, con durata da 1 a qualche secondo; ii) collassi, con durata minore di 1 s e tipica forma d'onda da impatto. In questa tesi, 397 eventi (16 rotture e 381 collassi) sono stati caratterizzati con il *software* NanoseismicSuite in termini di magnitudo locale M_L ed ipocentro. Mentre le rotture sono risultate distribuite nell'intero versante, i collassi si sono focalizzati in due diversi *cluster* spaziali sotto il livello di falda, ad una profondità in cui il carsismo produce cavità. I *cluster* sono stati trattati come due distinte sorgenti microsismogeniche ed una curva frequenza-magnitudo degli eventi è stata prodotta per ognuna, per descrivere l'attitudine a produrre eventi di diverso valore di magnitudo. È stata poi sviluppata una procedura automatizzata di analisi rapida degli eventi registrati della rete accelerometrica.

Infine, una matrice di pericolosità da frana è stata implementata per entrambi i casi di studio in base alla frequenza statistica degli eventi occorsi (i valori delle misure di rumore sismico per il caso di studio di Selmun e i valori di M_L dei collassi per il caso di studio del Peschiera) e la loro probabilità di eccedenza in un periodo fissato, fornendo un utile contributo nella gestione del relativo rischio da frana.

In conclusione, la presente tesi di Dottorato di Ricerca evidenzia come la sismica passiva possa essere considerata un utile strumento per investigare e monitorare processi di instabilità gravitativa dato che ha consentito di raggiungere i diversi obiettivi iniziali: valutare la suscettibilità da frana, stimarne la pericolosità ed, infine, implementare uno strumento che possa contribuire alla gestione del rischio connesso.

1. Introduction

Natural hazards are natural processes of evolution of the Earth that can have a negative effect on society when they interfere with human activities, as settlements, tourist sites and/or infrastructures. According to Dilley *et al.* (2005), approximately 19% of land area of the Earth and over 50% of its population are exposed to at least one natural hazard, including earthquakes, landslides, floods, volcanoes, cyclones and drought.

Landslides are one of the major natural hazards, causing large human and economic losses worldwide (Petley, 2012). Haque *et al.* (2016) observed that over the period between 1995 and 2004, a total of 1370 deaths and 784 injuries were reported from 476 landslides occurred in the 27 European countries (Fig. 1.1). In general, approximately from 1.3 to 3.6 million of people live in areas prone to landslide on European territory (Jaedicke *et al.*, 2014) and most of the settlements in Central Europe and Mediterranean area are potentially at risk of fatal landslides (Haque *et al.*, 2016). Exposure to landslide hazards is expected to increase due to rapid population growth in urban areas and the escalation of urbanization throughout many countries (Mateos *et al.*, 2017).

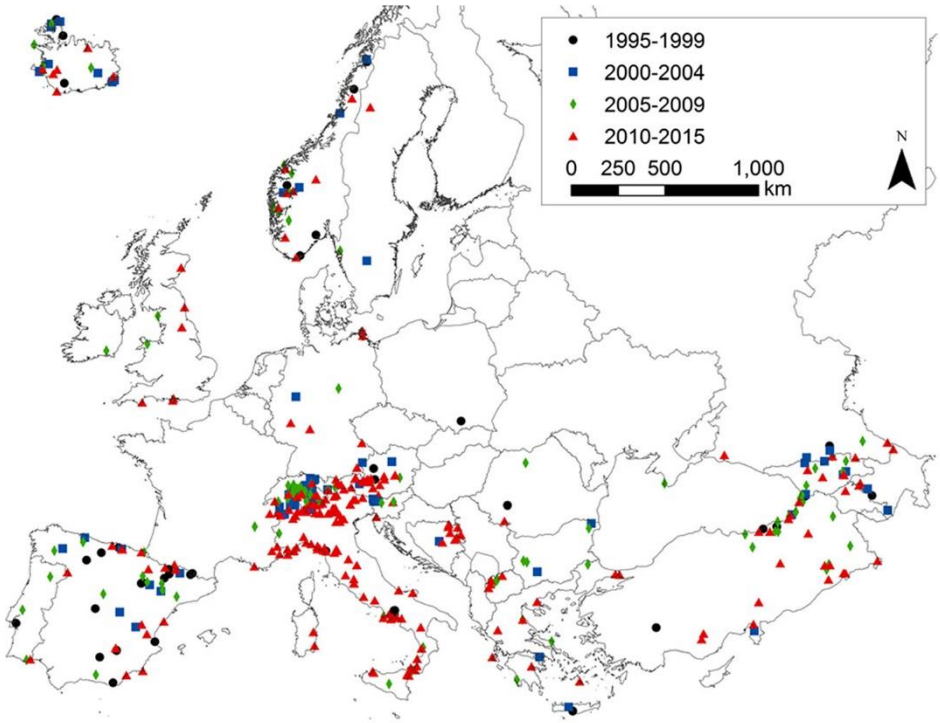

Fig. 1.1. Spatial distribution of fatal (death, injury and missing) landslides in Europe between 1995 and 2015. (from Haque *et al.*, 2016)

Among the European countries, Italy suffers the highest socioeconomic impact from landslides (Klose *et al.*, 2015). Italy is widely interested by gravity-induced slope instability phenomena because most of its territory consists of mountainous, hilly and coastal regions that are the environments mainly interested by landslides (Van Den Eeckhaut *et al.*, 2012). By studying the historical documents and the reports of landslides occurred in Italy between 1279 and 2002, Guzzetti *et al.* (2004) evidenced as fast-moving landslides in rock slope, including rockfalls, rockslides, rock avalanches and debris flows, caused the largest number of fatalities, probably due to their quick evolution. In light of the above, more efforts would be needed to manage hazard and risk associated with landslide processes, starting from the assessment of their hazard.

In coastal areas, landslides and related risk have always been widely studied in the scientific community due to the presence of human activities, settlements as well as tourist and cultural heritage sites (Guzzetti *et al.*, 1999; Senfaute *et al.*, 2009; Pennetta & Russo, 2011; Montoya-Montes *et al.*, 2012; Dewez *et al.*, 2013; Epifanio *et al.*, 2013; Martino & Mazzanti, 2014). Commonly, sea cliffs are subjected to retreat during their complex evolution, governed by a combination of sea erosion and gravity-induced instability processes on coastal cliff slopes (Hampton *et al.*, 2004; Young & Ashford 2008; Dickson *et al.*, 2013; Rosser *et al.*, 2013). Such processes may produce landslides involving from a single sea cliff up to several hundred meters of coast (Hutchinson *et al.*, 1991; Della Seta *et al.*, 2013).

Mountainous areas are the environment in which the most of the landslides occurs worldwide (Van Den Eeckhaut *et al.*, 2012). As a matter of fact, landsliding is a frequent erosional process of relief evolution in mountain belt, controlled and triggered by factors as fluvial slope undercutting, earthquakes, rainstorms and excess of internal stress thresholds (Korup *et al.*, 2010). Studies of landslides in mountainous regions have always been very common because gravity-induced slope instability processes threat villages (Wasowski & Del Gaudio, 2000; Esposito *et al.*, 2007; Bozzano *et al.*, 2008a), touristic and cultural heritage sites (Lollino & Audisio, 2006; Fanti *et al.*, 2013) or strategic infrastructures, e.g. plant drainages of aqueducts (Martino *et al.*, 2004; Maffei *et al.*, 2005), hydroelectric power plants (Discenza *et al.*, 2011) and highways (Rodríguez-Peces *et al.*, 2011; Bozzano *et al.*, 2012; Delgado *et al.*, 2015). The scale of gravity-induced

slope instabilities in mountainous environment varying from falls of a single rock block up to deep-seated gravitational deformations involving the entire slope of a relief.

In the last century, the exigence of defencing human activities by slope gravity-induced instability processes produced a large number of publications in which basic concept as risk, vulnerability, hazard and susceptibility related to landslides are defined and developed; these concepts are still used in the studies of landslides nowadays.

Landslides are natural phenomena related to the landscape evolution, defined as the movement of a mass of rock, debris or earth down a slope, triggered by variety of external natural stimulus or human activities, such as intense rainfall, earthquake shaking, water level change, storm waves, rapid erosion, deforestation or excavation (Hutchinson, 1968; Varnes & IAEG, 1984; Cruden, 1991; Dai *et al.*, 2002).

Varnes & IAEG (1984) reported the definition of risk proposed by UNDRO (United Nations Disaster Relief Organization) and UNESCO (United Nations Educational, Scientific and Cultural Organization). In general, the total risk (R_t) associated to a specific natural event is computed by considering the hazard of the expected event (H), the element at risk (E) and its vulnerability (V) to the expected event, according to the following equation [Eq. 1.1]:

$$R_t = E \times H \times V \qquad [1.1]$$

Population, properties and human activities in a given area and exposed to the analysed event represent the element at risk (E); it is expressed as economic value. The vulnerability (V) represents the expected degree of loss for the considered element or for a set of elements resulting from the occurrence of a natural phenomenon having a given magnitude; such an element typically requires an evaluation based on engineering approaches. The natural phenomenon is considered in probabilistic terms: the hazard (H) indicates the probability of occurrence within a specific period of time and within a given area of a potentially damaging phenomenon having a given magnitude. Considering the landslide processes, the landslide hazard assessment is the field in which geosciences and, in particular, applied geology are employed towards evaluation and management of landslide risk.

Hungr (1997) defined the hazard assessment as the first stage to infer the landslide risk: recognition of the landslide types, determination of locations and magnitudes, estimation of probabilities of occurrence, runout analysis and determination of hazard

intensity as a function of location and probability. Therefore, since the landslide hazard is defined as spatiotemporal probability of an event having a given magnitude, its estimation requires the definition of a spatial probability as well as the temporal probability of the considered natural event (Galve *et al.*, 2016).

Regarding the spatial probability of the hazard, Brabb (1984) described the concept of landslide susceptibility for expressing the likelihood of a landslide occurrence in an area only based on the stability conditions of the local terrain, without consider the temporal probability of failure or the magnitude of the expected landslide. At the same time, Varnes & IAEG (1984) introduced the concept of landslide hazard zonation for describing the procedure of division of land surface into homogeneous areas and ranking of these areas according to their degree of stability, indicating actual or potential hazard due to mass movements and estimating the factors that can induce instability, without, in any case, a temporal probability of occurrence.

In the here-presented Ph.D. thesis, several geophysical measurements were carried out in two case studies of rock masses interested by gravity-induced slope instability processes for evaluating as passive seismic approaches can be a useful tool to: i) evaluate the landslide susceptibility and produce a landslide hazard zonation; ii) assess the landslide hazard (in terms of probability of occurrence); iii) manage the related risk. The two case studies were selected by considering the variation of the scale of the landslide processes as well as the natural environments interested by the instability: i) one rock cliff slope in coastal environment, on the island of Malta (Selmun case study); ii) one rock slope in mountainous area in Central Italy (Peschiera case study). In each case study, two different geophysical approaches were experimented: i) seismic noise analysis carried out by single-station measurements; ii) seismic monitoring operated through seismic array/network (permanent or temporary).

2. Passive seismic applied to landslides

2.1. State of the art of geophysical methods in landslide investigation

In the last decades, geophysical techniques have been widely applied to study gravity-induced slope instability processes. Bogoslovsky & Ogilvy (1977) produced a pioneering work that evidenced the potentiality of application of surface geophysical methods to characterise landslide. Afterwards, this review was largely updated by McCann & Forster (1990), Hack (2000), Jongmans & Garambois (2007) and Maurer *et al.* (2010) by considering all the improvements produced in geophysical investigation in terms of resolution increase of previous methods as well as development of new and innovative techniques.

Geophysics can be applied to evaluate fundamental features of mass involved in landslide processes, as dimension, geometry, lateral and vertical variations, content of water, rate of movement, dynamic behaviour. By geophysical methods, some physical variables are directly measured in situ and other dependent physical parameters, such as geotechnical parameters, can be deduced in an indirect manner only after elaboration of the first ones. Since geophysics provides indirect information on relevant geotechnical parameters, its tools have to be always integrated and calibrated with other geological and geotechnical data for producing a reliable interpretation. Therefore, geophysical and engineering geological surveys can be considered as two complementary investigation approaches for characterising landslides (Jongmans & Garambois, 2007).

Geophysical techniques present several advantages as flexibility, efficiency, easiness of instrument deployment and quickness of data processing; hence, they allow investigating large areas in relatively short time and provide information on the internal structure of soil or rock mass through non-invasive surveys. On the other hand, their disadvantages concern the fact that the solution for a set of data is not unique, therefore the derived results should require a previous calibration with geotechnical constrains obtained by conventional engineering geological surveys (ISRM, 1978) for arriving at a reliable estimation of the required geotechnical parameters.

By considering the countless bibliography produced in the last decades, Jongmans & Garambois (2007) in their review summarised: i) applicability of geophysical techniques in landslide investigation; ii) geological contest in which these techniques

generated reliable results; iii) main observations and results derived by these techniques; iv) potentialities and limitations of these techniques. The most of the geophysical investigation methods are applied in landslide investigations in presence of a marked geophysical contrast (i.e. slip surface and boundaries of landslides involved soft slopes or open fractures in rock slopes) that is the first and essential condition for characterising dimension, water content and movement of unstable mass according to McCann & Forster (1990).

Among the electrical methods, Electrical Resistivity Tomography method (ERT) can allow to define thickness and boundaries of soft landslides in soil or debris (Havenith *et al.*, 2000; Bichler *et al.*, 2004; Méric *et al.*, 2005; Friedel *et al.*, 2006; Sass *et al.*, 2008; Hilbert *et al.*, 2012), while Spontaneous Potential method (SP) can be useful to define dimensions and presence of groundwater level in large landslides (Lapenna *et al.*, 2003; Chambers *et al.*, 2011). Also Ground Penetrating Radar (GPR) is largely applied to evaluate thickness of shallow landslides due to its good resolution and light instrumentation (Bichler *et al.*, 2004; Friedel *et al.*, 2006; Sass *et al.*, 2008). Instead, gravimetric and electromagnetic analyses are quite rarely used to define the failure surface of landslides (Del Gaudio *et al.*, 2000; Méric *et al.*, 2005).

Seismic surveys are divided into two different main systems: active seismic methods and passive seismic methods. The substantial difference regards the source of seismic waves. In the active methods, seismic waves are controlled because an operator directly produces them though a controlled source (i.e. an explosive charge or a standard hammer). In passive methods, sensors record seismic waves produced by random and uncontrolled sources, natural (sea waves, wind, rivers) as well as related to human activities (cars, trains, industrial machineries). During the last decades, both methods have been strongly improved and used in different geological contexts because their application for engineering scopes and seismic microzonation induced manufacturers to produce instruments having high portability and easy deployment for recording data as well as several user friendly and open source software for their processing. Seismic methods generally can be applied in soil or debris landslides because the impedance contrast between the weakened layer represented by the landslide body and the surrounding intact material influences seismic waves and modifies their features.

Excluding borehole geophysical techniques that are very expensive and require long times to drill and arrange the boreholes, seismic reflection, seismic refraction, seismic tomography and MASW (Multichannel Analysis of Surface Waves) are the most common methods of active seismic applied in landslide investigation. All these methods have been applied mainly for defining dimensions, geometry, slip surface and, in some cases, velocity of seismic waves into the landslide body (Havenith *et al.*, 2000; Bichler *et al.*, 2004; Glade *et al.*, 2005; Méric *et al.*, 2005; Hibert *et al.*, 2012; Imposa *et al.*, 2017).

The already-examined geophysical methods allow to provide a 2D or 3D imaging of landslide mass, as its dimensions and geometry, and some basic features, as water content or seismic wave velocity. On the contrary, passive seismic can be applied also by including the time dimension, with the aim of observing the variation of specific effects or parameters during time. This feature makes passive seismic suitable both for investigating landslides and for monitoring the evolution of such processes in time, being therefore useful for susceptibility landslide analysis as well as hazard and risk management purposes. By considering its broader field of application in landslide studies, passive seismic was applied through two different approaches in this work: seismic ambient noise measurements and microseismic monitoring.

The following paragraphs will focus on the two passive seismic approaches, explaining their theoretical bases, reassuming their published applications for studying and monitoring of landslide, and addressing the prospects that led to choose them as investigation methods for the two case studies that were examined in this Ph.D. thesis.

2.2. Seismic ambient noise measurements

Over the last two decades, seismic passive methods based on recording and analysis of seismic noise has been the most used since its intense application in engineering design field and in the studies of seismic microzonation, in particular for evaluating site amplification phenomena interesting worldwide many settlements built on soft deposits.

Seismic noise is composed of ambient vibrations of the ground produced by random and uncontrolled sources, natural or related to human activity such as tides, sea waves striking the coasts, wind, trees, buildings, industrial machineries, road traffic, trains, human footsteps, etc. In general, seismic ambient noise cover a broad range of frequencies. Gutenberg (1958), Asten (1978) as well as Asten & Henstridge (1984)

deeply investigated seismic noise, discovering a relation between the type of source, its nature and the frequency content of the produced vibrations. They defined two different terms for classifying seismic noise: microseisms for vibrations related to natural sources with a typical frequency content in a low and medium range (usually lower than 5 Hz), microtremors for vibrations related to human activities characterised by medium and high frequencies (usually higher than 1 Hz).

The seismic noise wavefield is composed of a mixture of both body waves (P, SV and SH waves) and surface waves (Rayleigh and Love waves), whose proportions are not very clear. In general, all the authors who investigated the composition of seismic noise (Douze, 1964, 1967; Toksöz & Lacoss, 1968; Li *et al.*, 1984; Horike, 1985; Yamanaka *et al.*, 1994; Bonnefoy-Claudet *et al.*, 2006) assume that it consists mainly of surface waves, with a proportion variability related to the distance of sources as well as the geological conditions of site. For example, seismic noise is dominated by Rayleigh waves in presence of a large impedance contrast (Bonnefoy-Claudet *et al.*, 2006).

Seismic ambient noise analysis can be carried out mainly through two different approaches: single-station measurements, performed by deploying independent seismic sensors, and array measurements, based on simultaneous recording and combined analysis of data derived by several seismic sensors. The main methods for analysing seismic noise records were developed during the second half of the last century. The Spatial Autocorrelation analysis of signal (SPAC) by Aki (1957, 1965) and the Frequency-Wavenumber analysis (f-k) by Capon (1969) and Lacoss *et al.* (1969) were designed among the seismic array measurements, while the Horizontal-to-Vertical Spectral Ratio analysis (HVSR) by Nakamura (1989) was implemented for the single-station measurements. The technique of Site-to-Reference Spectral Ratio analysis was designed in the same period (Borcherdt, 1970, 1994; Spudich *et al.*, 1996) and is part of the passive seismic methods, but it cannot be properly included in the group of seismic noise analysis techniques because it compares records of earthquakes in different stations.

According to Bonnefoy-Claudet *et al.* (2006), the number of publications dealing with seismic noise analysis is strongly increased year after year starting from 1970, exceeding 500 papers in 2006; however, the most of these papers (about 95%) were focused on the application of seismic noise analysis in different specific sites and only few publications investigated the composition and the nature of the seismic noise

wavefield. Considering the large use of seismic noise in several case studies, a specific European Project (SESAME, 2004) was focused to define guidelines for applying seismic noise measurements in different geological contexts as well as to study extensively the nature of the ambient seismic noise wavefield.

In the last twenty years, the different approaches of seismic noise analysis have been applied in mountainous and coastal areas. As proved by several recently-published works, seismic noise measurements have been already used to investigate landslide-involved slopes (Havenith *et al.*, 2000, 2002; Del Gaudio & Wasowski, 2007; Danneels *et al.*, 2008; Del Gaudio *et al.*, 2008, 2014; Burjánek *et al.*, 2010, 2012; Renalier *et al.*, 2010; Moore *et al.*, 2011; Mainsant *et al.*, 2012; Torgoev *et al.*, 2013; Martino *et al.*, 2016; Yalcinkaya *et al.*, 2016; Del Gaudio 2017; Imposa *et al.*, 2017; Pazzi *et al.*, 2017), unstable blocks of rock cliffs (Got *et al.*, 2010; Lévy *et al.*, 2010, 2011; Panzera *et al.*, 2012; Bottelin *et al.*, 2013a, 2013b, 2014, 2017; Galea *et al.*, 2014; Iannucci *et al.*, 2015, 2016; Colombero *et al.*, 2017; Valentin *et al.*, 2017) and natural rock arches (Starr *et al.*, 2015; Moore *et al.*, 2016) by different approaches, e.g. HVSR analysis, f-k analysis, site-to-reference spectral ratio analysis, polarization analysis, analysis of amplitude noise variation in the frequency and time domains.

Generally, one aim of the cited studies was the investigation of the seismic response of landslides; as a matter of fact, in the case of seismic shaking the contrast of impedance between the landslide body and the surrounding intact material can be seen as responsible for triggering or reactivating the gravity-induced slope instability (Havenith *et al.*, 2003a, 2003b; Bozzano *et al.*, 2004, 2008b, 2011; Bourdeau & Havenith, 2008). Surely, the most widespread technique for analysing seismic noise measurements in landslide is the HVSR method, applied in almost all the cited works because it requires the deployment of portable instruments having fast acquisition and easy processing. According to the published results, HVSR analysis seems be useful to define the dimension of the landslide body and to study its seismic response, especially when it is applied jointly to a polarization analysis (Burjánek *et al.*, 2010, 2012; Galea *et al.*, 2014). As this jointed approach was also applied in the present Ph.D. thesis, some additional theoretical elements as well as some remarkable results obtained in landslide study will be discussed in the next two subparagraphs (see Subparagraph 2.2.1 for HVSR analysis and Subparagraph 2.2.2 for polarization analysis).

Probably, the most important issue in seismic response study of a landslide body focus on the identification of the mainly resonance frequency of the landslide itself. This feature can be used for monitoring the evolution of the gravity-induced slope instability, by borrowing an approach already experimented for detecting changes in stiffness of buildings and civil structures during their progressive damage (Doebling *et al.*, 1996; Kim & Stubbs, 2003; Clinton *et al.*, 2006). Michel *et al.* (2010) evidenced as the eigenmode frequency of buildings and civil structures can be also extracted from records of ambient vibrations.

By applying a monitoring approach based on seismic noise analysis, Got *et al.* (2010) and Lévy *et al.* (2010, 2011) presented the results obtained at the test site of Chamousset, in the Vercors Massif (French Alps), where a rock block of 21000 m^3 collapsed in November 2007. Four months before the collapse, several seismic sensors were installed on the unstable block as well as on the stable part of the test site; they were set in continuous recording mode for identifying the main resonance frequency of the unstable rock block and for monitoring its variations during time. The several published works about Chamousset test site evidenced as significant changes occurred in the range of the rock block resonance frequency approaching to the collapse, in particular a drop in the value of the resonance frequency (Lévy *et al.*, 2010) and a decrease in the amplitude of the base noise level (Got *et al.*, 2010).

In the screening of the continuous noise data recorded at Chamousset test site, the authors (Got *et al.*, 2010; Lévy *et al.*, 2010, 2011) evidenced also the presence of an high number of events similar to very-weak earthquakes, that increased approaching to the collapse of the unstable rock block. Such microearthquakes, known as microseismic events in literature, are related to the progressive failure and detachment of a rock block and can be considered as microseismic precursor of the main landslide event (Amitrano *et al.*, 2005, 2010; Senfaute *et al.*, 2009). The study of these microseismic events in continuous seismic data is part of another approach of passive geophysics called microseismic monitoring, not included between the ambient seismic noise measurement approaches because it specifically requires the detection and the analysis of microseismic events only. This method was also applied in the here-presented Ph.D. thesis, therefore various approaches for monitoring of microseismic events will be presented and discussed in a dedicated section (Paragraph 2.3).

2.2.1. HVSR analysis

The Horizontal-to-Vertical Spectral Ratio analysis (HVSR) was proposed by Nogoshi & Igarashi (1970, 1971) and was analytically implemented by Nakamura (1989) to evaluate the resonance frequency of a site (f_0), especially where there is a marked impedance contrast due to the presence of low shear-wave velocity layers above the seismic bedrock. HVSR technique is based on the analysis of records of the ambient seismic noise by single-station measurements. For each measurement point, spectra are computed by applying the Fourier Transform on the Horizontal components (H) and on the Vertical component (V) of the recorded time history; finally, the ratio between them is computed for each frequency. A peak in the distribution of the HVSR values vs. natural frequency can be interpreted both in terms of SH-wave resonance in soft surface layers as well as in terms of the ellipticity of particle motion when the ambient noise wave train is made up predominantly of surface waves (Bonnefoy-Claudet *et al.*, 2006). Since the seismic noise wavefield is expected to be a combination of both types, the HVSR curve contains information about the shear wave velocity profile in shallow sediments (Galea *et al.*, 2014).

HVSR analysis was developed and widely applied in engineering design field and seismic microzonation studies for investigating sedimentary sequences composed of planar, homogeneous and almost-horizontal strata, providing information about the thickness of the resonant layers and their mean seismic wave velocity by the following relation [Eq. 2.1]

$$f_0 = \frac{V_S}{4h} \qquad [2.1]$$

in which f_0 is the resonance frequency associated to the resonant layers, V_S the mean S-wave velocity value and h the total thickness.

Due to the similar sedimentary condition (i.e. planar, homogeneous and sub-horizontal strata), HVSR analysis has been mainly applied for investigating large landslides in soil or debris, in which a marked impedance contrast exists due to the slightly-dip slip surface and the landslide body represents the resonant layer (Havenith *et al.*, 2002; Bozzano *et al.*, 2008b, 2011; Danneels *et al.*, 2008; Del Gaudio *et al.*, 2008, 2014; Torgoev *et al.*, 2013; Martino *et al.*, 2016; Yalcinkaya *et al.*, 2016; Imposa *et al.*, 2017; Pazzi *et al.*, 2017).

Recently, HVSR analysis has been also applied in rock slopes involved in gravity-induced instability processes (Panzera *et al.*, 2012; Galea *et al.*, 2014; Iannucci *et al.*, 2015, 2016; Valentin *et al.*, 2017), whose evolution produce landslides characterised by sub-vertical fractures that often isolated single and unstable rock blocks. Panzera *et al.* (2012) and Galea *et al.* (2014) investigated the seismic response of two rock coastal areas involved in landslide processes in the North Western part of the island of Malta (Central Mediterranean Sea), respectively Xemxija Bay and Anchor Bay. In both case studies, HVSR analysis results showed a marked-different seismic response between the stable zones and the areas involved in the landslide process. As a matter of fact, all the HVSR curves obtained in the measurements points both on stable areas and on unstable zones evidenced a clear peak related to the stratigraphic succession of the area. On the other hand, the HVSR results obtained in the zones involved in landslide processes presented also one or more peaks at higher frequencies, related to the vibrational behaviour of the unstable rock blocks (Fig. 2.1).

Valentin *et al.* (2017) presented the results obtained at two different sites: Vercors Massif (French Alps) and Piton de La Fournaise (La Réunion Island, Indian Ocean). Both case studies are characterised by the presence of rock blocks isolated by sub-vertical fractures from the stable part of the slopes. By comparing the HVSR analysis on the unstable blocks and a numerical modelling of their dynamic response, the obtained results seem to confirm that the main peak in the HVSR curves is related to the resonance frequency of the analysed unstable rock block.

2.2.2. Polarization analysis

Vidale (1986) introduced in the seismological community the concept of polarization of the particle motion and a method to analyse it based on principal component analysis of the coherency matrix (i.e. complex covariance matrix), which is computed from analytical signals of a three-component seismogram and without time averaging.

Some works about the landslide investigation applied tools to study the polarization of the Fourier spectra as well as of the HVSR(f) function for obtaining the distribution of their values on the horizontal plane (Del Gaudio *et al.*, 2008, 2014; Panzera *et al.*, 2012; Martino *et al.*, 2016; Imposa *et al.*, 2017; Valentin *et al.*, 2017).

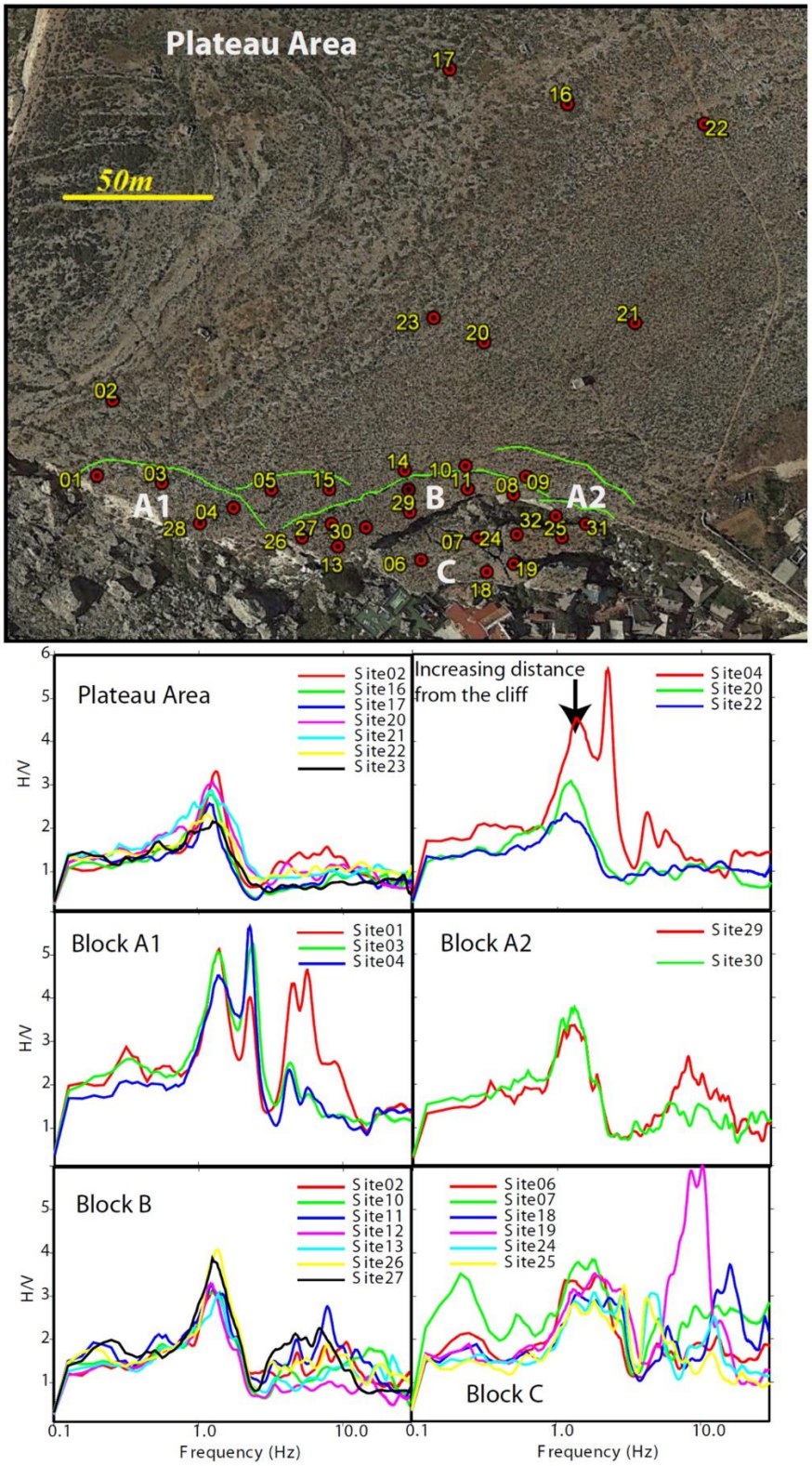

Fig. 2.1. Location of measurement stations at Anchor Bay case study (Malta, Central Mediterranean Sea) and summary of HVSR results on the stable area and on the different unstable blocks. (from Galea *et al.*, 2014)

Based on the hypothesis that wavefield within an unstable rock mass is dominated by normal mode vibration rather than horizontal propagation of seismic waves, Burjánek *et al.* (2010, 2012) implemented an analysis code (WAVEPOL) to perform polarization analysis on seismic noise measurements by adopting a Continuous Wavelet Transform (CWT), by carrying out a time-frequency domain analysis on a time history. WAVEPOL package allows to obtain a 3D ellipse representing the particle motion at each time-frequency pair. Burjánek *et al.* (2010) explained the theoretical bases of such an analysis, whose fundamental steps will be shown in the following. The continuous wavelet spectrum of the *i*th seismogram component x_i at time t and scale s is [Eq. 2.2]

$$W_i(t,s) = \frac{1}{\sqrt{|s|}} \int_{-\infty}^{+\infty} x_i(\tau) \psi^* \left(\frac{\tau - t}{s} \right) \mathrm{d}\tau \qquad [2.2]$$

in which ψ is the mother wavelet, and the asterisk denotes complex conjugation. If the CWT is calculated for all three components of the seismogram in the same way (i.e. using the same set of times and scales), the coherency matrix $\hat{C}$ can be generalized as [Eq. 2.3]

$$\hat{C}(t,s) = \begin{pmatrix} W_1^* W_1 & W_2^* W_1 & W_3^* W_1 \\ W_1^* W_2 & W_2^* W_2 & W_3^* W_2 \\ W_1^* W_3 & W_2^* W_3 & W_3^* W_3 \end{pmatrix} \qquad [2.3]$$

where $W_i = W_i(t,s)$ is the continuous wavelet spectrum defined in Equation 2.2, assuming a Morlet wavelet as the mother wavelet ψ. Following Vidale (1986), eigenvalues and eigenvectors of the coherency matrix $\hat{C}$ are then calculated. The normalised eigenvector (x_1, x_2, x_3) associated with the largest eigenvalue points in the direction of the largest amount of polarization. An optimum phase (α) is then found maximising X, the length of the real component of the eigenvector [Eq. 2.4]

$$X = \sqrt{\sum_{k=1}^{3} [\Re(x_k \cos\alpha + i x_k \sin\alpha)]^2} \qquad [2.4]$$

The optimum phase (α_0) is found by a grid search over the interval (0, π). The eigenvector (x_1, x_2, x_3) is then rotated in the complex plane by the angle α_0 [Eq. 2.5]

$$\tilde{x}_k = (x_k \cos\alpha_0 + i x_k \sin\alpha_0) \qquad [2.5]$$

The elliptical component of the polarization is estimated as [Eq. 2.6]

$$P_E = \frac{\sqrt{1 - X_0^2}}{X_0} \qquad [2.6]$$

where X_0 is the length of the real component of the vector ($\tilde{x}_1$, $\tilde{x}_2$, $\tilde{x}_3$). P_E equal to 0 represents purely linear particle motion, P_E equal to 1 indicates circular particle motion.

The strike of maximum polarization is [Eq. 2.7]

$$\phi = \frac{\pi}{2} - \tan^{-1}\frac{\Re(\tilde{x}_2)}{\Re(\tilde{x}_1)} \qquad [2.7]$$

and the dip of the direction of maximum polarization is [Eq. 2.8]

$$\delta = \tan^{-1}\frac{\Re(\tilde{x}_3)}{\sqrt{[\Re(\tilde{x}_1)]^2 + [\Re(\tilde{x}_2)]^2}} \qquad [2.8]$$

The strike defined in Equation 2.7 ranges from 0 to π, whereas the dip defined in Equation 2.8 ranges from −π/2 to π/2. The strike and dip angles describe the direction of maximum polarization in a 3D half-space: the dip represents inclination from the horizontal plane, while the strike indicates the azimuth in horizontal half-plane. All quantities in the equations presented above depend on both time (t) and scale (s).

WAVEPOL package (Burjánek *et al.*, 2012) outputs three different plots that represent the particle motion at each time-frequency pair: ellipticity diagram, polar strike plot and polar dip plot. It is possible to demonstrate polarization effects of the particle motion by combining the outputs from such an analysis, i.e. by observing for the same frequencies a high degree of linearity on the ellipticity diagram and a main azimuthal direction on the polar strike plot. The polarization analysis code developed by Burjánek *et al.* (2010, 2012) provides quite robust results about directivity effects of the particle motion, overcoming the bias that could be introduced by the denominator spectrum in the HVSR calculation (Panzera *et al.*, 2014).

Burjánek *et al.* (2010, 2012) applied the WAVEPOL analysis code on seismic noise data recorded at the landslides of Randa and Walkerschmatt, on Swiss Alps. In both cases, a strong directional amplification was observed in the unstable masses, in a direction normal to the fracture strike (Fig. 2.2). The same polarization analysis code was tested by Galea *et al.* (2014) on seismic noise measurements at Anchor Bay (Malta, Central Mediterranean Sea), evidencing on the unstable blocks a polarization roughly normal to the fracture directions as well as a high degree of linearity of the particle motion for some specific frequencies.

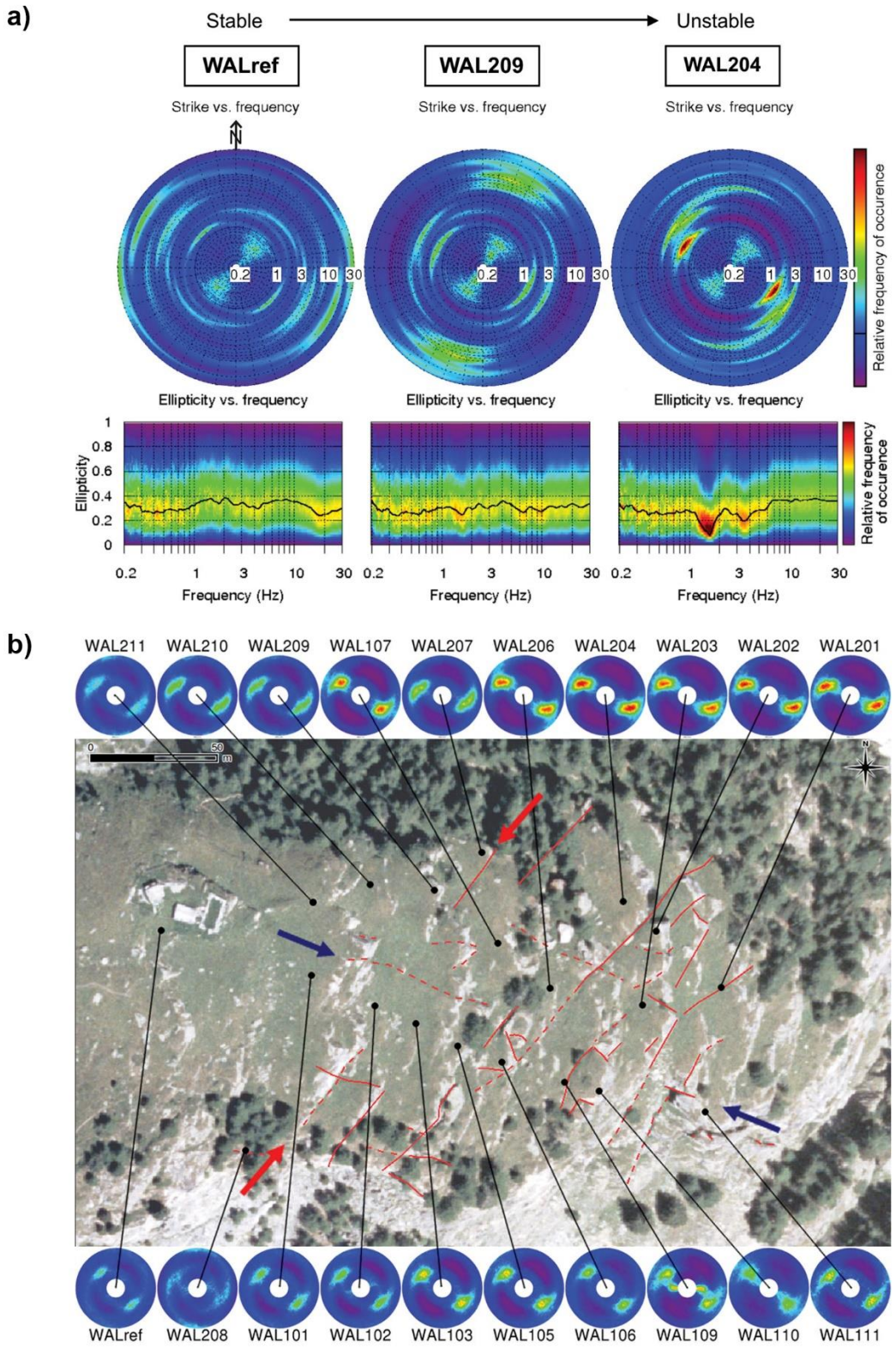

Fig. 2.2. Polarization analysis results at Randa case study (Swiss Alps): **a** polar strike plots and ellipticity diagrams by moving from the stable zone to the unstable zone (from left to right); **b** distribution of polar strike plots respect the open fractures (in red). (from Burjánek *et al.*, 2012)

2.3. Monitoring of microseismic events

As already evidenced in Paragraph 2.2, continuous seismic measurements in area involved in a landslide process can evidence the presence of events similar to very-weak earthquakes, known as microseismic events, related to the progressive failure and detachment of the unstable mass.

The presence in seismic records of "marks" due to events having different nature than earthquakes is a well-known issue in seismology. As a matter of fact, despite national and regional seismic networks are targeted for recording earthquakes, they allowed also to observe seismograms of nuclear explosions (Zucca *et al.*, 1996; Hafemeister, 2007), volcanic eruptions (Kanamori & Given, 1982; Hagerty *et al.*, 2000), snow avalanches (Lawrence & Williams, 1976) and landslides. Several examples about landslide events recorded and studied by seismic networks can be found in literature, from the destructive landslide of Vajont (Italian Alps) of 1963 (Delle Rose, 2012) to more recent examples of gravity-induced instability processes that involved different types of slope, material and environment, e.g. rockfalls in French Alps (Deparis *et al.*, 2008), debris flows in Himalaya (Burtin *et al.*, 2009), rockslides in Swiss Alps (Dammeier *et al.*, 2011) or the large soil landslides of Laguna Beach in California (Surinach *et al.*, 2005), Bingham Canyon in Utah (Hibert *et al.*, 2014) and Oso-Steelhead in Washington (Hibert *et al.*, 2015).

However, all the above-mentioned examples are related to large events having a significant level of energy. In the last two decades, the development of specific seismic sensors with even higher sensitivity allowed to record also events having very-low level of energy. The spread of these microseismometers or microaccelerometers, i.e. sensors devoted to record microseismic events, and their employment in specific networks aimed for monitoring of landslide processes evidenced the occurrence of microseismic events before the main event of slope instability. As a matter of fact, sequences of microseismic events can proceed from a transitional to a transgressive phase by indicating an incoming rock mass failure (Szwedzicki, 2003). In this regard, space and time occurrence analysis of microseismic events can be considered as a useful tool both for studying the landslide hazard and for managing the related risk, by monitoring the failure propagation as well as the possible occurrence of more critical conditions (i.e. generalised collapse).

Monitoring of microseismic events ranks at a field of intermediate scale between the study of acoustic emissions generated by laboratory tests for fracturing of rock samples (Lockner, 1993) and the characterisation of large energetic landslide events by regional and national seismic networks (Hibert *et al.*, 2017a). Occurrence of microseismicity in rock masses are well known in mining engineering since the end of the last century (Wong *et al.*, 1989; Gibowicz *et al.*, 1991; Feignier & Young, 1992; McGarr, 1992; Phillips *et al.*, 1997) and its study for monitoring the mining processes in quarries and mines became very popular in the last two decades (Cai *et al.*, 2001; Driad-Lebeau *et al.*, 2005; Li *et al.*, 2007; Wang & Ge, 2007; Alber *et al.*, 2009; Contrucci *et al.*, 2010; Hudyma & Potvin, 2010; Lebert *et al.*, 2011; Barzaghi & Ferulano, 2012; Liu *et al.*, 2013; Lu *et al.*, 2013; Cao *et al.*, 2016; Cheng *et al.*, 2017). Recently, microseismic monitoring systems were already tested for monitoring the construction stages of hydroelectric power stations by rock excavation (Xu *et al.*, 2011, 2014, 2015; Tang *et al.*, 2015) as well as the rock hydraulic fracturing induced in deep geothermal power plants by fluid-injection processes (Häge *et al.*, 2013; Edwards *et al.*, 2015; Zang *et al.*, 2017).

Application of microseismic approaches for monitoring of natural gravity-induced instability processes in rock masses can be more difficult than their application in contexts in which instability processes are controlled by human activities. As a matter of fact, the induced microseismicity related to human activities (e.g. mining processes, rock excavation, rock hydraulic fracturing) is mainly focused in specific zones of the rock mass where the engineering interventions can induce changes in the stress field, a subsequently opening of new fractures and/or propagation of pre-existent joints and a progressive failure. On the other hand, since such a well-defined trigger factor (i.e. having known occurrence in time and space) is not present in rock mass involved in natural landslide processes, application of microseismic studies to landslide monitoring requires a different approach for investigating and characterising the unstable area.

In the last fifteen years, some case studies have been instrumented with specific and experimental microseismic networks aimed to test their suitability for characterising and monitoring of gravity-induced instability processes, involving slopes in soil/debris (Amitrano *et al.*, 2007; Walter & Joswig, 2008, 2009; Walter *et al.*, 2009, 2011, 2012a, 2012b, 2013; Tonnellier *et al.*, 2013) or rock (Amitrano *et al.*, 2005, 2010; Spillmann *et al.*, 2007; Senfaute *et al.*, 2009; Got *et al.*, 2010; Helmstetter & Garambois, 2010; Wust-

Bloch, 2010; Lévy *et al.*, 2011; Lenti *et al.*, 2012, 2015; Fiorucci *et al.*, 2015, 2016a, 2017). In addition, several experiments were also conducted to analyse and characterise the waveforms of induced rockfalls (Bottelin *et al.*, 2014; Hibert *et al.*, 2017b).

Event detection, classification and location is a complex task in gravitational mass movements due to the different waveform of recorded microseismic events as well as to the different landslide-involved materials. In general, microseismic events are composed of high-frequency signals and cannot be recorded at long distance due to their low energy and fast attenuation, so microseismic sensors have to be deployed close enough to the source. Another important issue is the processing of microseismic events that requires specific tools, software and codes devoted to their analysis.

Amitrano *et al.* (2005) and Senfaute *et al.* (2009) analysed seismic continuous data recorded on a coastal chalk cliff at Mesnil-Val (Haute Normandie, France). About 15 h prior to a rockfall of 2000 m^3 involved a large portion of the cliff, they observed a high rise of microseismicity within the rock mass (224 microseismic events recorded) as well as a clear increase of the related energy (Fig. 2.3), in particular in the microaccelerometer located on the collapsed zone. Senfaute *et al.* (2009) evidenced also a progressive decrease of frequency spectrum of the recorded microseismic events approaching the rockfall. By monitoring the post-collapse microseismic activity after a rockfall occurred at Randa (Swiss Alps), Spillmann *et al.* (2007) observed similar microseismic events with magnitudes between -2.0 and -0.5 in the unstable rock mass. Also Got *et al.* (2010) and Lévy *et al.* (2011) at the Chamousset site (French Alps) recorded several microseismic events before the collapse of a 21000-m^3 rock block, but they were not able to recognise a microseismic precursor pattern because the monitoring system stopped working 2 weeks before the rockfall.

Some of the above-mentioned works (Walter & Joswig, 2008, 2009; Walter *et al.*, 2009, 2011, 2012a, 2012b, 2013; Tonnellier *et al.*, 2013; Fiorucci *et al.*, 2017) applied an innovative analysis technique called nanoseismic monitoring (Joswig, 2008), recently developed by Institute for Geophysics of University of Stuttgart for studying microseismicity with a low number of sensors. After considering the published results, this approach was chosen for being experimented in the here-presented work, therefore it will be deeper examined in the next section (Subparagraph 2.3.1).

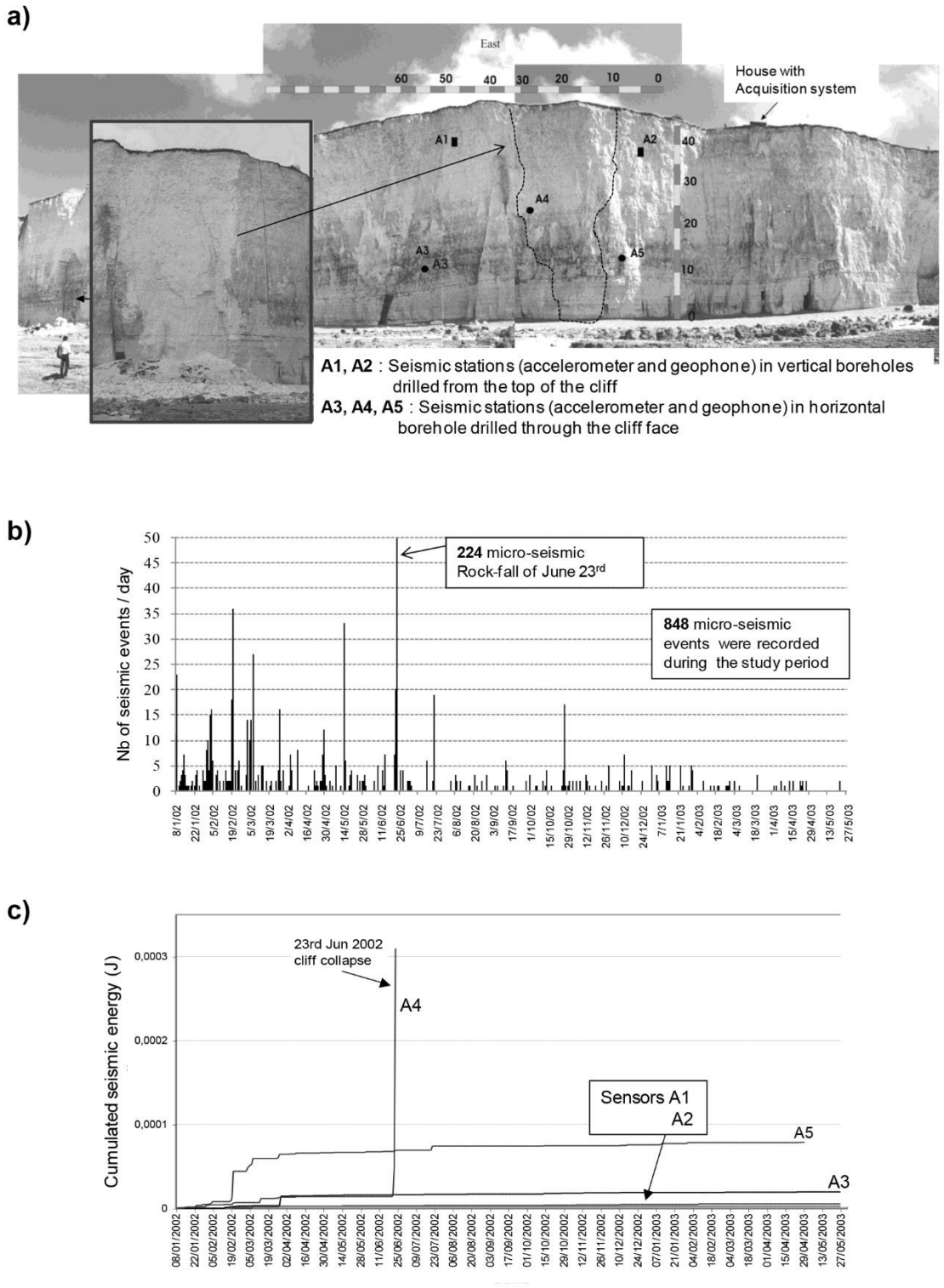

Fig. 2.3. Results obtained at the Mesnil-Val coastal cliff (Haute Normandie, France): **a** chalk cliff before and after the rockfall of 23rd June 2002 and sensor deployment; **b** number of recorded microseismic events per day; **c** cumulative seismic energy evolution per day for each sensor. (from Senfaute *et al.*, 2009)

2.3.1. Nanoseismic monitoring technique

Nanoseismic monitoring (Joswig, 2008) has been recently proposed for microseismicity studies by Institute for Geophysics of University of Stuttgart. Such an approach was designed in the framework of forensic seismology (Zucca, 1998; Douglas *et al.*, 2007) for searching potential nuclear activities through On-Site-Inspection (OSI) carried out with a limited use of instruments and operators, as required by the Comprehensive Test Ban Treaty Organization (CTBTO). In this regard, nanoseismic monitoring is able to detect and characterise events having extremely low energy, with an equivalent magnitude M_L lower than -3.0, also in unfavourable Signal-to-Noise Ratio (SNR) environmental conditions (i.e. events just above the base noise level) and by using only a single array composed of four sensors (Joswig, 2008).

The method of nanoseismic monitoring fills the gap between the traditional microseismic networks (Lee & Stewart, 1981), that do not resolve events in poor SNR conditions, and the other recent applications of passive seismic (Artman, 2006; Kochnev *et al.*, 2007), that require a large employment of sensors. The seismic data are recorded by a specific-geometry array called Seismic Navigating System (SNS) that is composed of four short-period sensors: one single three-component sensor at the centre of the array surrounded by three outer vertical-component sensors, at 120° and with a distance of 20-100 m from the central station (Fig. 2.4a). An array of only four sensors does not allow to perform any kind of f-k analysis, therefore nanoseismic monitoring applies jointly different interactive tools to characterise weak microseismic events. Joswig (2008) evidenced that the records from one single SNS array are sufficient to locate weak events in space and time.

The SNS records have to be managed by the NanoseismicSuite software (www.nanoseismic.net) that includes two main tools: SonoView for the event detection and HypoLine for the event characterisation. SonoView is designed to perform a manual data screening, that is a time-consuming procedure but allows to obtain the most complete detection of microseismic events. Automatic event detection requires to define a threshold that can be a difficult issue in case of events just above the noise level, inducing to record a large amount of false positive events (Spillmann *et al.*, 2007) or to lose the most weak events (Tonnellier *et al.*, 2013). SonoView allows to detect events by the sonogram computation (Fig. 2.4b) and the supersonogram compilation (Fig. 2.4c).

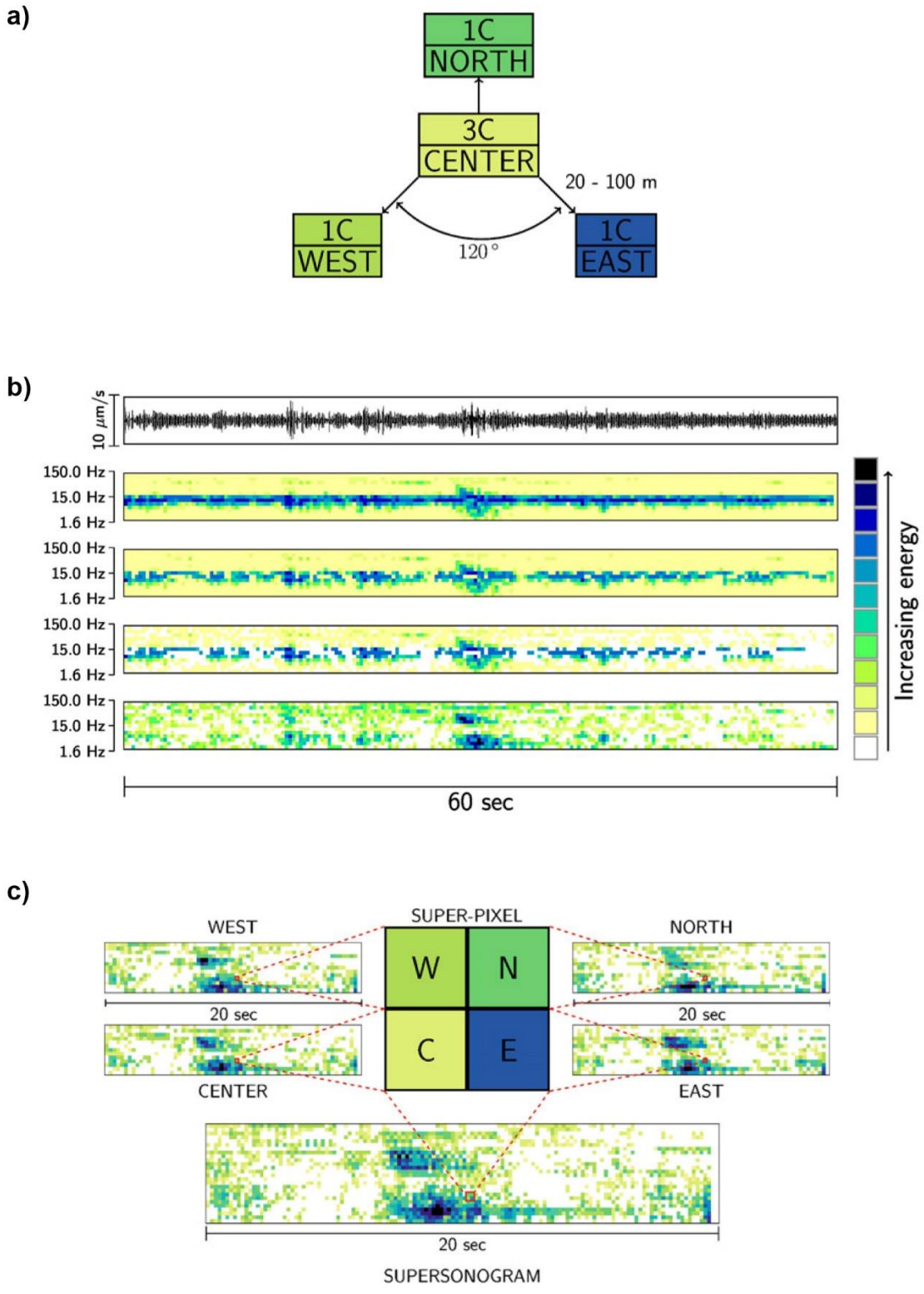

Fig. 2.4. Main principles of event detection by nanoseismic monitoring: **a** layout of a SNS array composed of one three-component station and three vertical-component stations; **b** steps of sonogram computation, from top to bottom: seismogram, power spectral density spectrogram, noise adaptation, blanking, prewhitening; **c** compilation of supersonogram from four sonograms of one SNS array. (from Sick *et al.*, 2014)

A sonogram (Joswig, 1993, 1995) is a modified spectrogram obtained by several computation steps (Fig. 2.4b), that are explained in detail by Sick *et al.* (2014) and will be shown in the following. Fist, on the recorded time history (time domain) a Short-Time Fourier Transform (STFT) is applied. It is split into 256 samples $x(\tau)$, which are tapered with a $\sin^2(\tau)$ windowing function and transformed by Fast Fourier Transform (FFT) to $X(\omega)$ with segment having 50% of overlap.

The resulting spectrograms (time-frequency domain) are based on the Power Spectral Density (PSD) from the STFT and are filtered in 13 half-octave wide passbands [Eq. 2.9]

$$A(\omega, t) = \sum_{\text{half-octave}} X(\omega)X(\omega)^* \qquad [2.9]$$

The amplitudes of the resultant time-frequency matrix are scaled logarithmically. If a log-normal noise distribution is assumed, the logarithmic-scaled spectrogram has a Gaussian distribution of noise with mean $\mu(\omega)$ and variance $\sigma(\omega)$. Noise adaptation has to be outlier resistant, and a more robust solution is to use the median $M(\omega) = M_{50}$ instead of the mean and $S(\omega) = M_{75} - M_{50}$ instead of the variance. $M(\omega)$ and $S(\omega)$ are both calculated for each frequency band, allowing individual adaptation. For noise adaptation, $2^{M(\omega)}$ is subtracted from the signal and only values greater than $2^{M(\omega)+S(\omega)}$ are allowed (blanking). Therefore, disturbing artifacts are eliminated from the signal visualisation [Eq. 2.10]

$$D(\omega, t) = \begin{cases} \log_2(A(\omega, t) - 2^{M(\omega)}), & A(\omega, t) > 2^{M(\omega)+S(\omega)} \\ 0, & \text{else} \end{cases} \qquad [2.10]$$

For further scaling, a log noise variance is applied by a prewhitening function [Eq. 2.11]

$$N_D(\omega) = \log_2 2^{M(\omega)+S(\omega)} - 2^{M(\omega)} \qquad [2.11]$$

where $D(\omega, t)$ and $N_D(\omega)$ are each rounded to the nearest integer value to suppress fine-grain amplitude differences less than $\sqrt{2}$.

Subtracting the frequency-resolved noise variance N_D from the logarithmic-scaled energy distribution performs a prewhitening where the significance of any local energy spot is rated and therefore color-coded as a multiple of the background noise variance [Eq. 2.12]

$$\text{SONO}(\omega, t) = \begin{cases} D(\omega, t) - N_D(\omega), & A(\omega, t) > 2^{M(\omega)+S(\omega)} \\ 0, & \text{else} \end{cases} \qquad [2.12]$$

This interpretation can be seen in the following formulation [Eq. 2.13]

$$\mathrm{SONO}(\omega,t)=\begin{cases}\log_2\left(\dfrac{A(\omega,t)-2^{M(\omega)}}{2^{M(\omega)+S(\omega)}-2^{M(\omega)}}\right), & A(\omega,t)>2^{M(\omega)+S(\omega)}\\ 0, & \text{else}\end{cases} \quad [2.13]$$

In summary, sonogram removes stationary background noise (Joswig, 1995) and allows to identify events by using the "memory image" concept as a detection tool (Joswig, 1990). Finally, the four vertical-component sonograms are combined into a supersonogram (Fig. 2.4c). The combination is done by jointing the single pixels, allowing to obtain a superpixel at each time-frequency pair. This visualisation aids in event detection because evidences the coherence of an event from the noise: incoherent signals are shown as spotted patterns, while coherent ones create consistent areas of similar colours.

The detected events are localised with HypoLine (Joswig, 2008), a tool based on a seismological approach. First, HypoLine needs a subsoil model with the velocity values of P-waves and S-waves and the thicknesses of the different layers. Then, it designs several shapes based on manual first-arrival picking of P-waves (t_P) and S-waves (t_S) on all the components of the analysed event: 4 circles are produced by the t_S-t_P difference at each station and 6 hyperboles are shaped by the t_P difference between different stations (Fig. 2.5a). Additionally, 2 beams are derived by the manual phases picking in the array mode. The best epicentre solution is characterised by the highest concentration of shapes, while the hypocentre depth is not derived by data inversion but is defined by the analysts by shifting the depth of the hypocentral plane for 10-m steps (Fig. 2.5b).

Finally, the assessment of the hypocentre allows to estimate a value of magnitude M_L for the analysed event. The M_L value is computed based on the maximum signal amplitude of S-waves recorded by the array central station and is corrected by a specific distance-magnitude curve (Fig. 2.5c). Such a curve is specially implemented for events having origin within 10 km by considering the relations produced by Richter (1958), Bakun & Joyner (1984), Bullen & Bolt (1985), Lahr (1989) and Di Grazia *et al.* (2001).

The analysist is assisted to obtain a robust solution by a jack-knifing approach that allows to identify the contribution of the single set constrains. All the constraints defined by the analyst (i.e. picking of first arrival and phases of the waves, epicentre, depth of hypocentre, magnitude) can be easily modified with a real-time update by the software, that aids the analyst to define the best solution for each detected event.

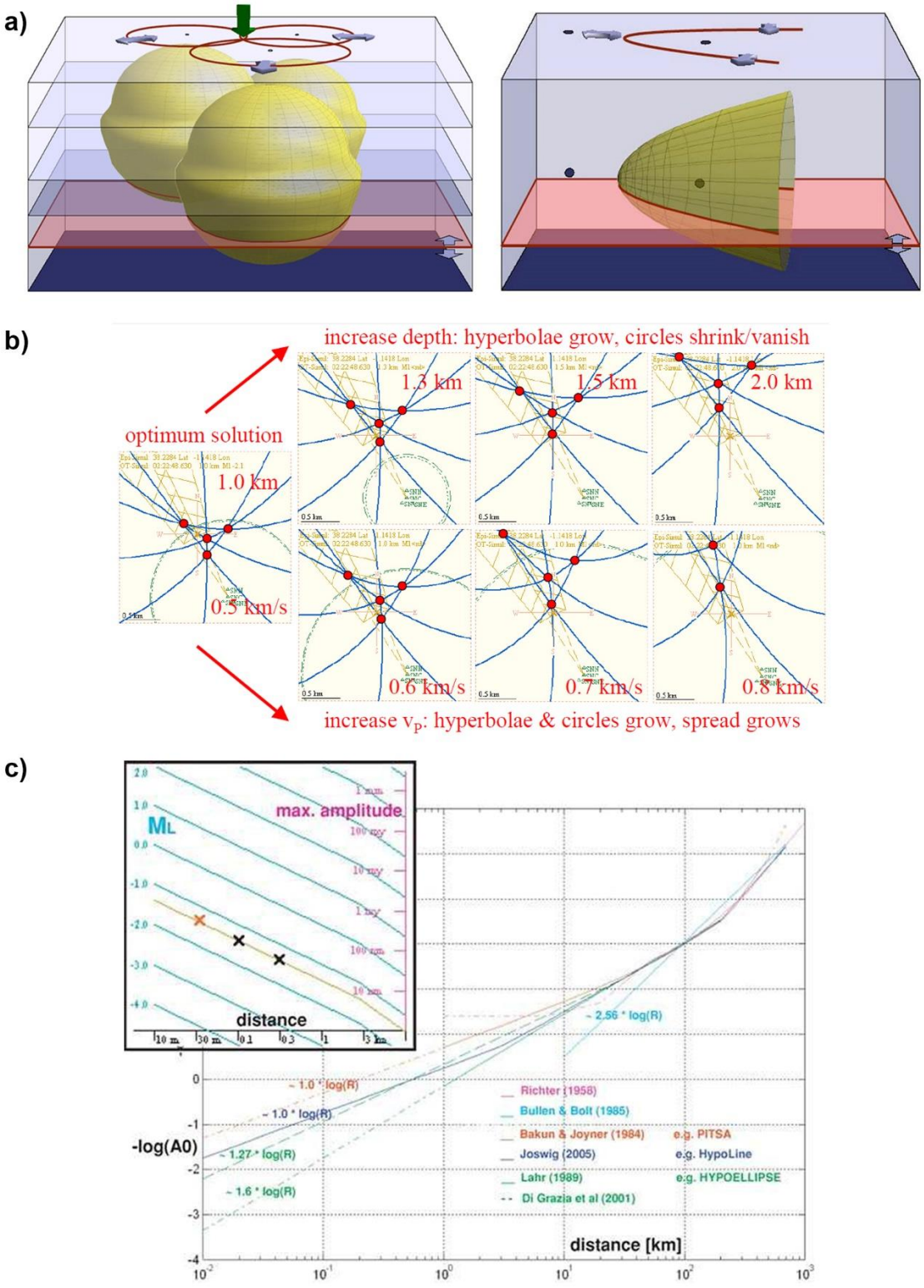

Fig. 2.5. Main principles of event location by nanoseismic monitoring: **a** circles produced by the t_S-t_P difference at each station (left) and hyperbole shaped by the t_P difference between different stations (right) (Joswig, 2008); **b** estimation of optimum depth and half space v_P by interactive parameter shifting (Joswig, 2008); **c** calibration of magnitude-distance relationship (top) and extrapolation of the M_L distance correction factor -log(*A0*) for events having origin within 10 km by different authors (bottom) (Wust-Bloch & Joswig, 2006).

Starting from the original purpose of explosion detection (Joswig, 2008), in the last ten years the reliability of nanoseismic monitoring to study vibrational events has been tested for different purpose and in various geological contexts. By considering its robust seismological bases, nanoseismic monitoring was applied in geodynamics for studying aftershocks of earthquakes (Häge & Joswig, 2009a) and for mapping active faults (Häge & Joswig, 2009b, 2009c). This technique produced results also for monitoring microseismicity induced by hydraulic stimulation of deep geothermal power plants (Häge *et al.*, 2013). The Ph.D. student already applied nanoseismic monitoring (Fiorucci *et al.*, 2016b) in the framework of his master thesis for detecting weak slope instability events induced by mining activities in the quarry district of Coreno Ausonio (Central Apennines, Italy).

Several experimental sites demonstrated the reliability of the nanoseismic monitoring technique also to detect, locate and follow the space-time distribution of vibrational events related to sinkhole development (Wust-Bloch & Joswig, 2006) or to gravity-induced instability process involved sandstone cliffs (Wust-Bloch, 2010) and soil slopes (Walter & Joswig, 2008, 2009; Walter *et al.*, 2009, 20011, 2012a, 2012b, 2013; Tonnellier *et al.*, 2013). A large catalogue of microseismic events was collected by Walter *et al.* (2009, 2012b) and Tonnellier *et al.* (2013) at the Super-Sauze landslide (French Alps), where a SNS array was installed permanently for several months. The detected microseismic events related to slope instability has been distinguished into two main group differing in duration, frequency content and waveform shape, one related to fall of rock block and another one related to landslide mass fracturing.

Currently, the Peschiera Spring Slope (Central Apennines, Italy) is the only site where nanoseismic monitoring has been applied for monitoring a landslide involved a rock slope. Fiorucci *et al.* (2017) showed the preliminary results obtained by applying this technique, confirming the detection of two different type of events related to slope instability as proposed by Walter *et al.* (2009, 2012b) and Tonnellier *et al.* (2013) for the Super-Sauze landslide. In the framework of the here-presented Ph.D. thesis, further and deeper analyses of the data acquired by the SNS array installed at the Peschiera Spring Slope were carried out and the obtained results will be presented in Paragraph 4.3.

2.3.2. Clustering of microseismic events

In their studies, Walter *et al.* (2012b) and Tonnellier *et al.* (2013) observed that sources of several microseismic events focused in specific zones of the Super-Sauze landslide, especially in the shearing zone between the unstable part of the slope and the more stable one.

The presence of rock mass zones in which microseismic events are concentrate is a well-known issue in mining engineering, also by considering the space and time control on the stress changes that can induce instability. Hudyma & Potvin (2010) produced a very extensive study by analysing the spatial distribution of the microseismic events induced by mining process in 35 deep mines of Australia and Canada. By analysing the distribution of the all detected microseismic events in each monitored mine (Fig. 2.6a), they were able to define different spatial clusters of events associated to different zones of the mine having different features (Fig. 2.6b). Then, they considered each defined cluster as a single microseismic source and compiled a frequency-magnitude curve for each source (Fig. 2.6c) according to the Gutenberg & Richter (1954) power law relation [Eq. 2.14]

$$\log_{10} N = a - bM \qquad [2.14]$$

where N is the cumulative number of events having magnitude higher than M, while a and b are constants.

The values of b for a given region with a large population of events is approximately equal to 1. The value of b can significantly vary by analysing the different sources into the region, representing a way to define the potential hazard of each source in term of probability of occurrence of events: for b values less than 1 the proportion of large events is higher than for the general population of events, therefore there is a higher probability of occurrence of events with large magnitude. Instead, for b value higher than 1 there is a comparatively lower probability to have events with large magnitude. Additionally, the M_L value obtained by the linear projection of the frequency-magnitude curve at y equal to 1 is considered a fair predictor of the magnitude of the largest expected event that can be produced by a source.

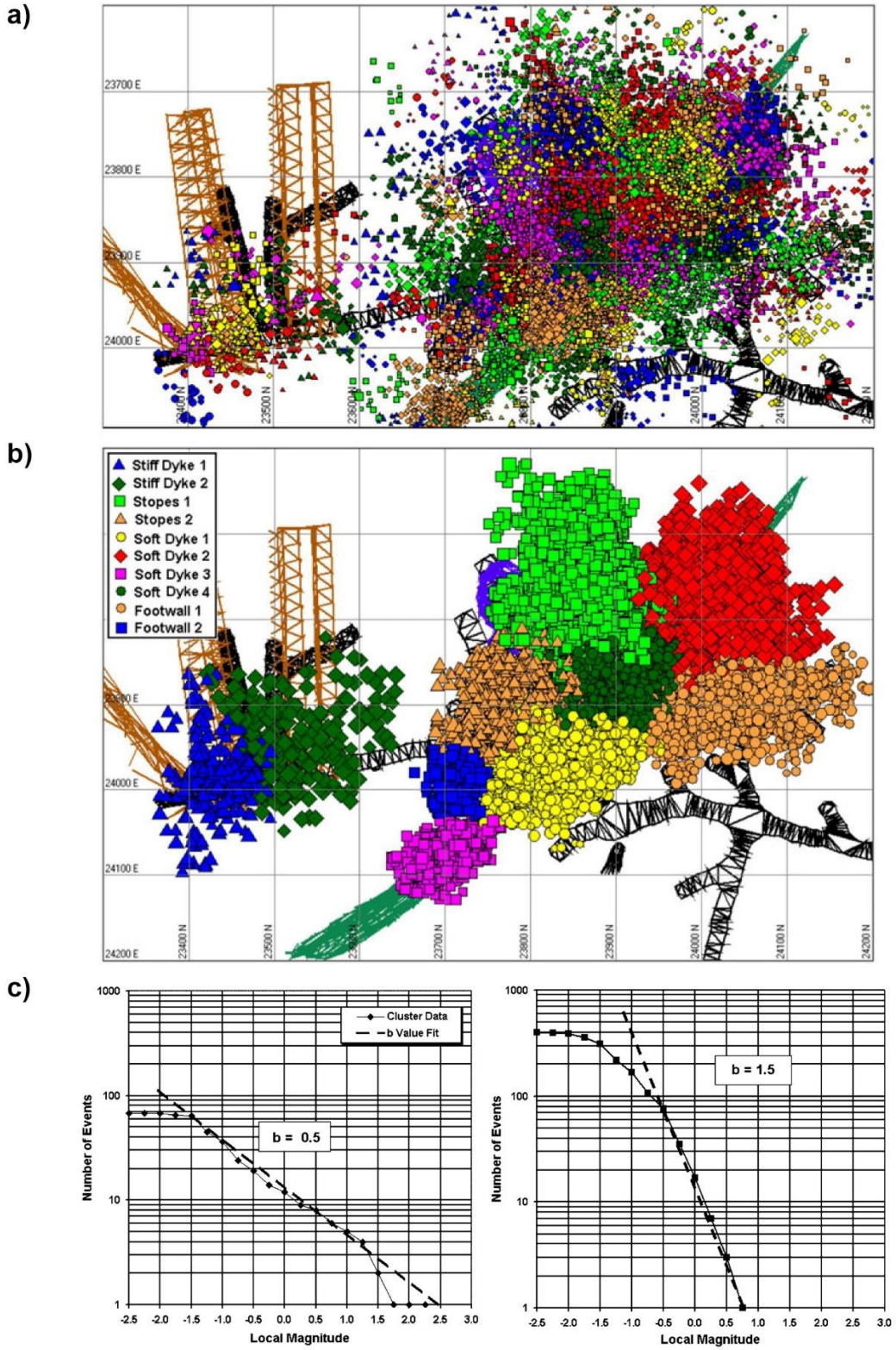

Fig. 2.6. Example of spatial clustering of microseismic events in deep mines of Australia and Canada: **a** location of the all detected events; **b** definition of spatial clusters associated to different microseismic sources; **c** compilation of frequency-magnitude curves for the different defined sources. (from Hudyma & Potvin, 2010)

3. Methodology

3.1. Experimental approach

In the here-presented Ph.D. thesis, different types of passive seismic measurements were carried out for experimenting as these techniques can be a useful support for applied geology towards the evaluation of landslide hazard as well as the management of the related risk, by integrating the traditional engineering geological surveys.

After an extensive review of geophysical methods applied to landslide investigation (Paragraph 2.1), passive seismic was selected due to its capability to be employed not only for providing a characterisation of landslide bodies as the other geophysical methods (e.g. dimensions, geometry, water content, seismic wave velocity), but also for observing variations of specific effects or parameters during time. As a matter of fact, several past applications demonstrated that passive seismic seems to be suitable for both investigating landslides and monitoring these processes, being therefore a useful tool for defining susceptibility landslide as well as hazard assessment and risk management. Between the various passive seismic methods, two different approaches were experimented in this work: i) seismic ambient noise measurements in single-station configuration (Paragraph 2.2); ii) seismic monitoring in array/network configuration (Paragraph 2.3).

For performing a complete experimentation, two case studies concerning rock masses involved in a gravity-induced instability process were selected. The choice of unstable rock masses was done because fast-moving landslides in rock slope (i.e. rockfalls, rockslides, rock avalanches, debris flows) are the most spread and the most destructive gravity-induced instability processes in Italy (Guzzetti *et al.*, 2004), therefore more efforts are require to manage such phenomena. The two different case studies were chosen by considering two different scales of the landslide process as well as two different natural environments. The first case study is the Selmun Promontory (Malta, Central Mediterranean Sea), a rock cliff slope in coastal environment involved in a lateral spreading phenomenon associated to falling of different-size rock blocks. The second case study is the Peschiera Spring Slope (Central Apennines, Italy), a rock slope in mountainous area involved in a large and complex mass movement. More details about the geological settings of the case studies and the landslide processes that interest them will be given in Paragraph 3.2.

In each case study, the application of the two types of passive seismic measurements was carried out for different purposes. On one side, seismic ambient noise measurements were carried out in single-station configuration and analysed through the HVSR technique (details in Subparagraph 2.2.1) of Nakamura (1989) and by using the WAVEPOL polarization analysis code (details in Subparagraph 2.2.2) implemented by Burjánek *et al.* (2010, 2012) for obtaining a complete seismic response characterisation of the unstable parts of the rock mass and of the stable zones of the slope. In particular, such an application of seismic ambient noise measurements was carried out to define features about the seismic response of the landslide mass related to its geological and geomorphological settings as well as to its vibrational behaviour. The final aim of the seismic ambient noise analyses was to evaluate the landslide susceptibility by defining zones having different stability level and, therefore, to produce a landslide hazard zonation. However, a reliable characterisation of the seismic response of the landslide mass can be also used in the management of landslide since it can represent a base to design a permanent seismic monitoring system based, for example, on variations of specific parameters of seismic ambient noise (Got *et al.*, 2010; Lévy *et al.*, 2010).

On the other side, seismic measurements were carried out also in array/network configuration through microseismic sensors that recorded in continuous mode in permanent or temporary installation. The seismic data were collected and analysed according to the nanoseismic monitoring technique (details in Subparagraph 2.3.1) proposed by Joswig (2008), with the aim of detecting and locating microseismic events related to the gravity-induced slope instability processes. Then, by using the clustering approach (details in Subparagraph 2.3.2) proposed by Hudyma & Potvin (2010), the spatial distribution of the microseismic events was studied for obtaining clusters of microseismic events and, subsequently, identifying the microseismic sources located into the unstable rock mass. Finally, each microseismic source was characterised by a frequency-magnitude curve, according to the Gutenberg & Richter (1954) power law relation. In summary, this second type of passive seismic measurements joints two different approaches currently applied in different contexts rather than rock mass landslides: nanoseismic monitoring, used for studying instability processes in soil slopes, and clustering of microseismic events, in use in mining engineering where its application is favoured by the knowledge in space and time of the induced stress changes. The here-

proposed method for monitoring of microseismic event is devoted to assess the landslide hazard in terms of probability of occurrence by producing a frequency-magnitude curve for each microseismic source identified within the unstable rock slope. Monitoring of microseismic events can be used also for managing the landslide risk by defining parameters that can anticipate a larger instability event, as frequency and/or cumulative energy of events occurred in a specific time interval (Lenti *et al.*, 2012).

3.2. Case studies

The methodology proposed by this work (Paragraph 3.1) was experimented in two case studies of rock masses involved in gravity-induced instability processes. As above mentioned, the two different case studies were selected for varying the scale of the landslide process and the natural environments interested by the instability, by performing a more-complete experimentation.

The Selmun case study will be presented in detail in Subparagraph 3.2.1. The Selmun Promontory represents an important touristic and cultural heritage site on the North Western coast of the island of Malta (Central Mediterranean Sea). Such a promontory is involved in a landslide process as demonstrated by the large block-size talus at its bottom and by the presence of a dense net of open fractures. Despite such an instability process threats the ruins of Għajn Ħadid Tower and the below beach, detailed studies about the Selmun Promontory landslide were not carried out. Therefore, in this Ph.D. thesis an extensive characterisation of the geological and geomorphological settings as well as several engineering geological surveys were carried out in the area before installing the geophysical instrumentation. Then, the seismic data acquisition was carried in the two configurations by temporary installation of sensors and dataloggers provided by Research Centre for Geological Risks (CERI) of Sapienza University of Rome; instruments of Department of Geosciences of University of Malta were also used for few measurements.

The Peschiera case study will be described in Subparagraph 3.2.2. The Peschiera Spring Slope is a rock slope in Central Apennines (Italy). This slope has been studied since the beginning of 2000s by researchers of Department of Earth Sciences of Sapienza University of Rome, in the framework of an agreement between ACEA-ATO2 S.p.A. and Research Centre for Geological Risks (CERI) of Sapienza for monitoring the landslide

process due to the presence of an important drainage plant within the slope. The advanced studies carried out in these years produced a detailed characterisation of the gravity-induced instability process and led to install a permanent system, property of ACEA-ATO2 S.p.A, for monitoring the landslide process. Such a monitoring system was integrated with a permanent SNS array in 2014, therefore this case study was select by considering the deep knowledge of the landslide process as well as the availability of continuous seismic data recorded through the nanoseismic monitoring approach.

3.2.1. Selmun case study

The Maltese Archipelago is composed of three main islands (Malta, Gozo and Comino) located in the middle of the Mediterranean Sea, about 100 km South from Sicily and 290 km East from Tunisia. The islands represent the only currently emergent part of an extensive shallow-water shelf that extends from Eastern Sicily to the Malta Graben, an important part of the threshold separating the Western and Eastern Mediterranean basins (Pedley *et al.*, 2011). Limestones and clays of Oligocene and Miocene epochs form the Maltese islands. The sequence of the sedimentary rocks of the Maltese Archipelago is composed of five main geological formations (Hyde, 1955; Pedley *et al.*, 1976, 1978, 2002; Gigli *et al.*, 2012), from the oldest (Fig. 3.1):

- Lower Coralline Limestone Formation (LCL), a hard and compact grey limestone of Oligocene age (Chattian), having thickness of about 140 m;

- Globigerina Limestone Formation (GL), a soft yellowish fine-grained limestone of Lower Miocene age (Aquitanian-Langhian) with a thickness from 20 m up to 200 m;

- Blue Clay Formation (BC), a very soft pelagic blue or greenish grey marl and limey clay of Middle Miocene age (Serravallian) with a thickness varying approximately between 20 m and 75 m;

- Greensand Formation (GS), massive, friable brown to dark green glauconite and gypsum grain-rich bioclastic limestone of Upper Miocene (Tortonian), having thickness less than 1 m in Malta and up to 10 m in central sector of Gozo;

- Upper Coralline Limestone Formation (UCL), pale grey and orange fossiliferous coarse-grained limestone, up to 160 m thick, of Upper Miocene in age (Tortonian-Messinian), composed of four different members.

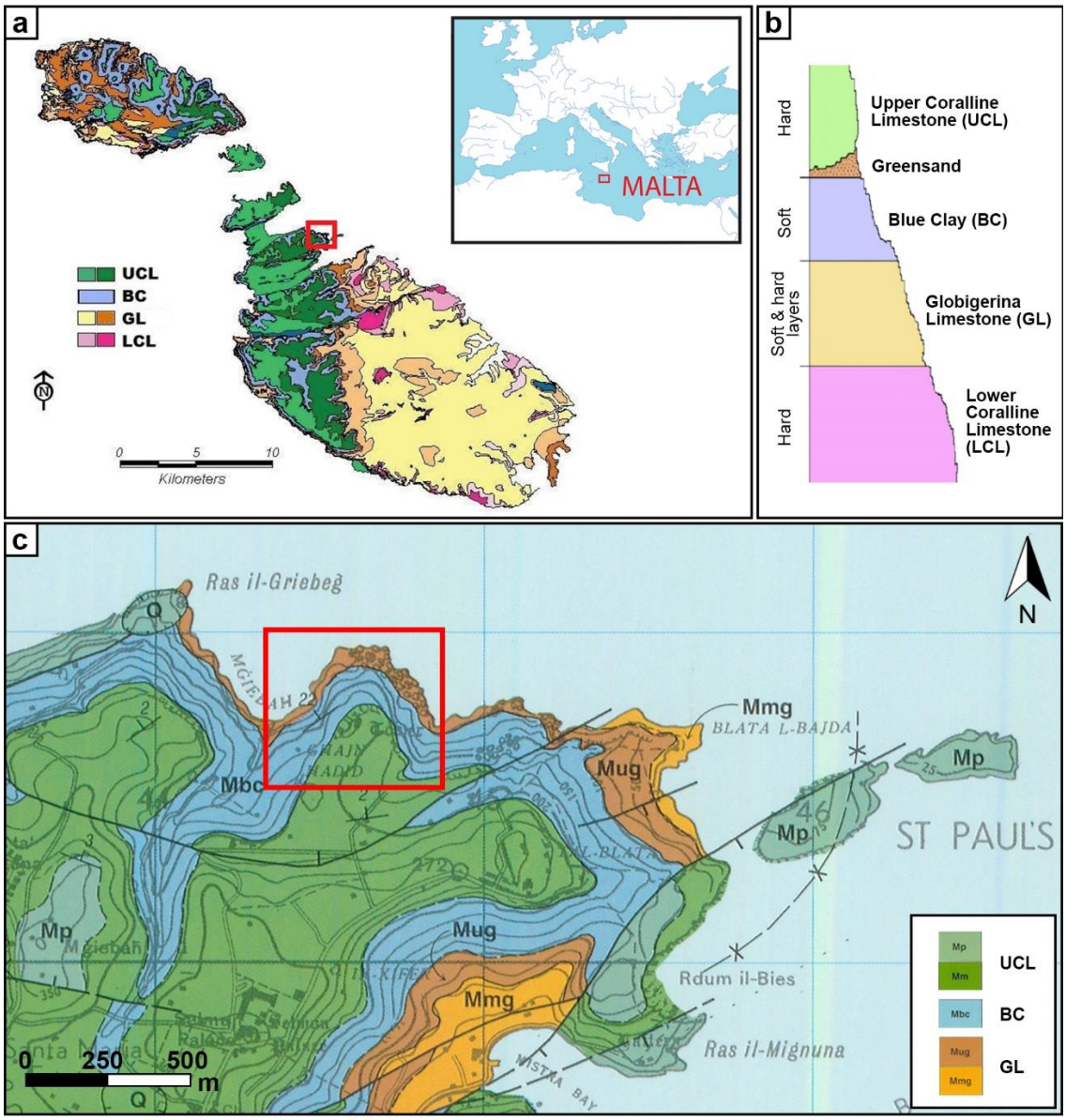

Fig. 3.1. Geology of the Maltese Archipelago: **a** geological map, position of the Maltese islands in the Mediterranean Sea and location of the Selmun area (in the red frame); **b** sketch of the sedimentary sequence; **c** excerpt of the Oil Exploration Directorate (1993) geological map in Selmun and St Paul's Bay areas and location of the Selmun Promontory (in the red frame).

Based on the geological setting, the island of Malta can be easily divided in two main sectors (Fig. 3.1a): the South Eastern part of Malta where only the two oldest formations outcrop, shaping relatively flat landscapes, and the North Western part of the island, where the full sedimentary sequence is generally conserved and the UCL and the BC mainly outcrop. Due to the outcropping geological formations, unstable cliff slopes cut in a summit UCL plateau overtopping gentle slopes of the BC (between 30° and 45°)

are the typical landscapes of the North Western part of Malta (Gigli *et al.*, 2012; Mantovani *et al.*, 2013; Galea *et al.*, 2014).

The Selmun Promontory, located on the North-facing coast of the North Western sector of Malta, is involved in a significant landslide process, as evidenced by the large block-size talus and the dense joint net on the rock plateau surface (Fig. 3.2). In particular, its geological succession, characterised by the overposition of stiff rocks on a plastic deposit (i.e. the stiff UCL on the plastic BC), leads to a lateral spreading phenomenon (Goudie, 2004): the horizontal deformation affecting the clayey materials, having visco-plastic behaviour, induces fracturing of the overlying stiff rock. Lateral spreading shapes a plateau of stiff rock bordered by jointed unstable cliffs, favouring the detachment of single rock blocks by typical gravity-induced instability mechanisms, i.e. planar sliding, wedge sliding, toppling and falling (Hoek & Bray, 1981). The resulting landslide process should be defined as a complex type according to Varnes (1978) and Hutchinson (1988).

During 2015 and 2016, field surveys and analysis of satellite image were carried out to better characterise the geological features of the Selmun Promontory. The stratigraphic succession of the Selmun Promontory (Figs 3.1c and 3.2a) is composed of 20-30 m of the UCL, 30 m of the BC and the GL at the base. All the formations show sub-horizontal or slightly NE-dipping (< 5°) strata. On the gentle slope, both the BC and the GL rarely outcrop because they are generally covered by a significant slope debris deposit resulting from the cliff slope evolution that has occurred until now. The observed slope debris is composed of UCL clasts having heterogeneous sizes (from centimetre-scale clasts up to metre-size blocks) embedded in weathered BC and residual material of limestone dissolution. The slope debris deposits reach several meters of thickness, especially in the part close to the UCL cliff wall where the largest-size rock blocks are located.

By considering its morphology, the Selmun Promontory can be schematised as suggested by Martino & Mazzanti (2014) for coastal slopes as the final stage of sea cliff evolution (Fig. 3.3), where the cliff is no more directly affected by sea erosion (except during exceptional storm events) but retreats primarily by gravity-induced instability processes. At this stage, a beach separates the old sea cliff from the current shoreline.

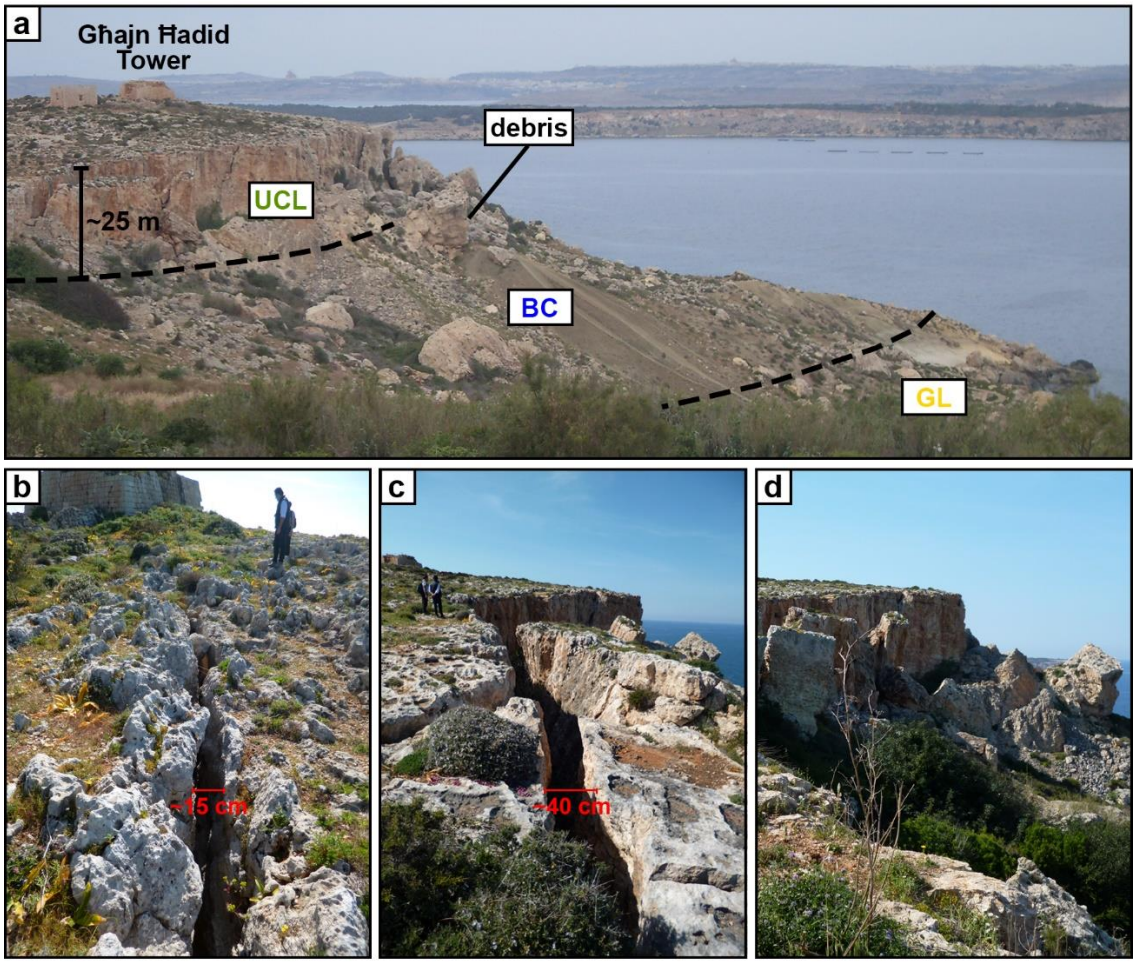

Fig. 3.2. Geological and geomorphological setting of the Selmun Promontory: **a** photograph showing the UCL cliff slope, the UCL-BC and BC-GL stratigraphic geological contacts and the debris covering the BC slope; **b c d** photographs showing the evolution in time of the landslide process, from the development of fractures in the UCL plateau (left) to the detachment of UCL rock blocks (right).

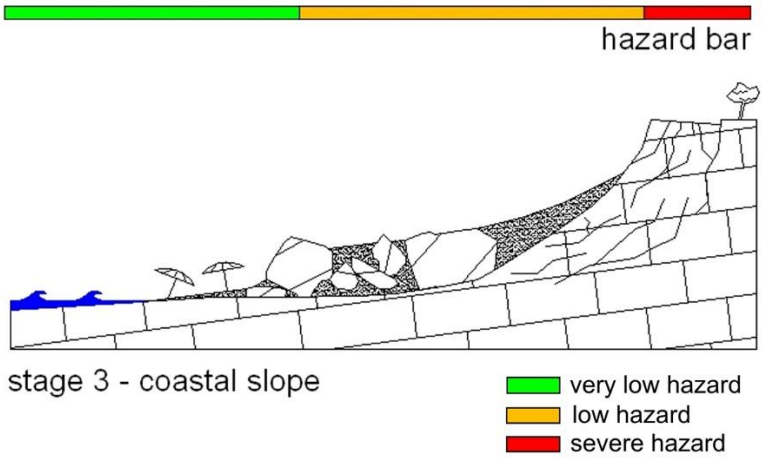

Fig. 3.3. Conceptual model of a cliff slope (last stage of a sea cliff evolution) and the related hazard levels. (from Martino & Mazzanti, 2014)

Detailed engineering geological field surveys were carried out to define geomechanical properties of the jointed rock mass composing the cliff slope of the Selmun Promontory (Iannucci *et al.*, 2017). First of all, the joints recognised in the rock mass (on the plateau surface as well as on the cliff wall) were mapped and plotted on a satellite view by combining information derived by a GPS device and field observations, such as direction and length of joint segments (with a decimetre resolution). Then, according to the ISRM standard (ISRM, 1978), each joint was characterised by defining: attitude (dip direction and dip), spacing, persistence, opening, filling, water flow, JCS coefficient (Joint surface Compressive Strength, indicating the joint wall compressive strength and derived using the Schmidt hammer) and JRC coefficient (Joint surface Roughness, indicating the joint wall roughness and obtained by the Barton comb). A GIS geo-database was implemented to inventory all the collected field data. Two main systems of sub-vertical joints were defined at the Selmun Promontory: J1 prevalent in the NW zone (mean dip direction 330°, strike 60°) and J2 prevalent in the SE one (mean dip direction 45°, strike 135°). The two joint systems have a dip direction approximately orthogonal to the plateau edge direction and, therefore, a strike similar to it (Fig. 3.4).

To characterise the rock mass matrix, 18 cubic samples of the UCL were analysed through laboratory tests performed in the Laboratory of Engineering Geology of the Department of Earth Science at Sapienza University of Rome. An average value of 26.37 kN/m^3 for the specific gravity of soil solids (γ_s) was obtained using the water pycnometer method (ASTM, 2006). A density (ρ) value of 2146 kg/m^3, equal to a natural specific gravity (γ_n) value of 21.05 kN/m^3, was obtained by using the hydrostatic weighing method (ISRM, 1979). The point load test (ASTM, 2008) estimated a uniaxial compressive strength (σ_c) in the range 63.0-79.8 MPa. Based on the sclerometer measurements (Schmidt hammer test) and on the γ_n value, an average JCS of 41.0 MPa was estimated for the analysed joints according to the correlation proposed by Barton & Choubey (1977). By considering only the rock matrix geomechanical features, UCL can be assumed as rock with medium strength according to the Deere & Miller (1966) classification for intact rock. In the edge zones, since the presence of the persistent and dense joint net composed of joints having high degree and medium roughness, the rock mass has to be considered as part of a weaker rock category (Sitharam *et al.*, 2001; Ramamurthy, 2004).

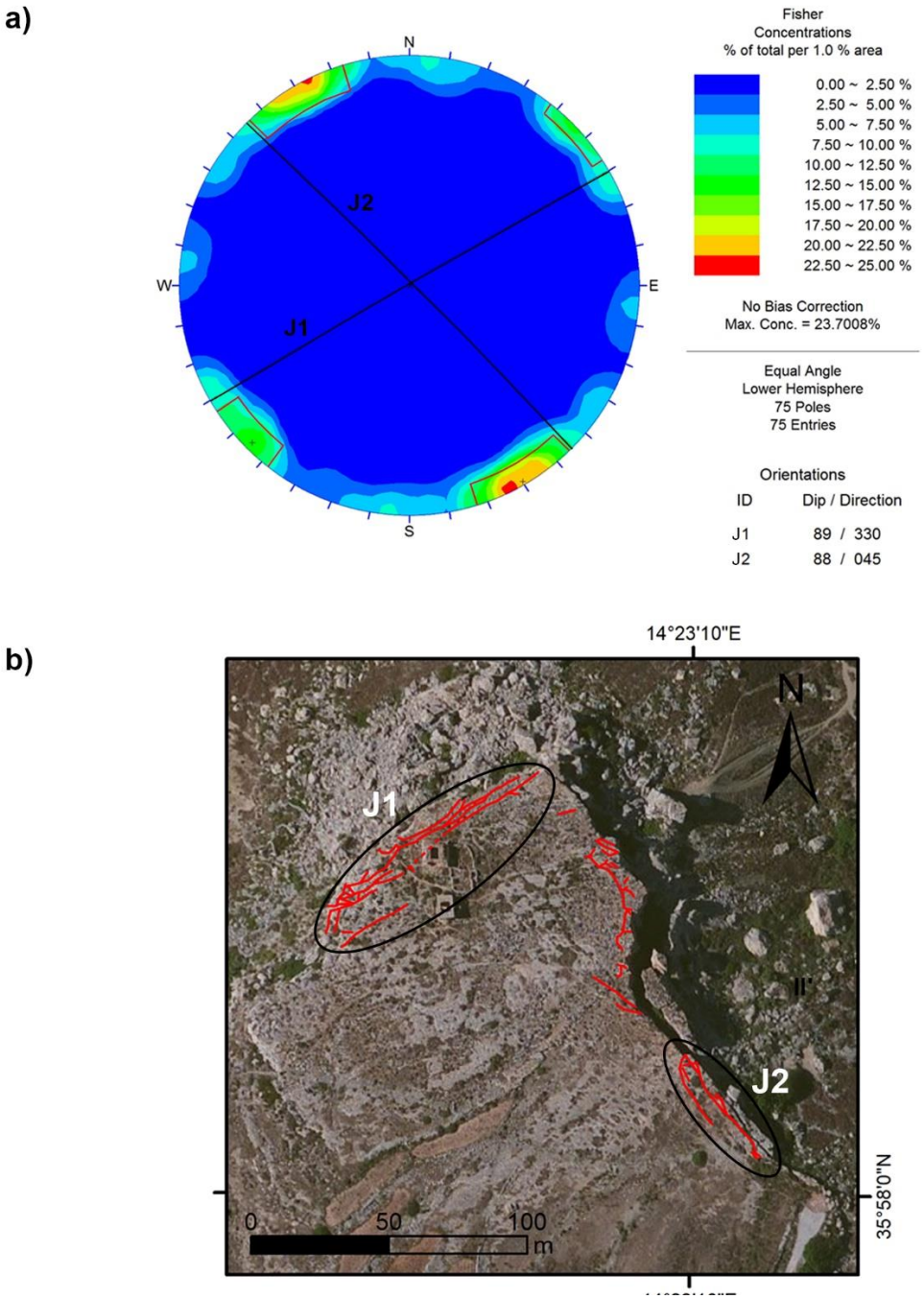

Fig. 3.4. Joint survey results on the Selmun Promontory: **a** stereographic projection (equal-angle lower-hemisphere) of joint poles surveyed, grouped forming two main systems (J1 and J2) whose mean planes are projected; **b** satellite view showing the location of the two main joint systems.

Rock mass joints						
ID system	**Dip direction and dip (°)**	**Opening (cm)**	**Vertical offset (cm)**	**Hydraulic conditions**	**JCS (MPa)**	**JRC**
J1	330/89	0-105 average 22	0-40 average 12	No flow	41.0	8-10
J2	45/88	0-70 average 16	0-30 average 16	No flow	41.0	8-10

Rock mass matrix		
Natural specific gravity γ_n (kN/m^3)	**Specific gravity of soil solid γ_s (kN/m^3)**	**Uniaxial Compressive Strength σ_c (MPa)**
21.05	26.37	63.0-79.8

Tab. 3.1. Summary of the main geomechanical properties of the rock mass (UCL) compiled through field activities and laboratory tests.

An engineering geological model of the Selmun Promontory was derived by combining all the collected geological and geomechanical data and by mapping the spatial distribution of the joint net (Fig. 3.5); from this model, two orthogonal cross-sections of the Selmun Promontory were obtained (Fig. 3.6).

Based on the engineering geological features, five zones were defined in the studied area (Fig. 3.5): one zone located in the inland plateau (A), characterised by the absence of ground fractures and unstable blocks; three zones located at the edge of the plateau (B, C and D), where a high density of ground fractures and unstable blocks exists; one zone located on the gentle slope (E), where the BC outcrops even if mainly covered by slope debris.

Such an engineering geological zonation, strongly focused on the characterisation of the instability process involving the Selmun Promontory, was then used for planning the passive seismic measurements. As a matter of fact, whereas on one hand the detailed spatial definition of the fracture net was employed for fixing the location of the single-station seismic noise measurements, on the other hand the knowledges acquired about the landslide phenomenon were used for defining the position in which to install the SNS array. A detailed description of acquisition and elaboration phases of seismic data will be given in Paragraph 3.3.

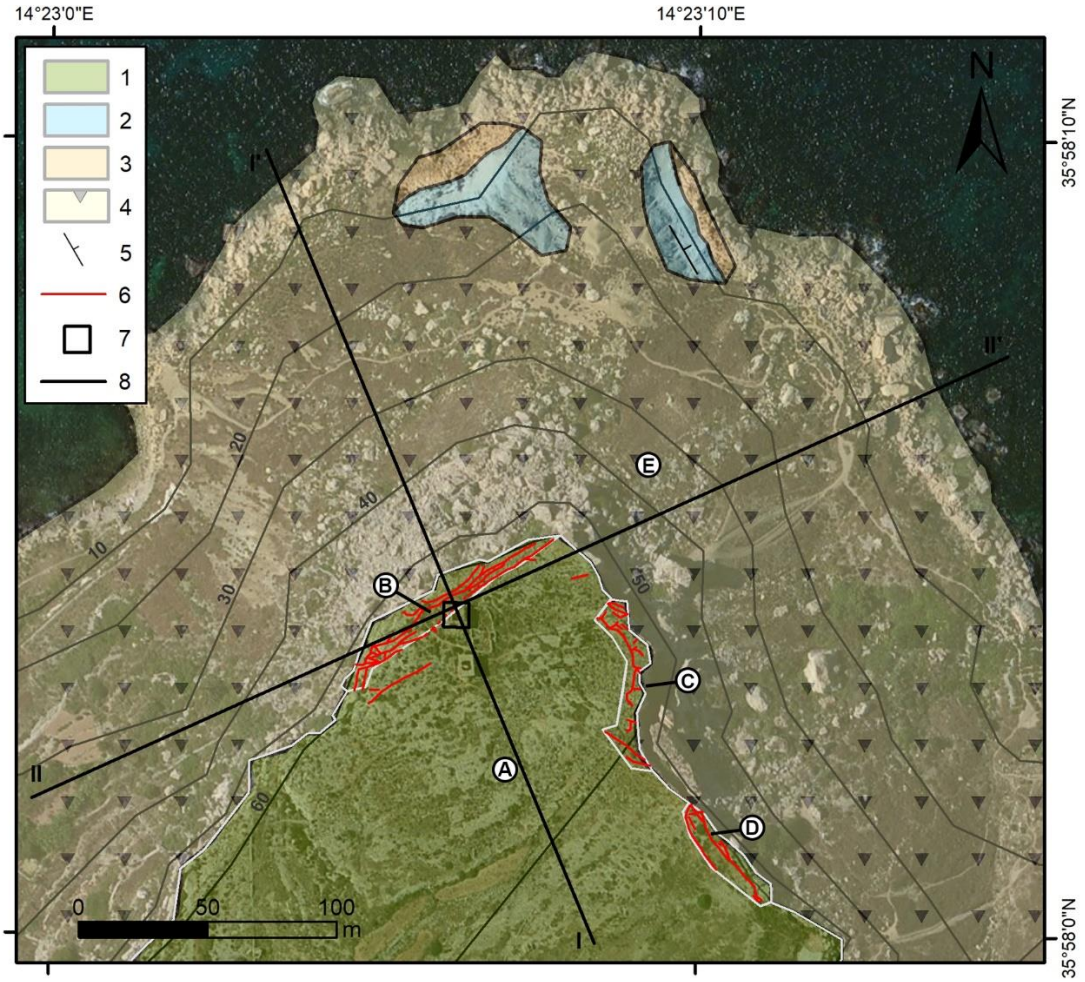

Fig. 3.5. Satellite view of the Selmun Promontory showing the geological setting: 1) UCL; 2) BC; 3) GL; 4) debris slope deposit; 5) attitude of strata; 6) fracture (the dashed line represents an inferred fracture); 7) Għajn Ħadid Tower; 8) cross-sections (see Fig. 3.6). Elevation is given by contour lines (m a.s.l.). The light grey lines indicate the different zones of Selmun (A-E).

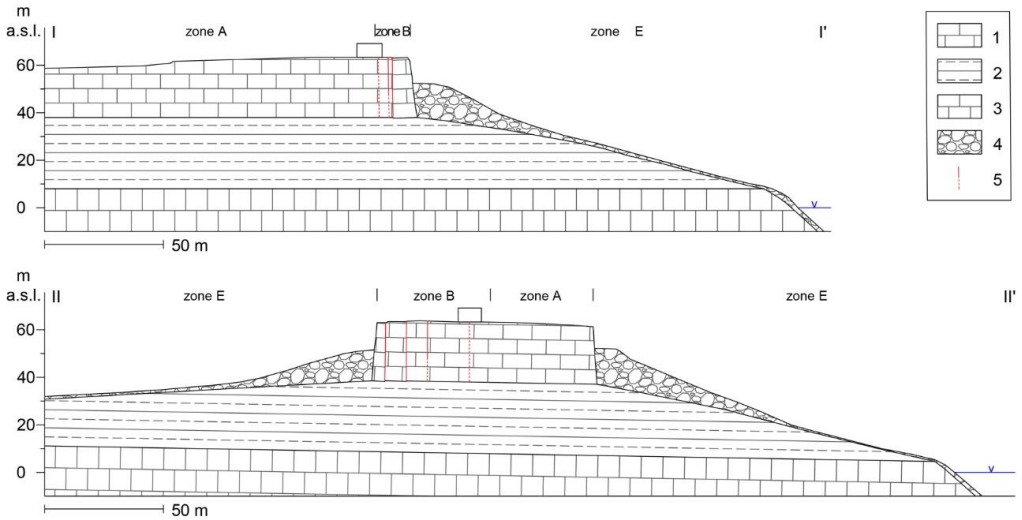

Fig. 3.6. Cross-sections (see Fig. 3.5) of the Selmun Promontory: 1) UCL; 2) BC; 3) GL; 4) debris slope deposit; 5) fracture (the dashed line represents an inferred fracture).

3.2.2. Peschiera case study

The Peschiera Springs Slope is located in Central Apennines (Italy), about 70 km North East from Rome. Such a slope corresponds to the South Western flank of Mt. Nuria and is composed of Malm-Lower Cretaceous limestones (Ciotoli *et al.*, 2001; Bigi & Costa Pisani, 2002). The structural setting of the slope is monoclinic, with EW-trending and N-dipping (30°-40°) strata; many faults cross the slope with roughly NS and N35E trends (Fig. 3.7). The slope hosts a major karst aquifer recharges by the drainage system of the Nuria-Velino-Western Fucino and Western Marsica Mountains (total drained area: 1016 km^2), whose Peschiera-Canetra Springs are the main discharge with a measured total water flow from 18 up to 21 m^3/s (Boni *et al.*, 1986, 1995). Since this large water availability, inside the slope is present the main drainage plant of Rome aqueducts.

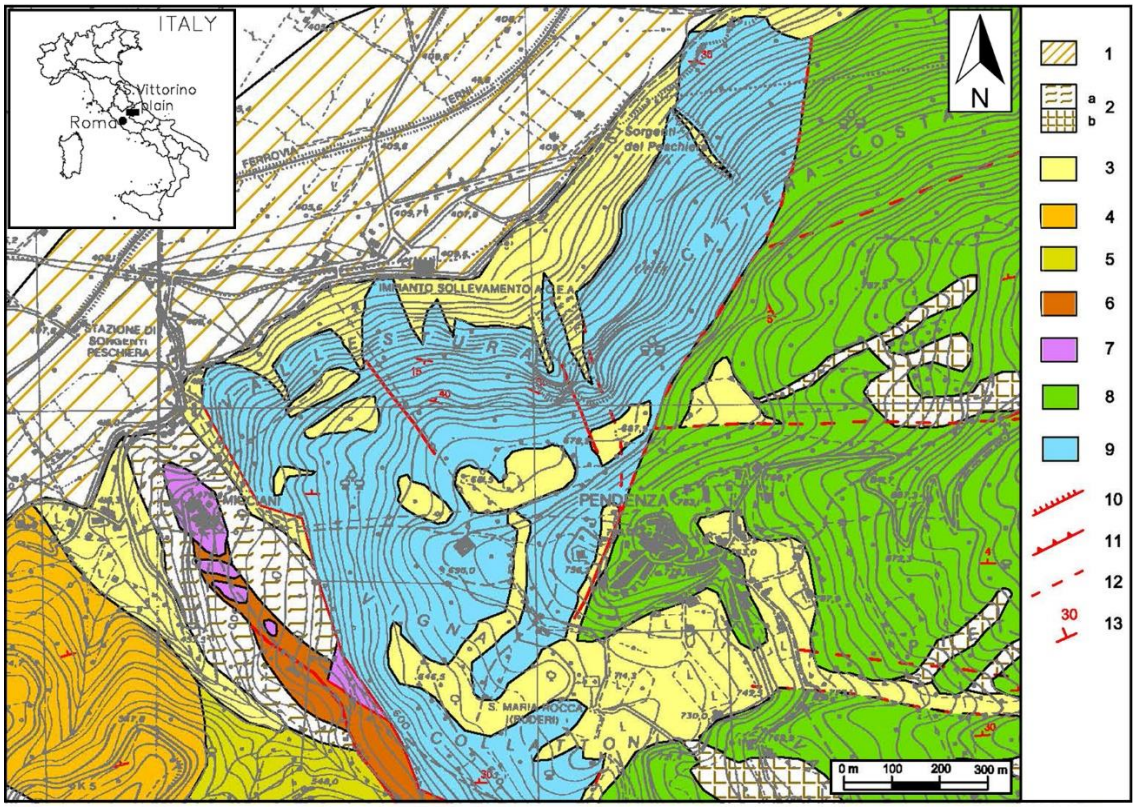

Fig. 3.7. Geological map of the Peschiera Springs slope: 1) recent alluvial deposits (Holocene); 2) eluvio-colluvial deposits (Holocene): a) silty clays and clayey silts, b) reddish soils; 3) slope debris (Upper Pleistocene-Holocene); 4) Fosso Canalicchio Formation (Upper Pliocene-Lower Pleistocene); 5) Sandy-Clayey Flysch (Upper Miocene); 6) marly limestone, marl and calcarenite (Lower Miocene); 7) Scaglia Formation (Upper Cretaceous-Lower Miocene); 8) Salpingoporella and Birdseyes limestone (Lower Cretaceous); 9) Coral and Echinoids limestone (Upper Jurassic); 10) fault; 11) thrust; 12) supposed fault; 13) attitude of strata. (from Fiorucci *et al.*, 2017)

Geomorphological surveys performed on the slope as well as a digital high-resolution (2 m) elevation model (DEM), derived by a Light Detection And Ranging (LIDAR) radar remote survey, were able to identify numerous landforms, e.g. scarps, trenches, sinkholes and tension cracks (Lenti *et al.*, 2012), indicative of slow, intense and pervasive deformations which affect the entire slope. Such deformations are caused by specific portions of the slope involved in landslide processes at different evolutionary stages, as proved by already published result from a stress-strain monitoring system installed within the drainage plant (Martino *et al.*, 2004; Maffei *et al.*, 2005).

In particular, three sectors of the slope with ongoing gravity-induced processes can be recognised: (I) a wide sector, including the Southern portion of the slope and its top, with evidences of incipient and low deformations, representing the early evolutionary stage; (II) a Western sector with evidences of mature and not yet advanced gravity-induced deformations, only concentrated close to the main trenches or scarps; (III) an Eastern sector, with evidences of advanced gravity-induced slope deformations, characterised by pronounced landforms, as scarps, trenches and sinkholes. Based on a frontal 3D view of the slope (Fig. 3.8), the rock mass spreading can be clearly observed in the Western portion of the slope, where it is associated with multiple transverse trenches (i.e. continuous transverse scarps combined with longitudinal trenches) that generate a radial displacement field. In the Eastern sector, an already-occurred rock mass landslide can be observed by the DEM; this event produced two debris fans clearly visible at the bottom of the slope. By the lateral 3D view of the DEM, the convex shape portion of slope involved in the ongoing rock spreading process is observable, while a concave shape is present in the scar area of the already occurred landslide.

The geological evolutionary model of the Peschiera Springs Slope reflects a complex deep-seated gravitational deformation, which initiated as a "sackung" phenomenon (Zischinsky, 1969; Savage & Varnes, 1987) and evolved from rock mass spreading (Hutchinson, 1988) to rock block mass deformation (Martino *et al.*, 2004). The spreading is associated with the collapse of underground caves due to major karst dissolution within relieved rock mass portions, corresponding to sub-vertical belts (Maffei *et al.*, 2005; Casini *et al.*, 2006). These collapses produced a loss of volume and induced depressions and sinkholes on the surface slope. Such a process dislodged rock blocks and increased the jointing of the rock mass. Furthermore, the collapse of

underground caves may be triggered by external stresses e.g. earthquakes (Maffei *et al.*, 2005). Teleseismic events may interact with the dislodged blocks causing a temporary increase in the strain rate that induces displacements along joints up to 2 mm within 24 h (Lenti *et al.*, 2015).

The ongoing deformational process that involves the Peschiera Springs slope also resulted from instrumental measurements performed through a geotechnical stress-strain monitoring system (average steady strain rate of 1 mm/y) as well as by a traditional accelerometric network installed inside the tunnels of the plant since 2008 (Lenti *et al.*, 2012, 2015). For managing the geological risk of the drainage plant, an alarm system based on both frequency of occurrence and cumulative energy of microseismic events was defined and tested (Lenti *et al.*, 2012; Fiorucci *et al.*, 2015). Additionally, in 2014 a SNS array was permanently installed within the plant. Fiorucci *et al.* (2017) reported and discussed the first outputs of this monitoring system, while the advanced results will be presented in this Ph.D. thesis (Paragraph 4.2). More details about acquisition and processing of seismic data will be given in the next section (Paragraph 3.3).

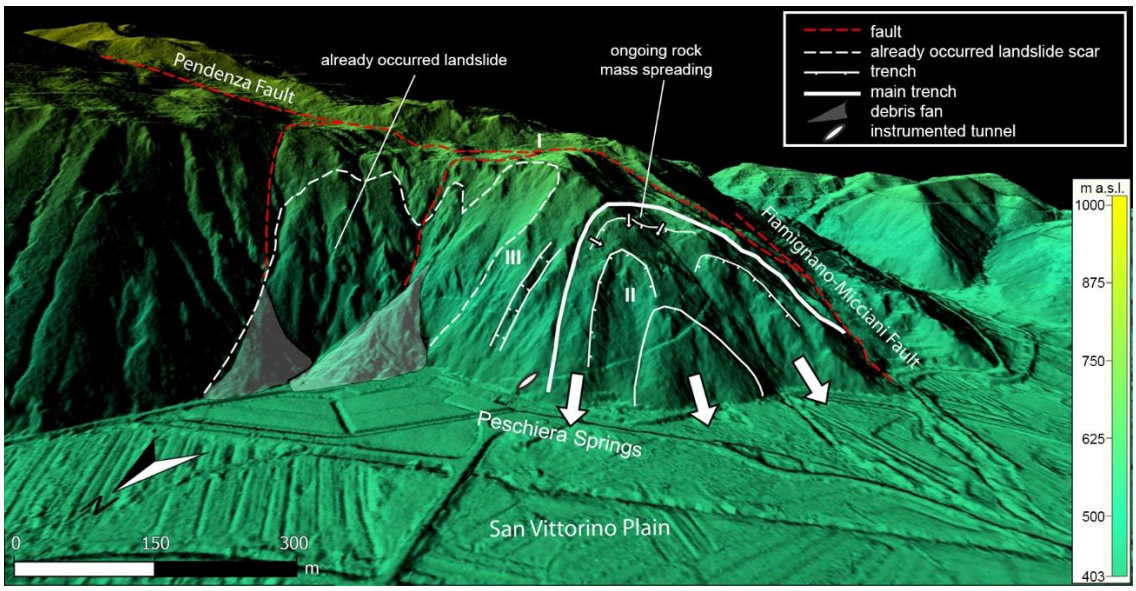

Fig. 3.8. 3D view of the Peschiera Springs Slope obtained from the 2-m-resolution DEM, showing the rock mass involved in the ongoing landslide processes and the main related landforms. Slope sectors (I, II and III) at different evolutionary stages are also shown. The slope shapes reveal a convexity in the Western sector, currently involved in rock spreading process, and a concavity in the Eastern sector where a general collapse already occurred. Arrows indicate the northward direction of the rock mass movement. (from Fiorucci *et al.*, 2017)

3.3. Seismic data acquisition and elaboration

As explained in detail in Paragraph 3.1, the experimental methodology proposed by this Ph.D. thesis makes use of two different types of passive seismic approaches with different aims: i) single-station measurements of seismic ambient noise; ii) monitoring of microseismic events recorded by array/network of sensors. The present section is focused about the description of the seismic data acquisition and on their processing.

For the Selmun case study, the seismic data were acquired through temporary installations of the available instruments, by varying the two configurations. As the others field activities described in Subparagraph 3.2.1, the Ph.D. student carried out the geophysical measurements during two different periods that he spent on Malta as visiting Ph.D. student at Department of Geosciences of University of Malta, i.e. September-November 2015 and September-October 2016.

At the Peschiera site, two seismic monitoring systems are permanently installed for studying the occurrence of microseismic events: a standard accelerometric network and a SNS array for the nanoseismic monitoring approach. Therefore, the Ph.D. student did only occasional daily transfers to the site.

3.3.1. Single-station measurements of seismic ambient noise

For the Selmun case study, single-station seismic ambient noise measurements were carried out in 116 sites over an area of approximately 0.1 km^2 during the 2015-2016 field activities. As evidenced by Figure 3.9 and Table 3.2, most of the noise measurement stations were distributed to cover the unstable zones of the cliff slope (zones B, C and D) as well as the stable UCL plateau (zone A), while a few measurements were carried out on the BC gentle slope (zone E). A 3-component seismometer was deployed at each station: 84 measurements were carried out using a LE-3D/5s seismometer by Lennartz Electronic GmbH coupled with a REF TEK 130-01 datalogger (property of CERI), set to a sampling frequency of 250 Hz (Fig. 3.10a); 32 measurements were carried out using a Tromino (www.tromino.eu) 3-component portable seismometer (property of University of Malta), set to a 128 Hz or 256 Hz sampling frequency (Fig. 3.10b). In both cases, the seismic ambient noise was recorded for 1 hour. In addition, 4 long seismic ambient noise measurements were carried out (SEL101, SEL102, SEL103 and SEL104).

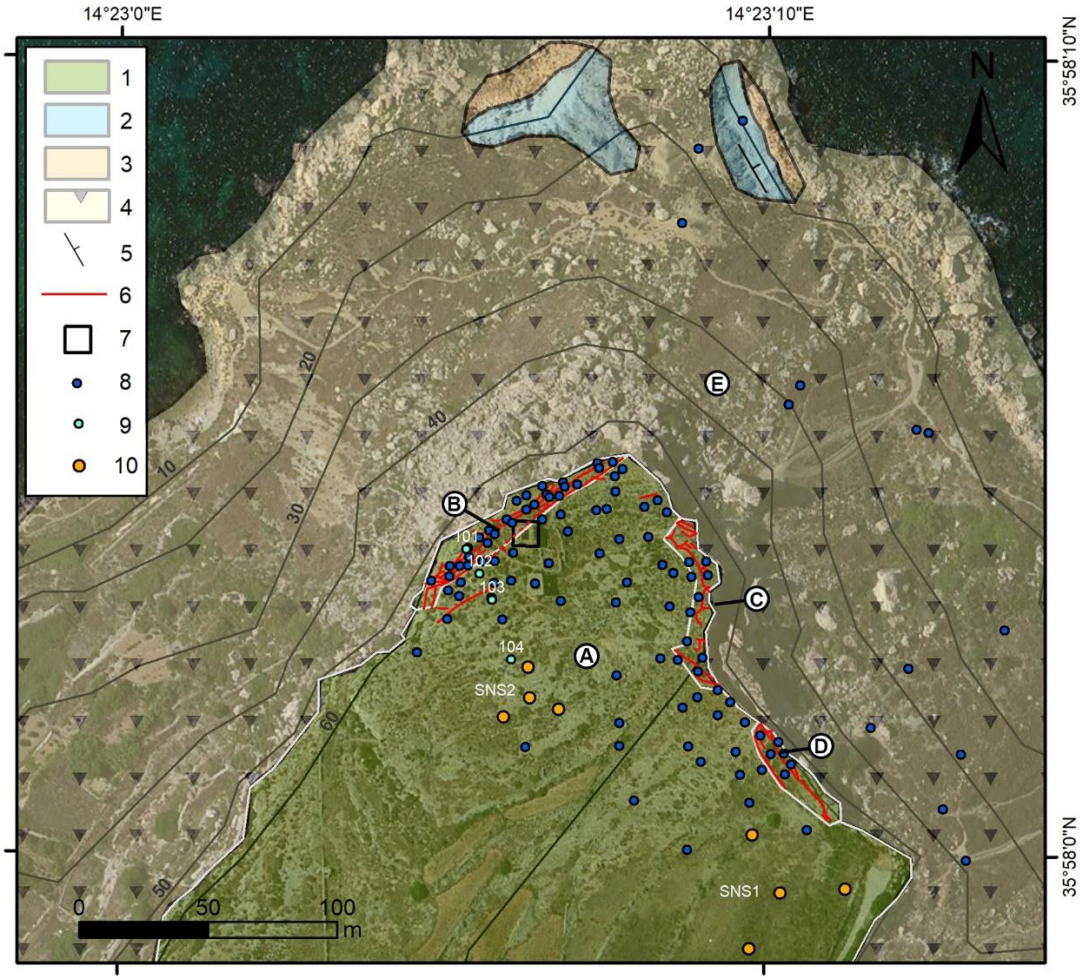

Fig. 3.9. Satellite view of the Selmun Promontory showing: 1) UCL; 2) BC; 3) GL; 4) debris slope deposit; 5) attitude of strata; 6) fracture; 7) Għajn Ħadid Tower; 8) 1-h seismic noise station; 9) long seismic noise station (with ID); 10) SNS array station. Elevation is given by contour lines (m a.s.l.). The light grey lines indicate the different zones of Selmun (A-E).

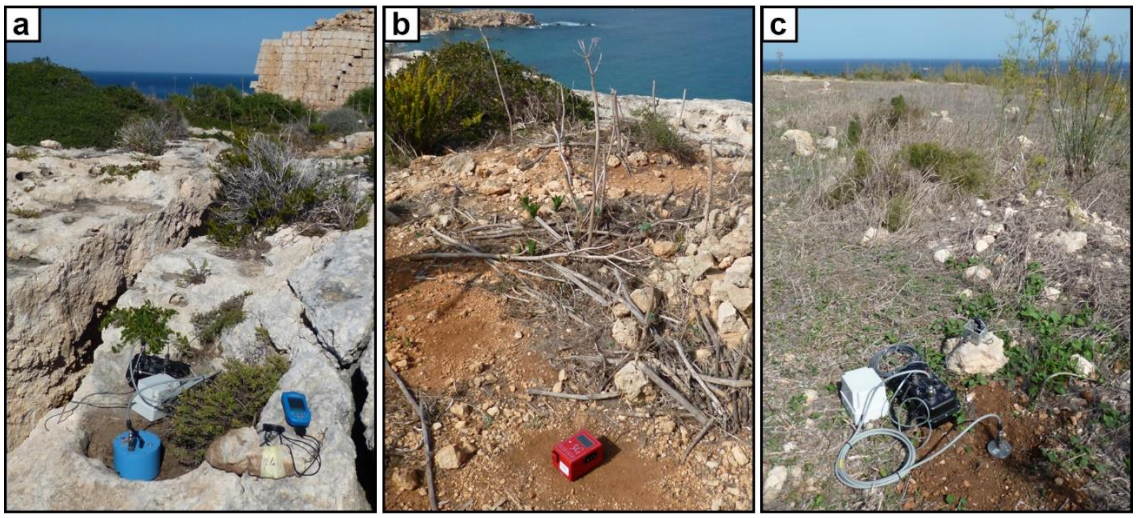

Fig. 3.10. Seismic data acquisition: **a** seismic noise station (Lennartz LE-3D/5s); **b** seismic noise station (Tromino); **c** SNS array station (Lennartz LE-3Dlite MkII).

ID zone	Area (m^2)	Measurements (n)	Measurement density (n/m^2)
A	27000	35	0.0013
B	1000	50	0.05
C	600	10	0.017
D	450	6	0.014
E	100000	15	0.00015

Tab. 3.2. Summary of the ambient noise measurements carried out in the several zones over the Selmun area (see Fig. 3.9).

At the Peschiera site, 8 single-station seismic ambient noise measurements were carried out on the slope in September 2013 (Fig. 3.11). Such geophysical surveys were aimed to study the seismic response on the slope to install several additional surface stations for integrating the pre-existent underground accelerometric network; more information about the application and the results obtained by this network will be given in the next section (Subparagraph 3.3.2). As for the Selmun case study, the seismic ambient noise measurements were carried out by deploying 3-component LE-3D/5s seismometers (period 5 s, flat transfer function 0.2-60 Hz, sensitivity 800 V/m/s) by Lennartz Electronic GmbH coupled with REFTEK 130-01 dataloggers, property of Research Centre for Geological Risks (CERI) of Sapienza University of Rome (Fig. 3.12a). The seismic ambient noise was recorded for 1 hour with a sampling frequency of 250 Hz.

By considering the past seismic ambient noise record availability, well distributed according to the distinguished sectors of the Peschiera landslide, and the difficulties to reach other zones of the slope due its steep sharp and its dense vegetation cover, the analysis of such measurements was considered enough for characterising preliminarily the seismic response of the slope.

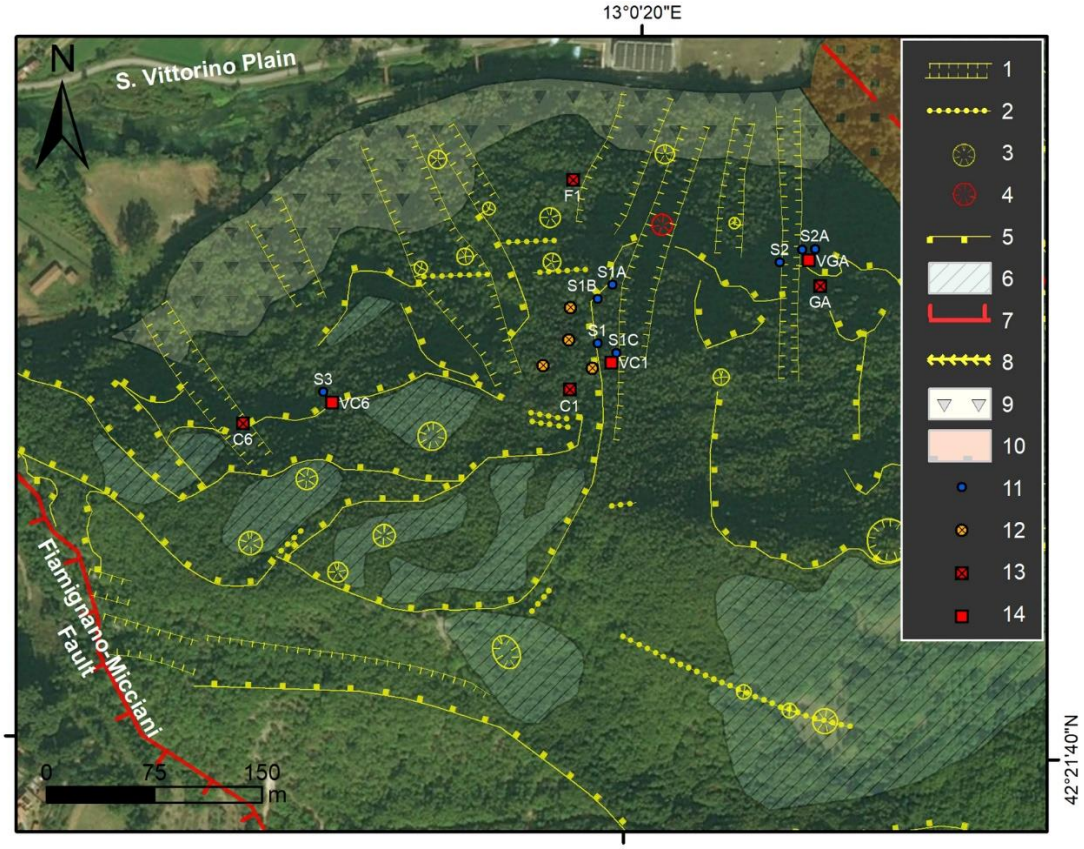

Fig. 3.11. Satellite view of the Peschiera Springs Slope showing: 1) trench; 2) tension crack; 3) sinkhole; 4) 1997 collapse of sinkhole; 5) scarp; 6) karstified flat; 7) fault; 8) gully; 9) slope debris; 10) debris fan deposit; 11) surface 1-h seismic noise station (with ID); 12) underground SNS array station; 13) underground and 14) surface accelerometric network station (with ID).

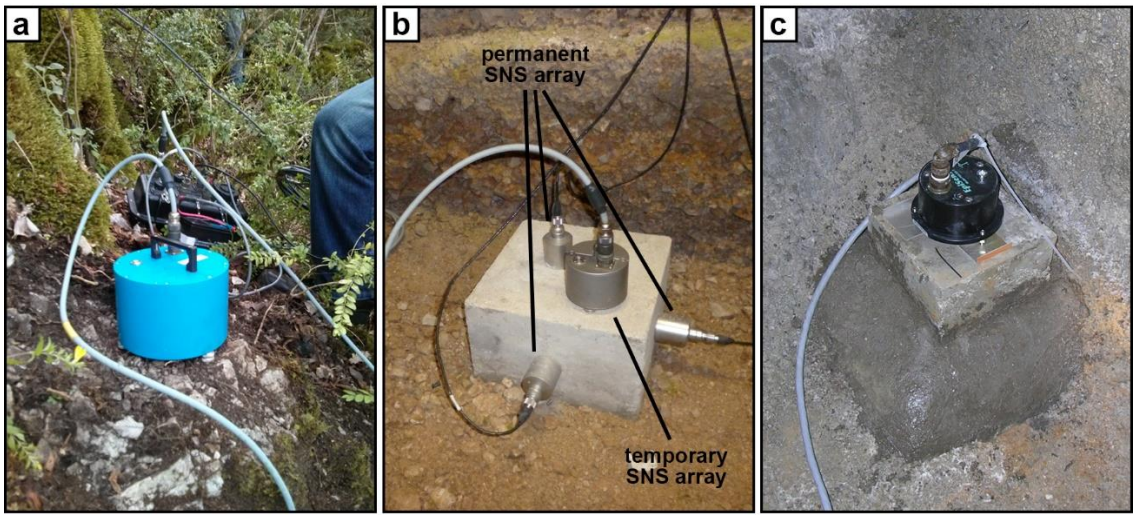

Fig. 3.12. Seismic data acquisition: **a** seismic noise station (Lennartz LE-3D/5s); **b** temporary (Lennartz LE-3Dlite MkII) and permanent (Brüel & Kjær type 8340) SNS array station; **c** accelerometric network station (Kinemetrics Episensor).

As already explained in Paragraph 3.1, for obtaining a complete seismic response characterisation of the investigated landslide, seismic ambient noise measurements were processed by using two different techniques: the HVSR analysis and the polarization analysis.

First, the Horizontal-to-Vertical Spectra Ratio (HVSR) analysis by Nakamura (1989) was carried out on the recoded seismic ambient noise data; theoretical explanations of this technique were given in Subparagraph 2.2.1. Seismic ambient noise data were elaborated by using the Geopsy open source software (www.geopsy.org). The time histories were divided into non-overlapping windows of 40 s and the Fast Fourier Transform (FFT) was computed for the three spatial components (North-South, East-West and Up-Down) in the frequency range between 1.0 and 60.0 Hz, by using a 5% cosine taper to each window. The obtained Fourier spectra of each window were smoothed by the Konno-Ohmachi function (Konno & Ohmachi, 1998). By taking the logarithmic average of the two horizontal components and averaging over the windows, the amplitude spectra and the H/V spectral ratio were finally computed for each single record. The results obtained by applying HVSR analysis for the two case studies will be presented in Subparagraph 4.1.1.

Then, the polarization analysis (Vidale, 1986) was carried out on the same time histories through the WAVEPOL code implemented by Burjánek *et al.* (2010, 2012); more information about polarization analysis principles as well as on the applied code were examined in Subparagraph 2.2.2. In summary, such an analysis produces two main outputs by applying a Continuous Wavelet Transform (CWT) on a time history: i) an ellipticity diagram describing the particle motion ellipticity for each frequency, where the ellipticity is defined as the ratio between the semi-minor axis and the semi-major axis of the ellipse (i.e. 1 represents circular particle motion and 0 purely linear motion); ii) a polar strike plot, representing for each frequency the azimuth of the semi-major axis projected to the horizontal plane from North. The combined interpretation of these outputs allows to point out the possible presence of polarization effects in the particle motion, observable as a high degree of linearity on the ellipticity diagram and an azimuthal direction on the polar strike plot for the same frequencies. The results obtained through the polarization analysis code will be shown in Subparagraph 4.1.2.

3.3.2. Systems for monitoring of microseismic events

For the Selmun case study, possible occurrence of microseismic events related to slope gravity-induced instabilities was monitored by nanoseismic monitoring (Joswig, 2008), whose theoretical bases are explained in Subparagraph 2.3.1. As shown in Figure 3.9, two SNS arrays recorded seismic data in two different positions on the Selmun Promontory; such arrays were alternatively installed during two different periods for some time-limited continuous recording campaigns, having last from 9 up to 72 h, and did not record seismic data simultaneously. Each SNS array station was equipped by one LE-3Dlite MkII seismometer (period 1 s, flat transfer function 1-100 Hz, sensitivity 800 V/m/s) by Lennartz Electronic GmbH and one REFTEK 130-01 datalogger (Fig. 3.10c) that acquired with a sampling frequency of 500 Hz. Table 3.3 summarises the SNS records carried out at the Selmun Promontory.

The seismic records on the array SNS1 position (Fig. 3.9) were carried out on September-October 2015 and on September 2016, according to the standard SNS geometry, therefore by opening the array with an aperture radius of about 25 m and by installing the sensors at a sufficient distance to the instability to make the most of the nanoseismic monitoring potentialities. For theoretical reasons explained by Joswig (2008), the beam shapes related to the waves phase picking are perfectly reliable at a distance at least 5 times the SNS array aperture.

Since a fast screening of the array SNS1 data did not allow to observe microseismic events, on October 2016 the nanoseismic monitoring records were carried out on the array SNS2 position (Fig. 3.9). The stations of the array SNS2 composed a SNS array having an aperture radius of about 12 m, smaller than the SNS standard aperture, and was located closer than the array SNS1 to the unstable plateau edge.

SNS array	Array aperture (m)	Installation period	Total of recorded seismic data (h)
SNS1	24.6-25.5	Sept.-Oct. 2015 September 2016	73
SNS2	11.8-12.5	October 2016	122

Tab. 3.3. Summary of the measurements carried out on the Selmun Promontory by the two SNS arrays, whose locations are shown in Fig. 3.9.

For the Peschiera case study, the monitoring of microseismic events related to the gravity-induced slope instability takes place by a standard accelerometric network and a SNS array (Fig. 3.11), installed in the framework of a convention between ACEA-ATO2 S.p.A. and Research Centre for Geological Risks (CERI) of Sapienza University of Rome for monitoring the landslide process. Both permanent seismic monitoring systems are property of ACEA-ATO2 S.p.A. and are managed by CERI in cooperation with Italian National Agency for New Technologies, Energy and Sustainable Economic Development (ENEA) and French Institute for Sciences and Technology for Transport, Development and Networks (IFSTTAR-Paris). Through the here-presented Ph.D. thesis, only a limited amount of the large available seismic data were analysed for two specific purposes: i) to obtain a characterisation of the landslide hazard by the SNS array records; ii) to integrate such a landslide hazard characterisation with the pre-existent alarm system based on the event detected by the accelerometric network.

On September 2008, four accelerometric stations (GA, C1, F1 and C6 in Figure 3.11) were installed within the drainage plant of the Peschiera Springs Slope in order to record both earthquakes and microseismic events related to the landslide process. Each station is equipped with a 3-component accelerometer Episensor (Fig. 3.12c), directly installed on bedrock, and connected to a digital datalogger Kinemetrics Granite that acquires with a 250 Hz sample frequency. The events are recorded by a triggering criteria based on duration and large-band frequency content (Lenti *et al.*, 2012). To automatically distinguish among different kinds of events, a specific script was implemented through Seismic Analysis Code (SAC) and Fortran on Unix platform. The software allows to classify the events on their physical properties, i.e. duration, frequency content, Arias Intensity (AI) and Peak Ground Accelerations (PGA) values, and to distinguish among earthquakes and different microseismic events originated within the slope. In particular, microseismic events are distinguished in: i) failures related to rock mass fracturing, with a duration from 1 to few seconds, a first arrival with a broad frequency content and a coda focused on low frequencies; ii) collapses, having a duration less than 1 s and a typical waveform of impact with a broad frequency content. The accelerometric network also records near-field and regional earthquakes as well as teleseisms (Lenti *et al.*, 2015).

For managing the landslide risk at the Peschiera drainage plant, the frequency of events (P) as well as the cumulative Arias Intensity (AI) of failures and collapses are

plotted as a function of time. To provide an alarm system, a frequency index [FI(P, t)] was defined as sum of two frequency indexes: the first one referred to earthquakes [FI_er(P, t)] and the other one related to microseismic events [FI_me(P, t)]. Moreover, the rate of the cumulative AI of the recorded microseismic events is used to define an energy index [EI(P, t)]. A final control index [CI(P, t)] was defined as a function of the sum of frequency and energy indexes [FI(P, t) + EI(P, t)]. This control index is daily computed for each station of the network and enables to associate each specific sector of the plant (represented by the corresponding accelerometric station) with three possible alarm levels: i) "ordinary" (OL) if [CI(P, t) = 1]; ii) "alert" (AL) if [CI(P, t) = 2]; iii) "emergency" (EL) if [CI(P, t) = 3]. To take into account energetic collapses or failures, "emergency" level is directly reached with a PGA value of 10^{-3} g, corresponding to the value that produced visible damages into the drainage plant (Lenti *et al.*, 2012).

Until September 2015, the accelerometric network recorded 2311 events among which 1031 earthquakes and 1280 microseismic events (i.e. failures and collapses). Since January 2014, a relevant increase in microseismic event detection was observed respect to the previous 7 years, mainly due to collapses. From January 2014 to September 2015, the accelerometric network recorded 689 collapses, grouped in 46 crises, where a crisis is given by at least 3 events within 24 h. As evidenced by the synoptic plot of Figure 3.13a, the time distribution of the recorded crises could be related to discharge variation, that probably influenced the stress field in the karstified rock mass. The cumulative number of the recorded collapses shows a significant change in rate in correspondence with the maximum daily total discharge recorded (Fig. 3.13a); consequently, in these specific periods (September 2011, June-July 2014 and June-July 2015) the control index CI often achieves the "emergency" level (Fig. 3.13b).

On November 2013, three additional accelerometers Episensor were installed on the slope surface (stations VGA, VC1 and VC6 in Figure 3.11), to integrate the pre-existent accelerometric network. Actually, such surface stations have been not yet integrated into the event detection and control index computation processes because they showed evident effects of site amplification. A correction procedure for these stations was proposed and tested in this Ph.D. thesis and will be explained in Paragraph 5.2.

The accelerometric network has been switched off since November 2015 for a significant refurbishment work that involves the drainage plant.

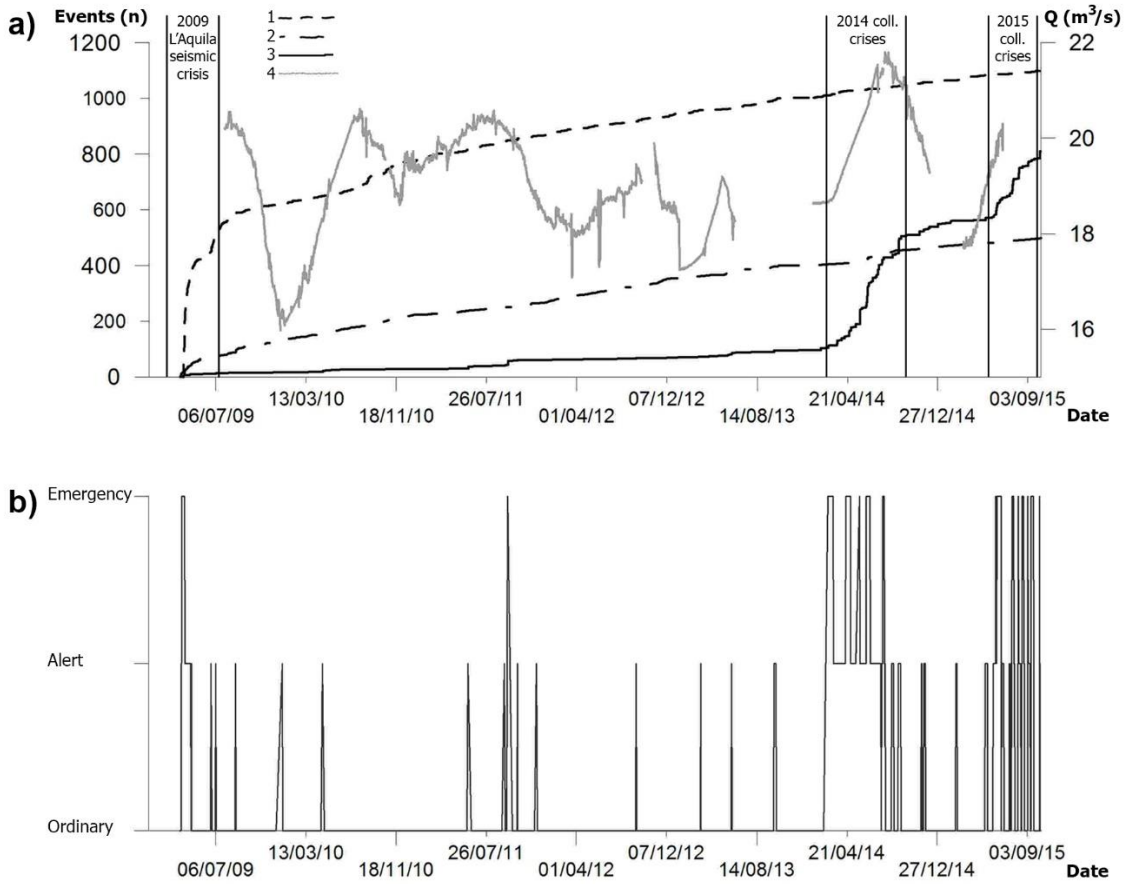

Fig. 3.13. Results of the accelerometric network of Peschiera case study: **a** cumulative numbers of 1) earthquakes, 2) failures and 3) collapses recorded by the accelerometric network and 4) daily total discharge (data are not available where line is interrupted); **b** variation of the alarm level at C1 station during the whole monitoring period (2008-2015) corresponding to the control index CI (ordinary = 1; alert = 2; emergency = 3). (from Fiorucci *et al.*, 2017)

During 2013, a 27-m-aperture SNS array was experimented in abandoned drainage tunnels within the slope (Fig. 3.11). Each station was equipped with one LE-3Dlite MkII seismometer by Lennartz Electronic GmbH and one REFTEK 130-01 datalogger (Fig. 3.12b) that acquired in continuous mode with a sampling frequency of 500 Hz. Based on the results obtained during the five measurement campaigns, a permanent SNS array was installed in 2014 to replace the temporary one. The permanent SNS array is composed of 6 Brüel & Kjær type 8340 microaccelerometric sensors (Fig. 3.12b), having high sensitivity (10 V/g) and flat response in a broad frequency range (0.1-1500 Hz), coupled with a 3-modules HBM QuantumX datalogger that acquires in continuous mode at a 600 Hz sampling frequency.

Fiorucci *et al.* (2017) presented the results obtained by the temporary SNS array as well as the first outputs derived from the analysis of the main events recorded by the permanent one, in term of detection of microseismic events and the distribution of their epicentre and hypocentre within the slope. As the accelerometric network, also the temporary and the permanent SNS array allowed to detect two types of different microseismic events originated within the slope and related to the gravity-induced instability, i.e. failures and collapses, distinguished by time duration and frequency content as well as by the considered physical parameters.

In terms of event location, the epicentral distribution of the microseismic events is in very good agreement with the spatial distribution of the main morphological landforms associated with the ongoing rock mass deformation that involves the Peschiera Springs slope. Moreover, the hypocentre distribution evidences as the instability events are mainly located below the groundwater level. In terms of event detection, a comparison between the events recorded in triggering mode by the accelerometric network and those manually detected by the SNS data screening was carried out for the 14 collapse crises occurred in 2015 (Fig. 3.14). Such a comparison allowed to observe that the SNS array was able to detect a number of events between 2 and 30 times higher respect to the number of collapses recorded by the accelerometric network in the same crisis.

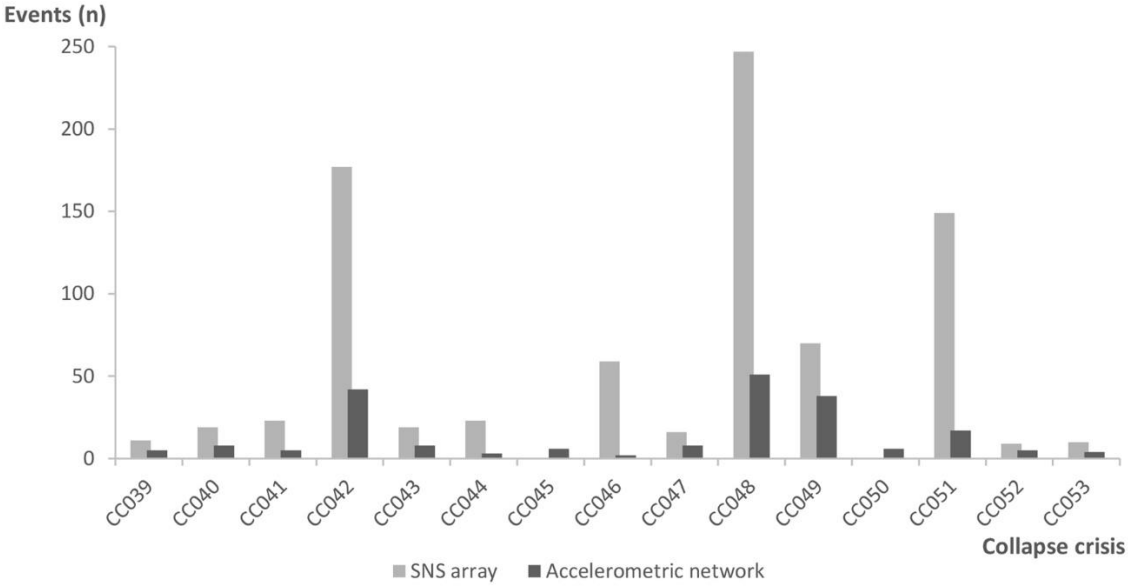

Fig. 3.14. Frequency histogram showing the collapses recorded at the Peschiera Spring Slope by the accelerometric network and the permanent SNS array during the 14 collapse crises occurred in 2015. (from Fiorucci *et al.*, 2017)

Differently from Fiorucci *et al.* (2017), in this work the permanent SNS data analysis was carried out also for the weaker events to obtain a characterisation not only focused on the most energetic events.

All the SNS array records carried out at sites of the two case studies were analysed by the software of nanoseismic monitoring (Joswig, 2008), after two specific workshops (i.e. May 2013 and August 2015) attended by the Ph.D. student at Institute for Geophysics of University of Stuttgart to become familiar with their use. As already explained in the Subparagraph 2.3.1, the NanoseismicSuite software (www.nanoseismic.net) includes two main tools: i) SonoView, devoted to detection of microseismic events, and ii) HypoLine, aimed to their characterisation in terms of assessment of epicentre, hypocentre and magnitude. In addition, a specific script, implemented in SAC code and devoted to compute the Peak Ground Acceleration (PGA) and the Arias Intensity (AI) values, allowed to obtain a physical characterisation of the detected events. Both parameters were computed on the three time histories of each event and, then, the values obtained for the North-South and the East-West components were averaged for obtaining the horizontal values of PGA and AI.

The results obtained in the two case studies in terms of detection and location of microseismic events will be shown in Subparagraph 4.2.1, while in Subparagraph 4.2.2 an event clustering process will be presented. Finally, for managing the landslide risk threating the drainage plant hosted into the Peschiera Spring Slope, an integration of the results obtained by the SNS array with the pre-existent alarm procedure based on the accelerometric network will be proposed in Paragraphs 5.2 and 6.3.

4. Results

4.1. Results of seismic ambient noise measurements

The present Ph.D. thesis section is focused about the exposition of the results obtained by the analysis of the seismic ambient noise measurements at single-station configuration carried out for the two case studies. According to the proposed experimental approach (Paragraph 3.1), the recorded time histories were analysed through two different methods: i) HVSR analysis carried out by using the Geopsy software (www.geopsy.org); ii) polarization and ellipticity analysis of the particle motion carried out through the WAVEPOL code implemented by Burjánek *et al.* (2010, 2012). Such methods of analysis and the related processing tools were explained in detail in Subparagraph 3.3.1, with also a description of the spatial distribution of the seismic ambient noise measurement stations for the both introduced case studies.

4.1.1. HVSR analysis results

For the Selmun case study, the results obtained by the HVSR analysis were grouped according to the five zones (A, B, C, D and E) previously defined in the area, in order to distinguish the seismic response related to engineering geological features. Such an engineering geological zonation was explained in detail in Subparagraph 3.2.1 and can be observed in Figure 3.9 with the location of the seismic ambient noise measurement stations.

As shown in Figure 4.1, all the stations located on the UCL plateau (i.e. both inland plateau and on the fractured plateau edge) show HVSR curves characterised by a ubiquitous resonance peak in a narrow frequency range of 1.5-2.0 Hz followed by a sharp dip of the ratio. The HVSR peak at 1.5-2.0 Hz can be considered representative of the fundamental frequency of the site (f_0) since this peak is always present in the Maltese archipelago where the UCL-BC-GL sedimentary sequence is located, as evidenced by the studies carried out at Dingli, Mdina, Wardija, Xemxija, Mellieħa, Anchor Bay, Mgarr, Nadur, Rabat, Golden Bay and Bahrija (Panzera *et al.*, 2012, 2013; Vella *et al.*, 2013; Galea *et al.*, 2014; Farrugia *et al.*, 2016, 2017; Pischiutta *et al.*, 2017). This feature of the HVSR curves (peak at 1.5-2.0 Hz followed by a dip below 1.0 over a wide frequency range) was interpreted as related to the difference of seismic wave velocity values

between the three geological formations that compose the sedimentary sequence. The dip of the HVSR(f) function is presumably due to the shallow shear-wave velocity inversion at the interface between the competent UCL and the plastic BC, while the peak can be related to Rayleigh wave ellipticity and/or trapping of SH waves in the BC low-velocity layer (Galea *et al.*, 2014).

On the other hand, the HVSR(f) functions on the UCL plateau show marked differences in the seismic response between the unstable zones and the stable plateau area at frequencies higher than 3.0 Hz (Fig. 4.1). As a matter of fact, in the measurements carried out within and in proximity of the unstable zones, the HVSR curves show significant resonance peaks at higher frequency (3.0-60.0 Hz) that are not present in the measurements carried out on the stable plateau zone. In addition, peaks of the HVSR(f) functions are much more evident in areas having higher density of fractures and blocks, as the jointed edge of the UCL plateau. Zone B shows a prevalent HVSR peak at frequency around 3.5 Hz, while the other jointed edge zones (C and D) do not show peculiar characteristic in the HVSR peaks.

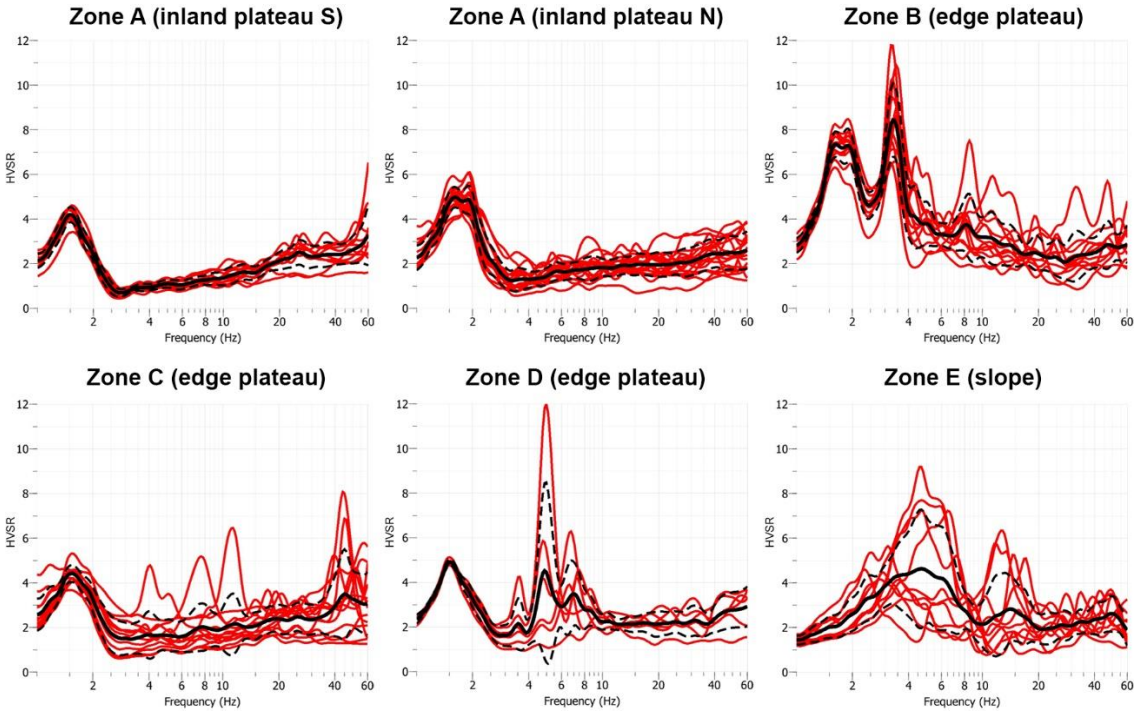

Fig. 4.1. HVSR(f) functions grouped for different zones of the Selmun Promontory (see Figure 3.9): the red curves represent examples of obtained HVSR(f) among the 116 measures, the solid black line is the average HVSR(f) function obtained by all curves in each zone and the dashed black lines show the standard deviation of all curves in each zone.

The HVSR(f) functions resulting from the noise measurements carried out on the BC slope show a first main peak at higher frequencies than the stations located on the UCL plateau, in a range between 2.4 and 6.5 Hz. Such a peak can be related to the resonance in the BC layer due to the lower values of the seismic wave velocity compared to the underlying GL layer. A quick and rough evaluation of the fundamental frequency of a resonant layer (f_0) can be theoretically obtained by Equation 2.1, that considers the S-wave velocity of the layer and its thickness.

BC are characterised by a S-wave velocity of 300-400 m/s (Panzera *et al.*, 2012; Farrugia *et al.*, 2016, 2017) and their maximum thickness at the Selmun Promontory is 30 m. The seismic noise measurements were carried out on the debris deposit, about 1-5 m thick. For the measurements carried out in the higher part of the slope, a total thickness of the BC-debris layer of 35 m and a mean S-wave velocity of 350 m/s can be assumed, by considering also the poorer geomechanical features of the debris. Such parameters allow to obtain a fundamental frequency (f_0) of about 2.5 Hz in the higher part of the slope, that increase at 5 Hz by halving the thickness of the BC-debris layer, a condition existing in the middle part of the slope. The obtained values of fundamental frequency (f_0) are in agreement with those obtained by Panzera *et al.* (2012) at several sites on Malta where BC outcrop, i.e. Rabat, Mdina, Wardija and Mellieħa.

The HVSR(f) functions in this area show additional peaks at higher frequencies that can be related to the resonance in the debris deposit due to its local features (i.e. thickness and/or weathering), since most of the measurements on the BC clay were carried out on the debris that covers the slope, as evidenced in Figure 3.9.

Figure 4.2 summarises the HVSR results for the Selmun area, displaying the spatial distribution of the frequency values and the HVSR(f) function amplitudes of the first HVSR peak. A significant variation of this peak can be observed in terms of frequency value as well as of HVSR amplitude value on the UCL plateau (zones A-D). On this area, the frequency value of the first peak of the HVSR(f) function varies between 1.5 and 1.8 Hz. On the other side, the variation of the main peak HVSR amplitude seems to be strongly related to the location of the measurement points. As a matter of fact, the HVSR(f) function amplitude increases on moving from the inner plateau towards the edge of the plateau, where the joint density significantly increases. In particular, the Southern portion of zone A is characterised by HVSR(f) amplitude values between 2.0 and 4.0 and

the Northern portion of zone A between 4.0 and 6.0, while in zone B the HVSR(f) amplitude range from 6.0 to 10.0.

On the BC slope (zone E), the frequency value of the first peak of the HVSR(f) function varies over a wider range compared to that on the UCL plateau, i.e. between 2.4 and 6.5 Hz. Additionally, stations located in the higher part of the slope show lower resonance frequencies than the stations in the lower part. This variation can be explained by the decreasing thickness of BC layer on going down-slope, as shown in the engineering geological cross-sections shown in Figure 3.6.

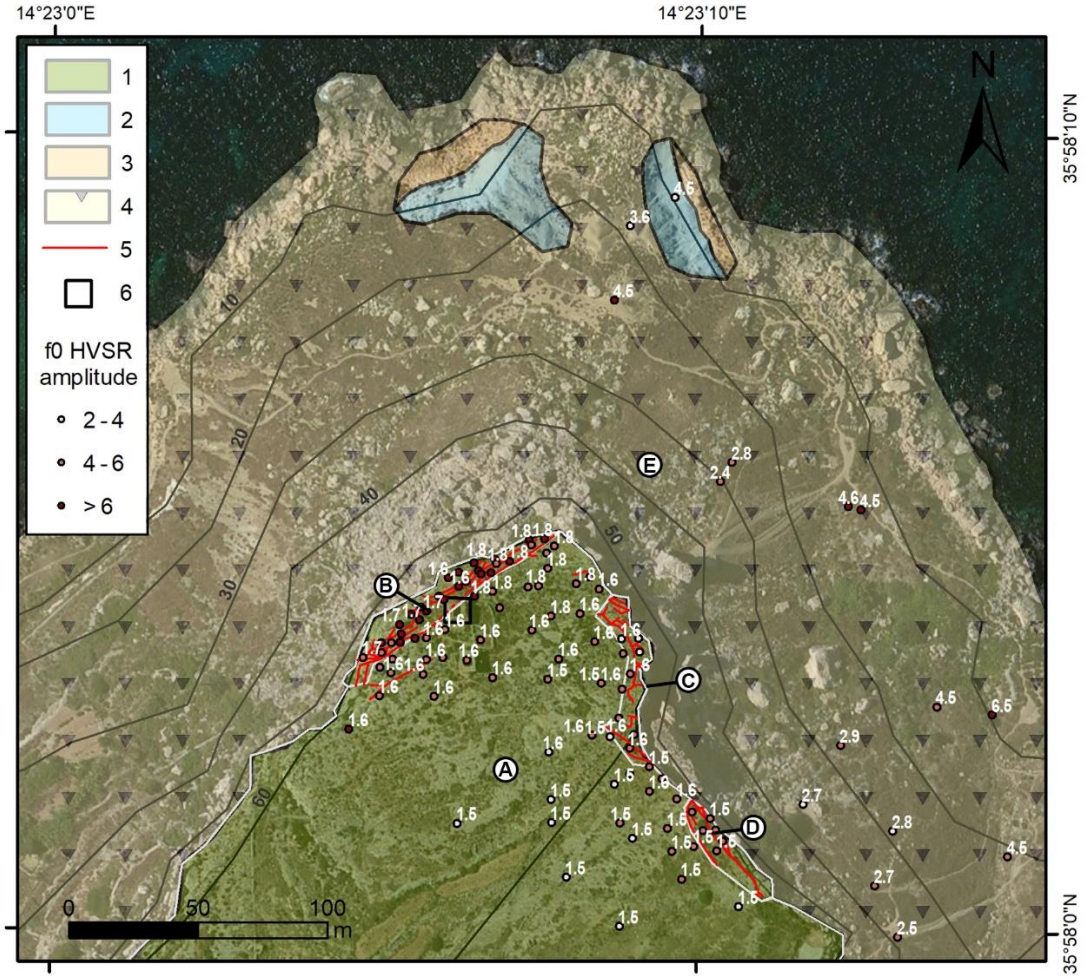

Fig. 4.2. Satellite view of the Selmun area showing the measurement points (dots) and the values (in white) of the first peak of the HVSR(f) function (colour scale): 1) UCL; 2) BC; 3) GL; 4) debris slope deposit; 5) fracture (the dashed line represents an inferred fracture); 6) Għajn Ħadid Tower. The light grey lines indicate the different zones of Selmun (A-E).

For the Peschiera case study, the results obtained by the HVSR analysis are shown in Figure 4.3; the HVRS curves of stations S2B and S1B are not shown because they are very similar respectively to those obtained at stations S2A and S1A due to their proximal position. The precise location of the seismic ambient noise measurement stations on the Peschiera Spring Slope can be observed in Figure 3.11.

The results obtained by the measurements carried out in the central portion of the slope (S1, S1A, S1B and S1C) evidence an important peak of the HVSR(f) functions at about 4 Hz, in some cases followed by several other peaks at higher frequencies. The HVSR peak at 4 Hz is characterised by a value of amplitude varying between 5 and 7, while the other peaks have even higher value, where they exist. On the other hand, all the HVSR(f) functions resulting from the noise measurements related to the Eastern portion of the slope (S2, S2A and S2B) show a peak at about 7 Hz and the presence of other peaks at various frequency values, even higher than 3 Hz; the HVSR(f) amplitude value ranges between 3 and 5. Finally, the HVSR(f) function obtained by the analysis of the station S3, located in the Western part of the Peschiera Spring Slope, do not present significant peaks.

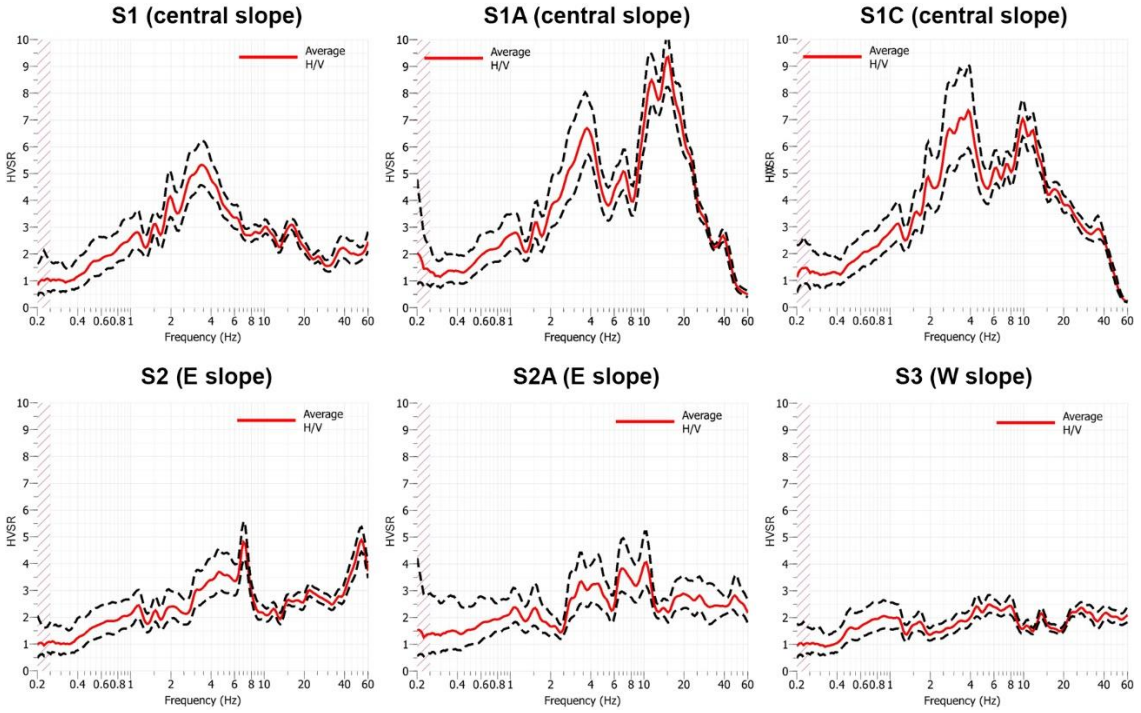

Fig. 4.3. HVSR(f) functions (the dashed black lines show the standard deviation of the curve) obtained on the Peschiera Spring Slope (see Figure 3.11 for the station locations).

In general, the analysis of the HVSR(f) functions obtained on the Peschiera Spring Slope do not allow to observe a uniform response of the whole landslide body but they seem to show features related to the local conditions of the slope portion. In fact, by HVSR analysis, it was possible to observe the absence of a marked seismic resonance for the Western part of the slope and a seismic resonance for its central and Eastern parts, respectively at 4 Hz and 7 Hz, plus other punctual resonance effects strictly related to the measurement points. Such a result is in good agreement with the complex geometry of the landslide mass, large and composed by sectors involved in landslide processes at different evolutionary stages as already evidenced in Subparagraph 3.2.2.

4.1.2. Polarization analysis results

For the Selmun case study, the polarization analysis carried out through the WAVEPOL code (Burjánek *et al.*, 2010, 2012) confirms the peculiar features observed in the HVSR analysis and provides additional evidence to support the different seismic response in the various zones on the Selmun Promontory. Figures 4.4 and 4.5 show several representative examples of the results obtained by the polarization analysis, compared with those of the HVSR analysis, in measurements located on the different zones of the Selmun Promontory. Based on the polarization analysis, two features emerge with reference to specific frequency ranges: i) the ellipse axes ratio, which decreases when the linearity of the particle motion increases; ii) the azimuthal distribution of the particle motion, which reveals a main direction of polarization of the particle motion.

By analysing all the results obtained on the UCL plateau as well as on the BC slope, the frequencies associated with the first peak of the HVSR(f) function (i.e. 1.5-1.8 Hz for the UCL plateau and 2.4-6.5 Hz for the BC slope) do not show evidence of polarization of the particle motion. As a matter of fact, even if the ellipticity diagrams for both zones show quite a high degree of linearity (an ellipse axes ratio in a 0.1-0.2 range), the polar strike plots do not demonstrate a main direction of the particle motion at the same frequencies. This confirms the hypothesis that the first peak of HVSR(f) function is mainly related to the stratigraphic setting (i.e. 1D resonance effect) and to the multi-directional nature of the ambient noise.

On the inland UCL plateau (i.e. zone A), the noise analysis shows no evidence of either peaks of the HVSR(f) function (beyond the f_0 peak) or polarization effects of the

particle motion, except for a few cases where these effects can be observed at frequency values higher than 30 Hz and are probably related to very local elements (e.g. thin and shallow soil layers characterised by low V_s values).

Zone B shows strong directivity effects at the same frequency of the 1D resonance after the f_0 peak, which already resulted by the HVSR analysis. As a matter of fact, the results obtained by the polarization analysis show that in zone B the 3.3-3.5 Hz frequency range is characterised by marked features of linearity (ellipse axes ratio between 0.0 and 0.1) and by a strong azimuthal polarization of the particle motion. In particular, all the polar strike plots show a directivity of the particle motion at azimuthal values between 135° and 150°, values similar to the mean dip direction of the joint system prevalent in zone B (J1, see Figure 3.4).

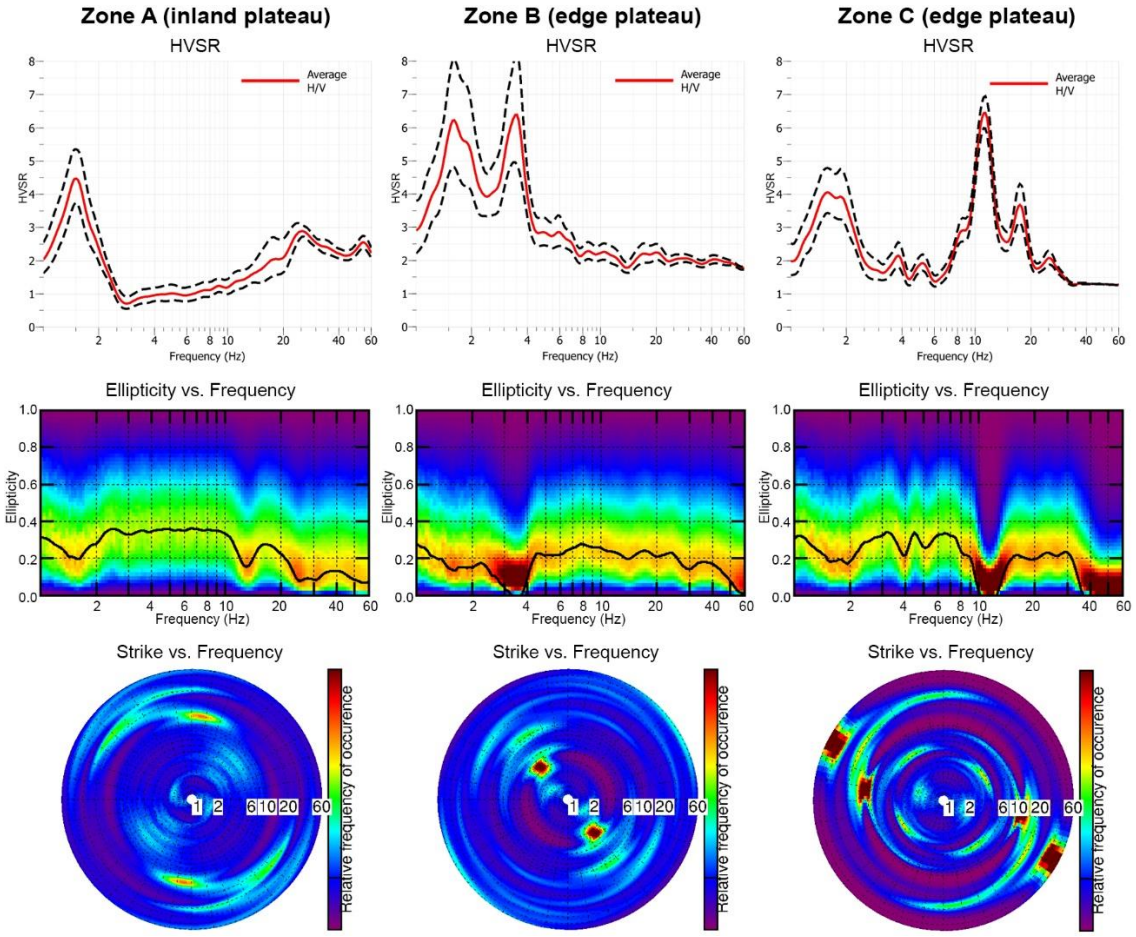

Fig. 4.4. Representative examples of HVSR(f) function (the dashed black lines show the standard deviation of the curve), ellipticity diagram and polar strike plot (same palette colour for relative frequency of occurrence) obtained for zones A, B and C of the Selmun Promontory.

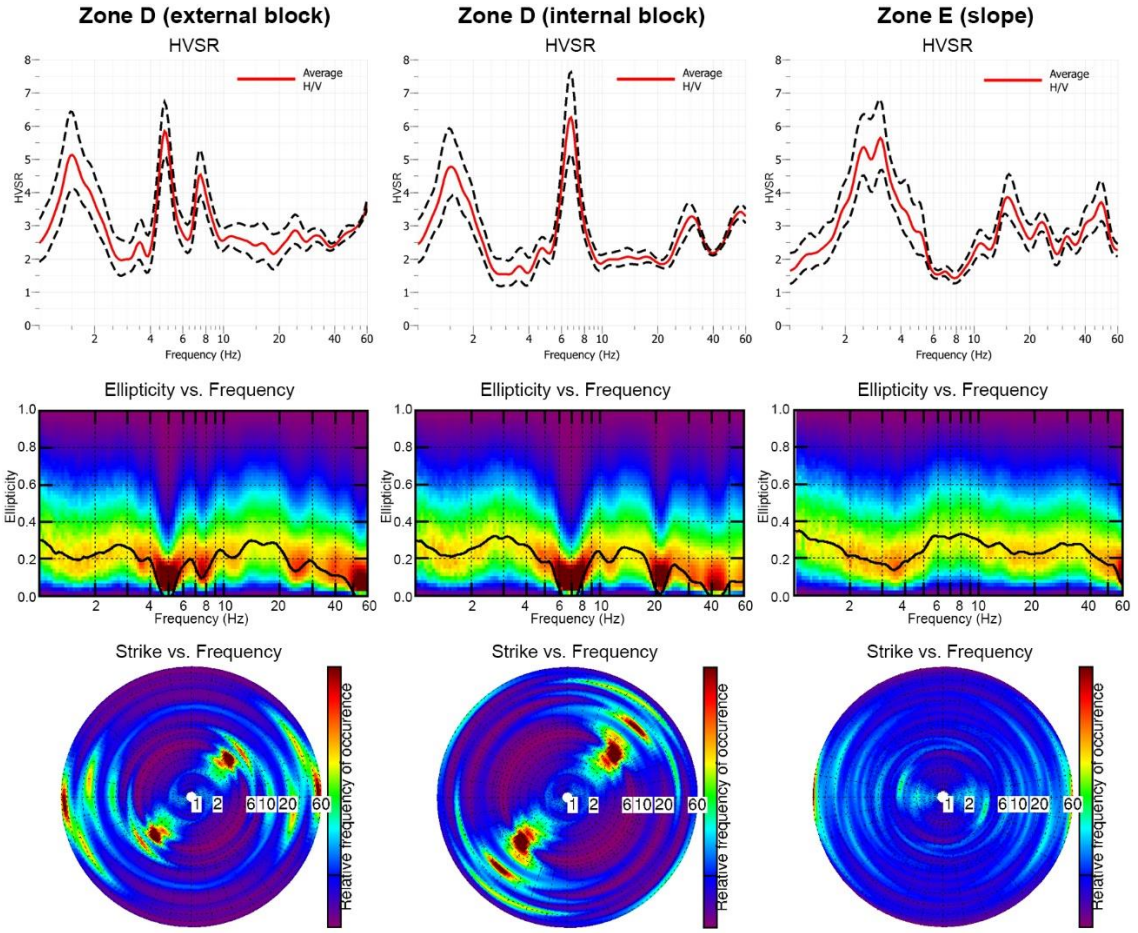

Fig. 4.5. Representative examples of HVSR(f) function (the dashed black lines show the standard deviation of the curve), ellipticity diagram and polar strike plot (same palette colour for relative frequency of occurrence) obtained for zones D and E of the Selmun Promontory.

By considering the polarization effects in zone D, they exist along the azimuthal direction 45-50°, values similar to the dip direction of the main joint system of the area (J2, see Figure 3.4). Nevertheless, these effects occur at two specific frequency values: 5 Hz in the portion of the plateau closest to the cliff (0-5 m from the edge) and 7 Hz in the internal portion of the plateau (5-10 m from the edge). Also in zone C there is evidence of polarization effects along a direction similar to the joint dip direction, but they do not occur in a specific range of frequency. Finally, in zone E, the analysis does not show polarization effects as well as ellipticity features, despite the several peaks observed in the HVSR(f) functions.

Figure 4.6 summarises on a satellite view the results obtained through the polarization analysis at the Selmun Promontory. This map shows the spatial distribution of the first polarised frequency values (only for frequencies lower than 30 Hz), the corresponding azimuthal directions of the particle motion and the associated ellipticity values. In addition, the noise measurement stations that do not evidenced neither ellipticity features nor polarization effects of the particle motion are represented by black dots.

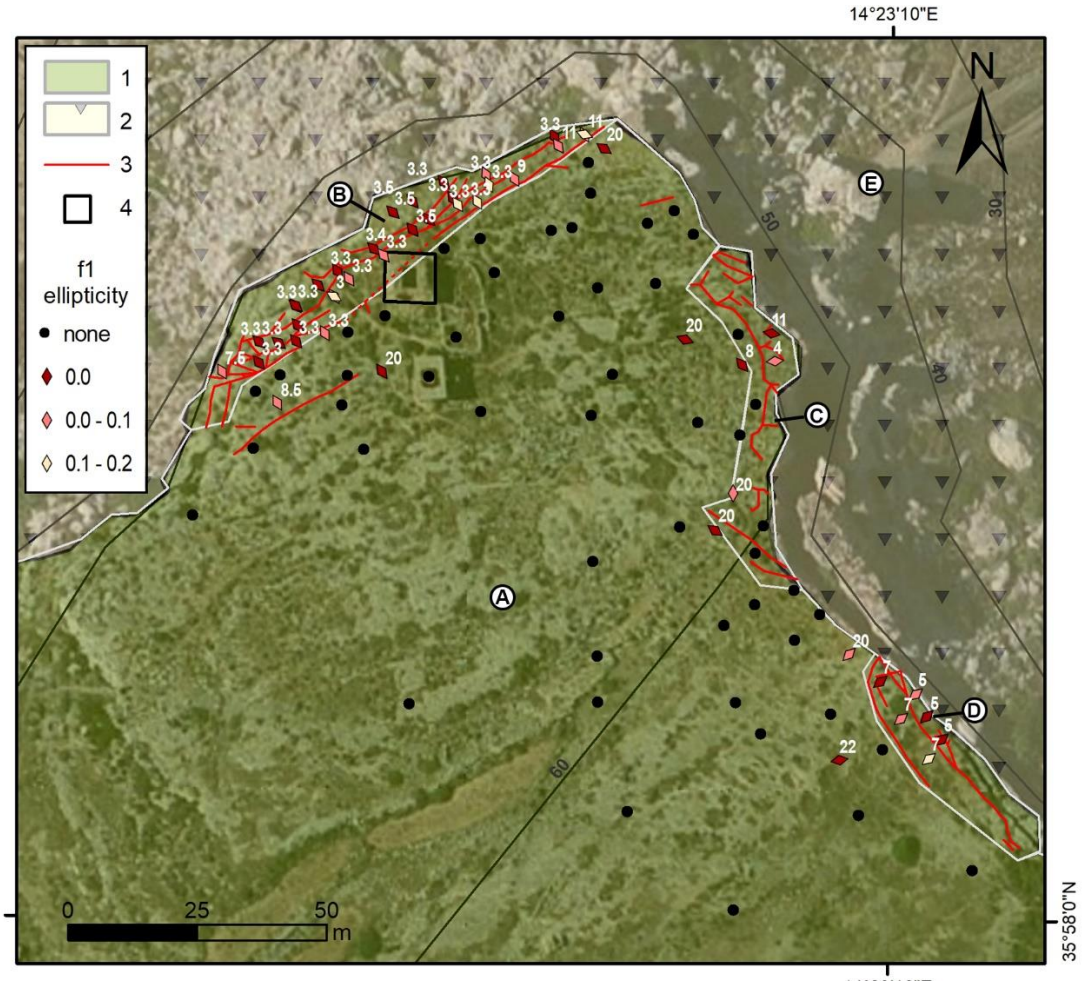

Fig. 4.6. Satellite view of the Selmun Promontory summarising the results of polarization analysis for the first (lower value) polarized frequency: 1) UCL; 2) debris slope deposit; 3) fracture (the dashed line represents an inferred fracture); 4) Għajn Ħadid Tower. Each symbol indicates a noise measurement point: the label displays the value of the first polarized frequency; the arrow is oriented in the polarization azimuth; the colour scale indicates the ellipticity intensity. Black dots indicates noise measurement points without polarization effects. The light grey lines indicate the different zones of Selmun (A-E).

The spatial distribution of the results confirms the absence of polarized frequency on the stable plateau (zone A), while highlighting different behaviours in the unstable areas (zones B, C and D). In particular, even though zone B is characterised by the denser joint net identified though the engineering geological surveys, its uniform seismic response seems to be related to the vibrational behaviour of a unique rock block characterised by a single polarized frequency at 3.3-3.5 Hz. On the other hand, in zone D the seismic response seems to be related to two different and independently vibrating rock blocks, each characterised by an own value of polarized frequency (5 and 7 Hz).

For the Peschiera case study, some representative results obtained by the polarization analysis carried out on the different portions of the slope are shown in Figure 4.7. Such results, compared to the respective function of the HVSR analysis, allowed to define additional and specific features of the different seismic response in the various zones of the Peschiera Spring Slope.

By considering the polarization analysis results obtained on the central portion of the slope (noise measurement stations S1, S1A, S1B and S1C, see Figure 3.11), they do not show evidence of polarization of the particle motion for the frequency associated with the main peak of the HVSR(f) function, at about 4 Hz. As a matter of fact, even if the ellipticity diagrams show a significant degree of linearity (an ellipse axes ratio between 0.1-0.2), the polar strike plots do not evidence a main azimuthal direction of the particle motion at the same frequency. These results are similar to those obtained for the first peak of HVSR(f) function at the Selmun case study, that resulted related to the stratigraphic setting (i.e. 1D resonance effect). Since the absence of polarization effects and the features similar to a peak related to the fundamental frequency of the site (f_0), the peak of HVSR(f) function at about 4 Hz obtained in the central zone of the Peschiera Spring Slope could be associated to the resonance in a weak layer characterised by a low V_S value, e.g. a deposit of debris slope, rather than to the vibrational behaviour of an unstable block.

In the Eastern zone of the Peschiera Spring Slope (noise measurement station S2, S2A and S2B), the polarization analysis evidences the presence of a marked effect of linearity (ellipse axes ratio between 0.0-0.1) as well as a strong azimuthal polarization of the particle motion at about 7 Hz. Such effects resulted at the same frequency of the 1D resonance peak obtained by the HVSR analysis. As evidenced by the polar plots, the polarization of the particle motion at 7 Hz is focused roughly North-South, in a direction

perpendicular to the main scarp in that portion of the slope according to Maffei *et al.* (2005). Since the contemporary presence at 7 Hz of both a peak in the HVSR(f) function and polarization features of the particle motion, the results can be associated to the vibrational behaviour of a rock block composing the complex landslide system. This hypothesis is coherent with the diffused instability processes evidenced by Maffei *et al.* (2005) and with the large cyclicity of the deformations observed by Martino *et al.* (2004) in the Eastern portion of the Peschiera Spring Slope. Finally, the results of seismic ambient noise measurement carried out in the Western zone of the Peschiera Spring Slope (noise measurement station S3) do not show neither the presence of peaks in the HVSR(f) function nor evidences of marked features of polarization and linearity of the particle motion. Therefore, this specific slope zone does not seem to be interested either by 1D resonance effects or by surface unstable rock blocks.

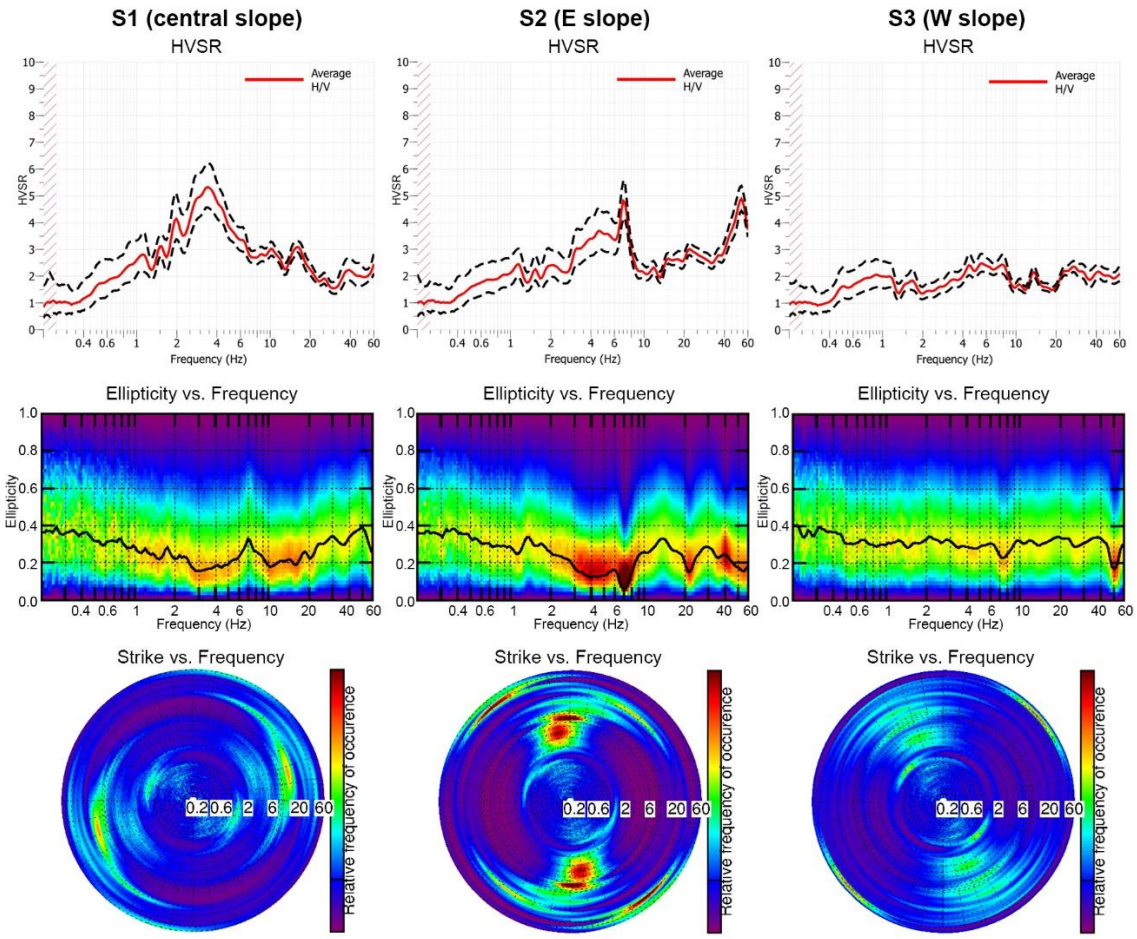

Fig. 4.7. Representative examples of HVSR(f) function (the dashed black lines show the standard deviation of the curve), ellipticity diagram and polar strike plot obtained for central, Eastern and Western portion of the Peschiera Spring Slope.

In summary, the analysis of seismic noise measurements at the Peschiera Spring Slope evidences a central part of the complex landside characterised by a 1D resonance effect at 4 Hz, a Easter part having effects of polarization of the particle motion at 7 Hz and a Western part with absence of both 1D resonance effects and polarization of the particle motion.

The results obtained in both the case studies (i.e. polarization effects of the particle motion mainly in a direction perpendicular to the joint direction) are in very good agreement with those obtained by Burjánek *et al.* (2010) and Moore *et al.* (2011) at the landslide of Randa (Swiss Alps) as well as by Galea *et al.* (2014) at the unstable sea cliff of Anchor Bay (even in the North-Western part of Malta but on the South-facing coast), both already presented in Subparagraph 2.2.2.

4.1.3. Zonation based on vibrational effects

The results obtained by analysing the 1-h seismic ambient noise time histories though the HVSR analysis and the polarization analysis allow to observe specific features of the seismic response of the several zones individuated in the two case studies. From a slope stability point of view, such a zonation can provide additional information about the stability level of the distinguished unstable zones and aid towards the assessment of their different landslide susceptibility (Brabb, 1984), in the framework of a landslide hazard zonation (Varnes & IAEG, 1984).

For the Selmun site, the different features of the seismic response of the zones distinguished on the Selmun Promontory by engineering geological survey can be observed in Figure 4.8. In this figure, the results obtained for each noise station were projected and interpolated along the cross-section I-I' (see Figure 3.9 for location) with a gridding process using a triangulation with linear interpolation method. Additional seismic noise stations were projected on the cross-section to increase the density of results and improve the interpolation process: for the UCL plateau, we interpolated stations in a 20-m buffer from the track; for the BC slope we interpolated stations using an equal-altitude criteria, since the thicknesses variation of the BC layer and the debris deposit are negligible at the same altitude.

Figure 4.8 shows three contour plots where the x-axis represents the distance along the cross-section and the y-axis corresponds to frequency. The colour scale represents respectively: the amplitude of the HVSR(f) function (Fig. 4.8a), the ellipticity of the particle motion (Fig. 4.8b), the frequency of occurrence of the polarized frequency for every azimuthal direction (Fig. 4.8c).

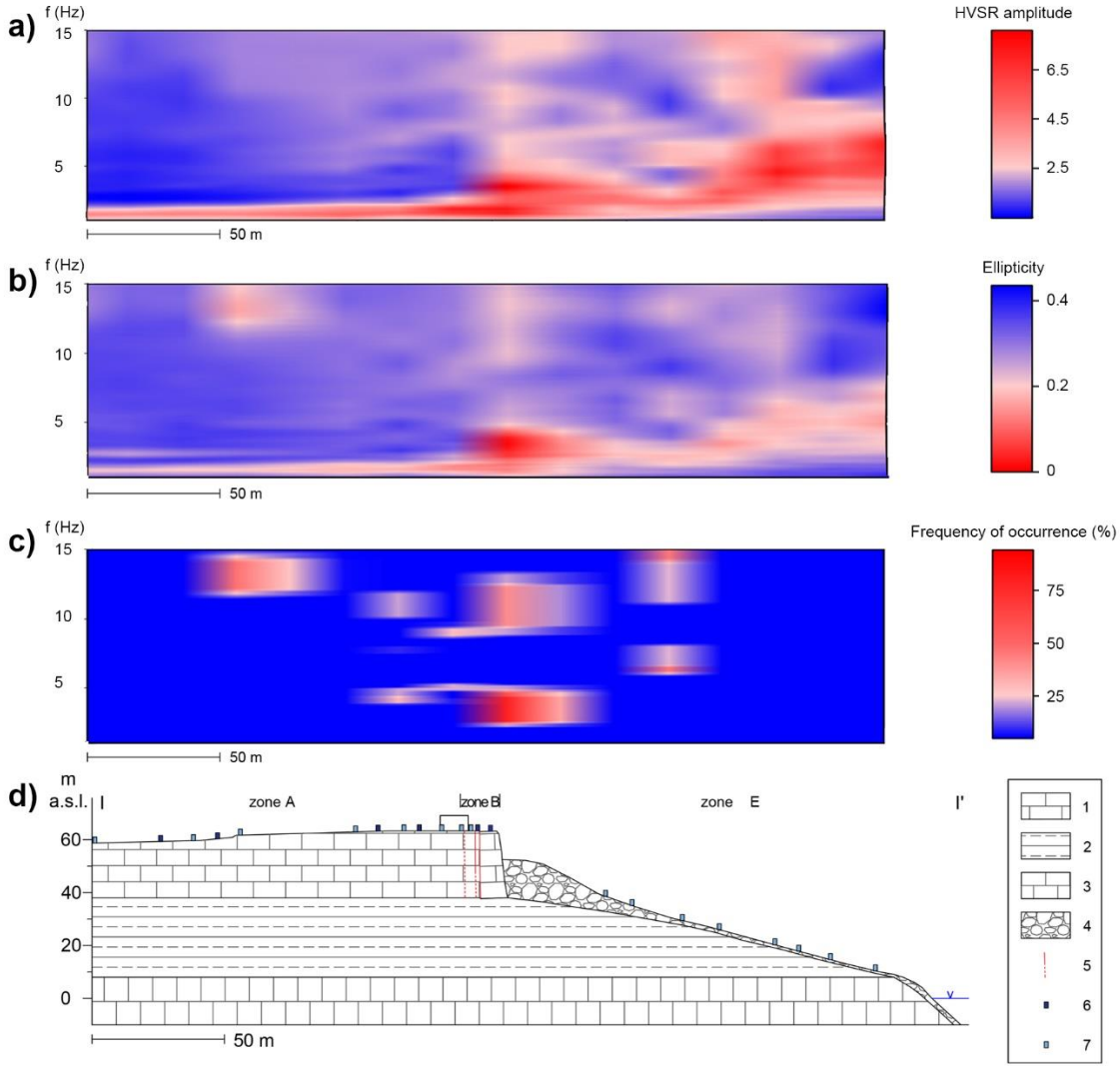

Fig. 4.8. Interpolation of the ambient noise measurement results at the Selmun Promontory along the cross-section I-I' (see Figure 3.5) as a function of distance (x-axis) vs. frequency (y-axis): **a** HVSR(f) amplitude; **b** ellipticity of the particle motion; **c** frequency of occurrence of polarized frequency; **d** cross-section I-I': 1) UCL; 2) BC; 3) GL; 4) debris slope deposit; 5) fracture (the dashed line represents an inferred fracture); 6) seismic noise measurement station located just along the cross-section; 7) seismic noise measurement station projected on the cross-section (using a 20-m buffer on the UCL plateau and an equal-altitude criteria on the BC slope).

The above-presented graphs illustrate the different seismic response of the zones distinguished in the Selmun Promontory and allow to evidence its features respect to the engineering geological setting of the area. The non-polarized fundamental frequency of the site (f_0) on the UCL plateau is at 1.5-2.0 Hz and the amplitude of the HVSR(f) function tends to increase on moving from the inner plateau towards the unstable plateau edge, where the strongly-polarized particle motion at 3.3-3.5 Hz results in correspondence of the main joints (zone B). On the BC slope (zone E), the value of the non-polarized fundamental frequency of the site (f_0) increases with the decreasing thickness of the BC layer.

Evidences that seismic energy concentrated in a specific range of frequency (typically higher than 3.0 Hz) can be related to the vibrational behaviour of unstable rock blocks has been shown in previous studies, as already evidenced by Got *el al.* (2010) and Lévy *et al*. (2010) at the Chamousset test site as well as by Galea *et al.* (2014) at Anchor Bay. The seismic response of a rock block is related to its eigenmodes, which depend on both the geometrical features and mechanical properties of the rock block.

In particular, as suggested by Got *el al.* (2010) the order of magnitude of the flexion mode of a rock block can be evaluated by the following equation [Eq. 4.1] proposed by Blevins (2001):

$$f_{ij} = \frac{\pi e}{2}\left[\left(\frac{i}{a}\right)^2 + \left(\frac{j}{b}\right)^2\right]\sqrt{\frac{E}{12\rho(1-\nu^2)}} \qquad [4.1]$$

where i and j are the numbers of vibration antinodes (equal to 1 for the first resonance frequency), E the Young modulus, ν the Poisson ratio, ρ the density and a, b and e respectively the z (thickness), x (length, dimension parallel to the rear fracture), and y (width, dimension perpendicular to the rear fracture) dimensions of the rock block.. A ρ value of 2146 kg/m^3 was considered by the results of the laboratory tests. A standard value of 0.25 was assumed for ν, while E resulted equal to 1.15*10^9 by the following equation [Eq. 4.2]:

$$E = \frac{5}{6}\rho {V_p}^2 \qquad [4.2]$$

where V_p is the P-wave velocity values, that can be assessed equal to 800 m/s for UCL based on the available literature (Farrugia *et al.*, 2016, 2017). Both values of ν and E are in a range typical for a weak rock considering the presence of vertical and persistent joints

in zone B, as already evidenced by the engineering geological characterisation of the rock mass.

The values of dimensions a, b and e for the whole zone B were assumed respectively equal to 30 m, 100 m and 8.5 m by using the engineering geological model (Figs 3.5 and 3.6). The whole thickness of the UCL layer was assumed for the a value, by considering the joints persistent up to the top of the BC layer. On the other hand, the values of b and e were assumed by considering the joint distribution: the first was assumed based on the length of the rear fracture of zone B, while the second by considering the mean width of zone B perpendicularly to the rear fracture. In this way, a value of about 3.5 Hz was obtained for the first resonance frequency, in a very good agreement with the experimental value measured at Selmun Promontory, in zone B, by the seismic noise analysis.

A reliable characterisation of the resonance eigenmodes of an unstable rock block is an important technical constraint which may be used to propose defence strategies for managing the landslide risk, for example in the case of seismic shaking. As already evidenced in Paragraph 2.2, several recently published works evidenced that seismic shaking can be considered as responsible for triggering or reactivating of gravity-induced slope instability processes at different scales (Havenith *et al.*, 2002, 2003a, 2003b; Bozzano *et al.*, 2004, 2008b, 2011; Bourdeau & Havenith, 2008; Lenti *et al.*, 2015; Martino *et al.*, 2017).

At the Selmun Promontory, the damage to the Għajn Ħadid Tower occurred mainly on October 12th 1856 during the seismic shaking related to the Crete earthquake (M_W 7.7) that caused damage to buildings all along the Maltese Archipelago (Galea, 2007). In the light of this, it is possible to conjecture that the damage of the tower was due to the interaction between the seismic waves and the polarized resonance frequency of the rock blocks at zone B, which favoured displacement along pre-existent joints and/or formation of new joints and facilitated the masonry collapse (Fig. 4.9).

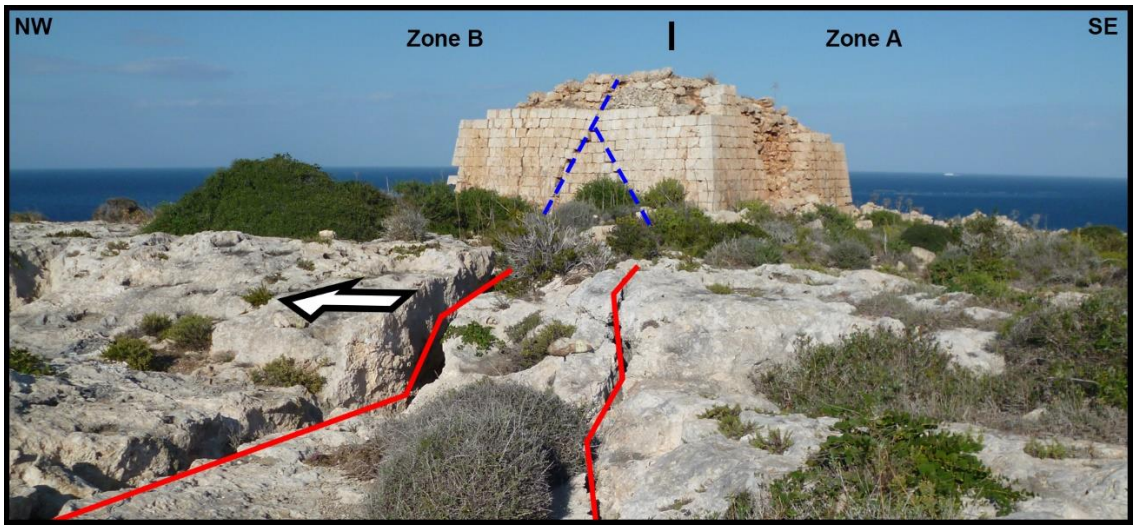

Fig. 4.9. Photograph of the Selmun Promontory showing the two joints passing under the Għajn Ħadid Tower (red solid lines) and two main fractures large cracks crossing related to the masonry (blue dashed lines) related to its collapse (blue dashed lines); the arrow indicates the direction of the polarization in zone B.

By considering the obtained results, zone B shows a higher landslide susceptibility than the other zones distinguished on the Selmun Promontory. This can be deducted by its seismic response that shows features of linearity and polarization of the particle motion, existing in a frequency range compatible with the main eigenmode of a rock block having the dimensions of zone B itself. Since these features are very marked, they can be easily associate to a high mobility of the unstable mass. In addition, despite the presence of a dense net of fractures, zone B shows a homogenous seismic response; therefore, in case of gravity-induced mass movement, the maximum landslide event can involve the whole zone, producing an event having higher intensity than the detachment of a single rock block from the UCL plateau edge.

Features of linearity and polarization of the particle motion in seismic response are less marked in the other unstable zones of the UCL plateau, therefore they could be associated to a relatively lower susceptibility to landslide than zone B; a lower intensity of the expected maximum event can also define since the litterer volume of rock mass involved. In the stable zones of the inland UCL plateau, both fracture net as well as linearity and polarization of the particle motion are absent, therefore zone A can be associate to a very low landslide susceptibility.

Such results can be the basis to design a monitoring system for early warning, in particular by considering the definition of the zone B eigenmode and its higher landslide

susceptibility. One early warning strategy can be based on analysis of continuous records of ambient seismic noise, with the purpose of capturing anomalies of the noise parameters in specific frequency ranges that could be related to changes in the vibrational behaviour of the unstable rock block, as evidenced by Got *et al*. (2010) and Lévy *et al*. (2010). In this regard, a preliminary study of long seismic noise records carried out at the Selmun Promontory will be exposed in Paragraph 5.1, that was carried out for evaluating the possibility to install permanent sensors devoted to the early warning.

Finally, a characteristic value of critical weakening displacement u_c was computed for each unstable rock block of the Selmun Promontory showing features of ellipticity and polarization of the particle motion, that can be associated to a high mobility of the unstable rock blocks. The definition of a characteristic threshold can be useful to evaluate the order of a displacement (e.g. related to seismic shaking) that potentially leads to the complete detachment of an unstable rock block due to the complete break of the rock bridge present along the pre-existent main fracture. According to Got *et al.* (2010), u_c is defined as the average displacement needed to create the fracture surface and consume the fracture energy when relaxing completely the rock mass strength. The displacement that induces general failure can be assumed as mainly horizontal and in a direction normal to the fracture.

By following the computation procedure proposed by Got *et al.* (2010), the characteristic u_c value for an unstable rock block can be assessed by the following equation [Eq. 4.3]:

$$u_c \sim \frac{G}{\sigma_t} \qquad [4.3]$$

where G is the fracture energy release rate and σ_t is the limit tensional stress of the rock mass.

The parameter G is defined as the ratio between the work dW_s needed for creating a new fracture having surface dS [Eq. 4.4]:

$$G = \frac{dW_s}{dS} \qquad [4.4]$$

and, by assuming that the rock block has a sub-horizontal movement under its own weight, G can be evaluated thought field observation by the following equation [Eq. 4.5]:

$$G \sim \frac{1}{4}\rho g \frac{e}{b} u^2 \qquad [4.5]$$

in which ρ is the rock density, g the gravitational acceleration, e and b respectively the x (thickness) and z (height) dimensions of the rock block and u the average opening of the fracture.

According to Got *et al.* (2010), the limit tensional stress σ_t of a rock mass having a macroscopic Young modulus E and containing a fracture of height b can be computed through the equation [Eq. 4.6] by Lawn (1993):

$$\sigma_t = \sqrt{\frac{EG}{\pi b}} \qquad [4.6]$$

where E can be assessed by Equation 4.2.

Table 4.1 summarises the characteristic values of u_c computed for the three different unstable rock blocks that evidenced marked features of linearity and polarization of the particle motion at the Selmun Promontory. The first rock block represents the whole zone B; the other two blocks are related to the internal and the external blocks composing the zone D that can be considered as two separated elements since the different polarized frequency resulted by the analysis (Fig. 4.6). Some parameters related to the UCL features were considered invariable between the three blocks: a E value of $1.15*10^9$ was computed according to Equation 4.2, while a ρ value of 2146 kg/m^3 was assumed by laboratory tests. On the other hand, the values of e (thickness) and b (height) of the rock blocks as well as the value of u (average opening of the fracture) were derived by the engineering geological model (Figs 3.5 and 3.6) of the Selmun Promontory and by the field surveys (Tab. 3.1). Table 4.1 evidences as a major displacement is needed to obtain the complete detachment of the rock block composing the zone B than the other two blocks.

Block	**e (m)**	**b (m)**	**u (m)**	**G (J/m^2)**	**σ_t (Pa)**	**u_c (mm)**
B	8.5	30	0.22	72.3	29668.0	2.44
D external	4	20	0.16	27.0	22202.3	1.22
D internal	6	20	0.16	40.5	27192.1	1.49

Tab. 4.1. Characteristic values of u_c computed for the three different unstable rock blocks at the Selmun Promontory.

For the Peschiera case study, the analysis seismic ambient noise measurements both by the HVSR analysis and by the polarization analysis allowed to define three different seismic responses related to the three parts of the slope, as evidenced in the previous Ph.D. thesis sections (Subparagraphs 4.1.1 and 4.1.2).

As a matter of fact, the central part of the complex landside is characterised by a 1D resonance effect at 4 Hz, evidenced by a peak in the HVSR(f) function. Such a peak does not show evidence of polarization, therefore it can be associate to the resonance effects in a surface layer having lower seismic velocity, as a debris slope deposit or an already occurred landslide deposit. The existence of a resonance frequency have to be considered for slope stability analysis because its interaction with seismic waves can induce a mobilisation or a reactivation of the resonant mass.

On the other hand, in the Eastern part of the Peschiera Spring Slope, it was possible to observe a peak in the HVSR(f) function at 7 Hz, characterised by effects of linearity and polarization of the particle motion. Such features could be related to the vibrational behaviour of an unstable rock mass, as evidenced by the results obtained at the Selmun Promontory as well as in other studies already published, e.g. Burjánek *et al.* (2010, 2012) and Moore *et al.* (2011) in Swiss Alps and Galea *et al.* (2014) at Anchor Bay.

The Western part of the Peschiera Spring Slope is characterises by the absence of both linearity and polarization of the particle motion. Such features could be related to the slow and constant deformation involving this portion of the slope, evidenced by the stress-strain monitoring system (Martino *et al.*, 2004; Maffei *et al.*, 2005), that probably does not generate particular marker in the seismic response. However, the Western and the Southern part of the slope are interested by deep collapse of underground cavities due to major karst dissolution, mainly focused below the groundwater level (Fiorucci *et al.*, 2017). Such processes are monitored by the SNS array, whose results will be exposed in the following section of the thesis (Paragraph 4.2).

The results obtained by the seismic noise measurements carried out on the Peschiera Spring Slope evidence some specific features of its seismic response, but the few measurements available do not allow to produce a detailed definition of the landslide susceptibility. A higher distribution of measurement points would be needed for obtaining a complete and reliable characterisation of the seismic response on the Peschiera Spring Slope.

4.2. Results of microseismic event monitoring

The present section is focused about the exposition of the results obtained by the analysis of the SNS records carried out at the two case studies. The recoded seismic data were analysed by the two main tools of the NanoseismicSuite software (www.nanoseismic.net): SonoView for detection of microseismic events and HypoLine for their characterisation (i.e. epicentre, hypocentre and magnitude assessment). A detailed explanation of such tools can be found in the Subparagraph 2.3.1, while an introduction of the SNS array measurements carried out in both case studies is presented in Subparagraph 3.3.2.

4.2.1. Detection and location of microseismic events

For the Selmun case study, the screening through SonoView of the data recorded by the array SNS1 did not allow to detect microseismic events, as already mentioned in Subparagraph 3.3.2. On the contrary, a few microseismic events were recorded by the array SNS2 (Fig. 4.10) that was installed subsequently and in a position closer to the unstable slope cliff zones. Unfortunately, one of the outer stations (i.e. station S1E) of the array did not work properly, therefore the characterisation and the location of such events by only 3 stations was more difficult and less precise.

First, several induced rockfall were recorded. The induced rockfall events were produced on October 10th 2016 by a controlled release from the edge of the plateau of rock blocks having dimensions of 25-40 cm. Such events were induced both for checking the recording reliability of the array SNS2 and for fixing a subsoil model in HypoLine, since they are characterised by a known origin in time and space. By changing the subsoil properties in the software, the best fit between modelled and real locations was obtained with a homogeneous half-space model having a P-wave velocity of 0.8 km/s and a standard V_P/V_S ratio of 1.73. Such seismic wave velocity values are in good agreement with those available in the literature (Farrugia *et al.*, 2016, 2017). Induced rockfall events show a duration of 1-3 s and have a frequency content focused between 5 and 180 Hz (Fig. 4.11). The M_L values for such events ranges from -2.2 to -1.8.

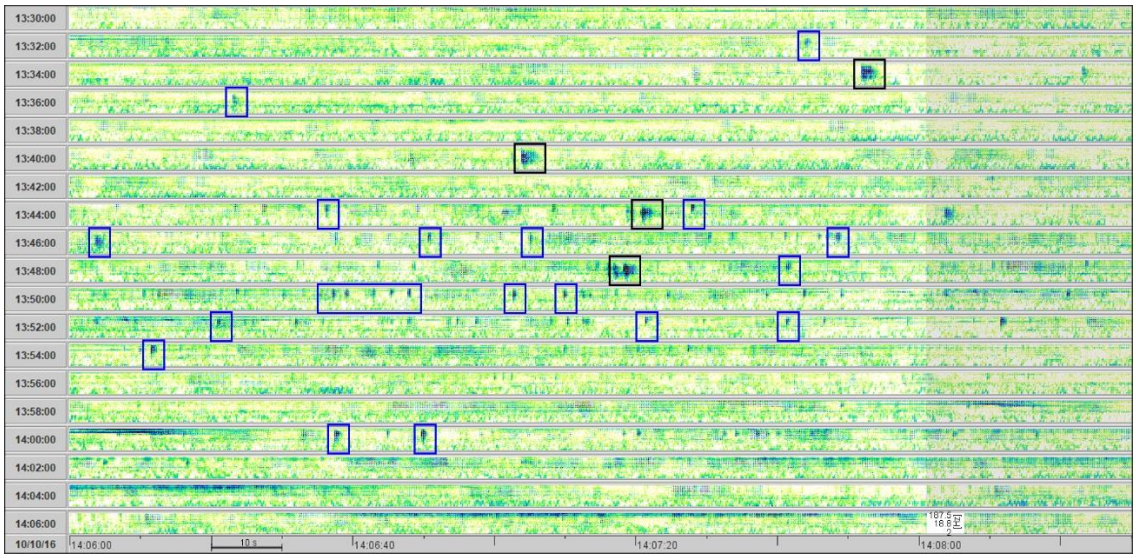

Fig. 4.10. Supersonogram from 13:30 UTC to 14:08 UTC of October 10th 2016 obtained at the Selmun Promontory by the SNS array; the black frames indicate induced rockfalls, the blue frames indicate collapses.

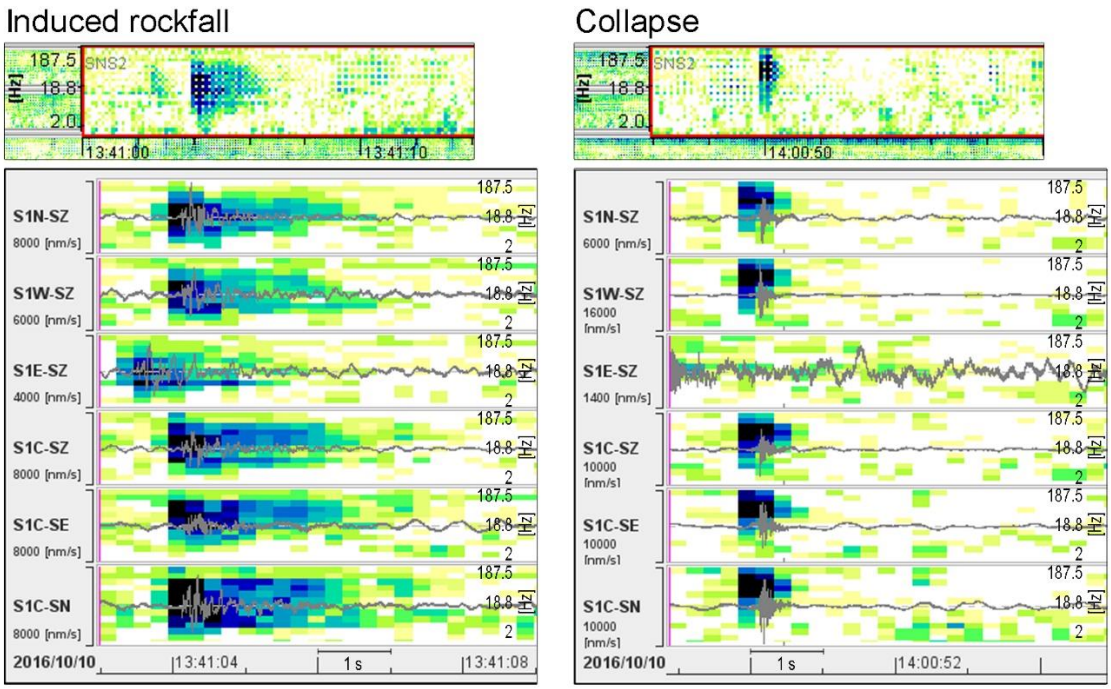

Fig. 4.11. Supersonogram (top), sonograms and over-layered time histories (bottom) of the two types of events recorded at the Selmun Promontory by the SNS array: induced rockfall (left) and collapse (right), both occurred on 16/10/2016. The upper 3 traces belong to the 3 outer vertical-component stations, the lower 3 traces belong to the central 3-component station.

In addition, 20 natural microseismic events were also detected on October 10th 2016 (Fig 4.10). Such natural microseismic events are characterised by a waveform similar to the collapse events related to gravity-induced instability processes (Fiorucci *et al.*, 2016b,

2017) since they are characterised by short duration (1 s or less) and their supersonogram typically enlightens a frequency range between 5 and 187.5 Hz (Fig. 4.11). Through the previously fixed subsoil model, the hypocentre coordinates were assessed for 17 collapses by using HypoLine. Figure 4.12 shows the epicentre distribution and evidences that collapses are originated from the unstable NW edge of the cliff slope, confirming that they are related to the landslide process. The M_L of collapses recorded at Selmun varies between -2.2 and -1.8. By the physical characterisation analysis, PGA_h and PGA_v values of collapses result between 10^{-4} and 10^{-3} m/s^2, while AI_h varies from 10^{-9} up to 10^{-8} m/s and AI_v ranges between 10^{-10} and 10^{-8} m/s.

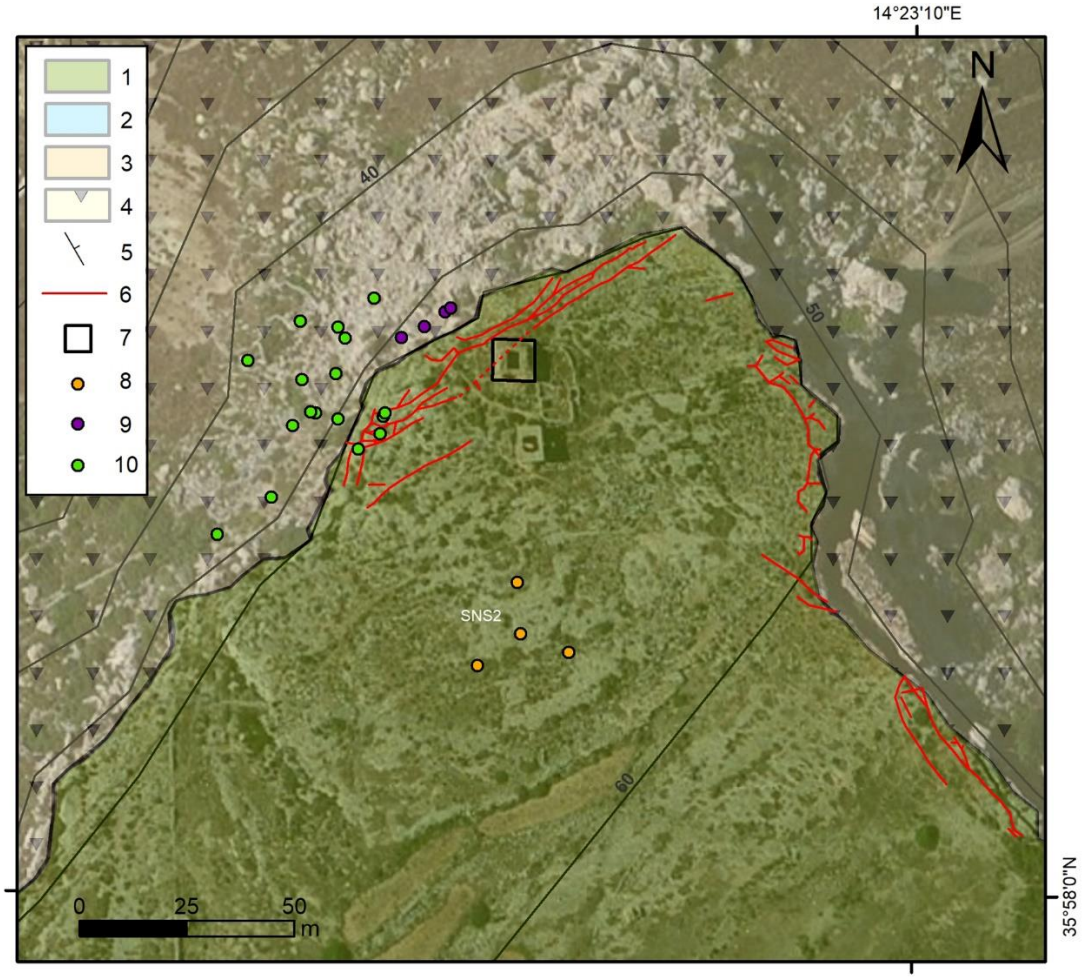

Fig. 4.12. Satellite view of the Selmun Promontory showing: 1) UCL; 2) BC; 3) GL; 4) debris slope deposit; 5) attitude of strata; 6) fracture (the dashed line represents an inferred fracture); 7) Għajn Ħadid Tower; 8) SNS array station; 9) induced rockfall epicentre; 10) collapse epicentre. Elevation is given by contour lines (m a.s.l.).

For the Peschiera case study, as already observed by Lenti *et al.* (2012) and Fiorucci *et al.* (2017), two different types of microseismic events related to gravity-induced slope instability process were detected by the SNS array: failures related to rock mass fracturing and collapses (Fig. 4.13). The screening of the SNS seismic data by SonoView allowed to detect more than 700 microseismic events in 2015, of which only 16 were classified as failures while the largest part of microseismic events presented the typical waveform of collapses. Collapses were typically concentrated in specific periods (Fig. 4.14) and formed collapse crises (i.e. occurrence of at least 3 events within 24 h). As exposed by Fiorucci *et al.* (2017), 14 collapses crises were recorded in 2015, mainly between May and July 2015 and on October 2015. In this Ph.D. thesis, the characterisation was carried out for 397 events, among which all the 16 detected failures and 381 collapses grouped some crises occurred between February and July 2015, representing the period in which the maximum number of collapses occurred.

Failures are characterised by a duration of 3-7 s and their supersonograms evidence a frequency content between 5 and 200 Hz upon the first arrival of P-waves and a coda focused in a lower frequency range, typically between 2 and 50 Hz (Fig. 4.13). The computed M_L values range from -2.3 up to -1.1. The physical analysis of the recorded failures outputs that PGA_h and PGA_v range from 10^{-5} up to 10^{-3} m/s^2, while AI_h and AI_v vary between 10^{-10} and 10^{-8} m/s.

On the other hand, the collapse supersonograms allow to observe that such events typically produce a sudden increase in intensity at certain frequencies, thus revealing their paroxysmal and impulsive nature; spikes are caused by the impacts of falling rock materials. Collapses typically enlighten the whole frequency band of the supersonogram (Fig. 4.13), in a range from about 2 up to 225 Hz with broadband spikes, therefore they are characterised by a higher frequency content respect to failures. The time duration of collapses varies from less than 1 s to about 2 s. The time duration increases up to 3 or 4 s in case of collapses of higher intensity or of multiple consecutive events. M_L values for collapse vary from -2.8 up to -0.3. Considering the physical parameters obtained for collapses, PGA_h and PGA_v are characterised by values between 10^{-5} and 10^{-2} m/s^2, while AI_h and AI_v range from 10^{-11} up to 10^{-7} m/s.

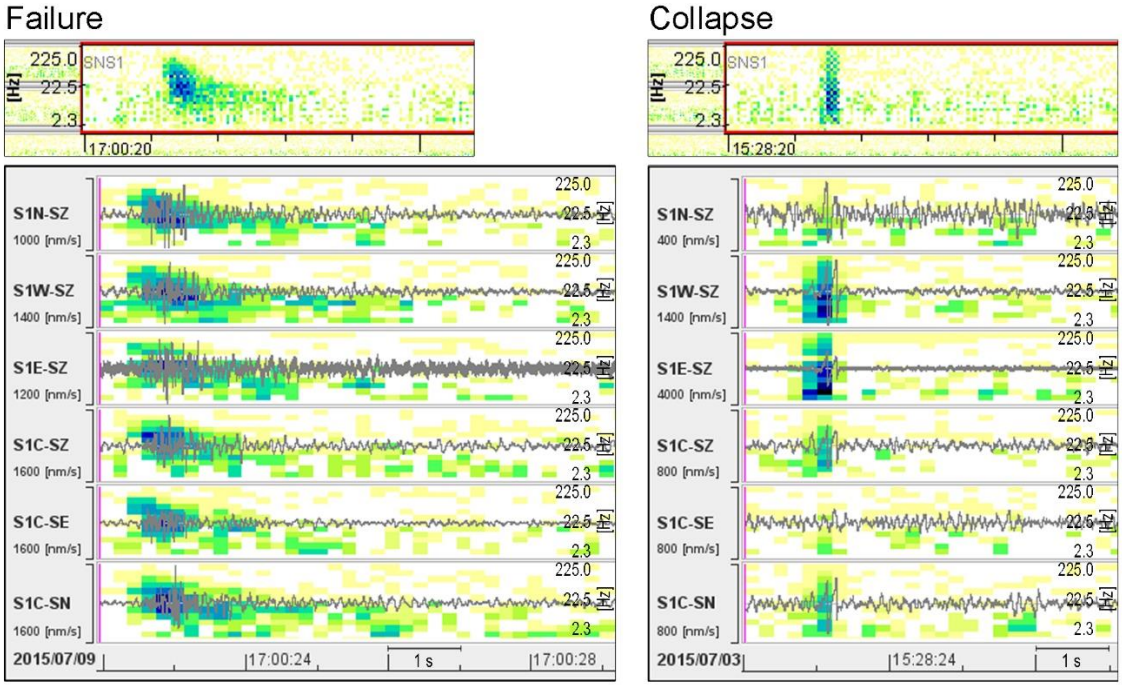

Fig. 4.13. Supersonogram (top), sonograms and over-layered time histories (bottom) of the two types of events recorded at the Peschiera Spring Slope by the SNS array: failure (left) occurred on 09/07/2015 and collapse (right) occurred on 03/07/2015. The upper 3 traces belong to the 3 outer vertical-component stations, the lower 3 traces belong to the central 3-component station.

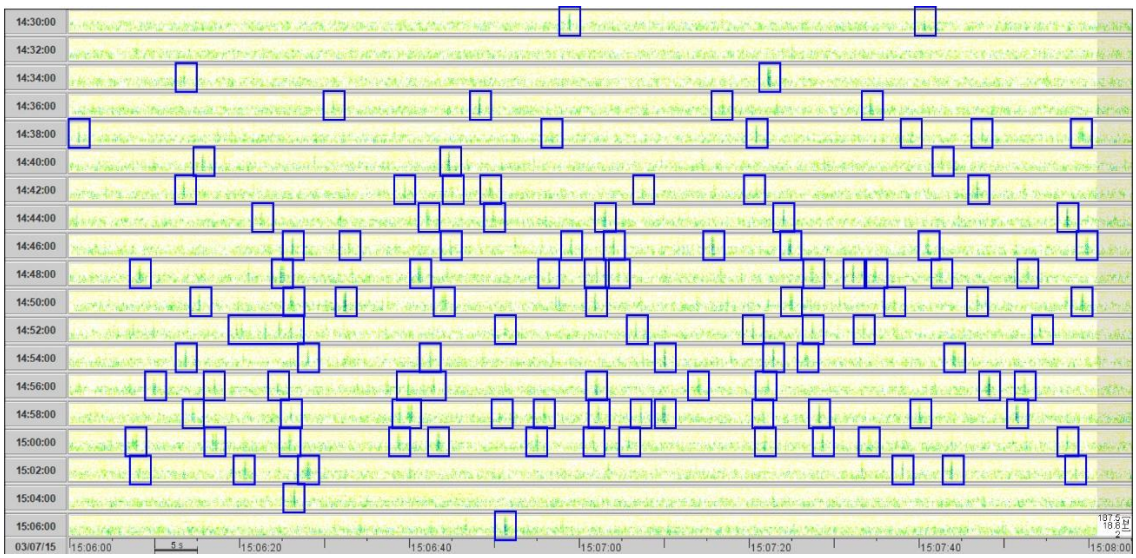

Fig. 4.14. Supersonogram from 14:30 UTC to 15:08 UTC of July 3rd 2015 obtained at the Peschiera Spring Slope by the SNS array; the blue frames indicate collapses.

In HypoLine, a simplified model of homogeneous half-space having P-waves velocity of 2.6 km/s and S-waves velocity of 1.5 km/s was applied for obtaining the epicentre and hypocentre coordinates for each microseismic event. The seismic wave

velocity values were attributed based on geophysical investigations performed on the slope and within the drainage plant by ACEA S.p.A and an analogous subsoil model was validated by Fiorucci *et al.* (2017).

Figure 4.15 shows the epicentre distribution of the events analysed at the Peschiera Spring Slope. By analysing the epicentre distribution of the failures, they result mainly concentrated on the faults that traverse the slope, in particular near to the Fiamignano-Micciani Fault, while few events are localised along landforms as trenches and subvertical scarp. On the other hands, collapses seem to be focused in a specific part of the rock mass that is located in the Southern portion of the slope. By considering the landform distribution, currently such slope portion seems to be in an early stage of deformation process and is located just behind the portion of the slope at a mature stage, characterised by a constant deformation.

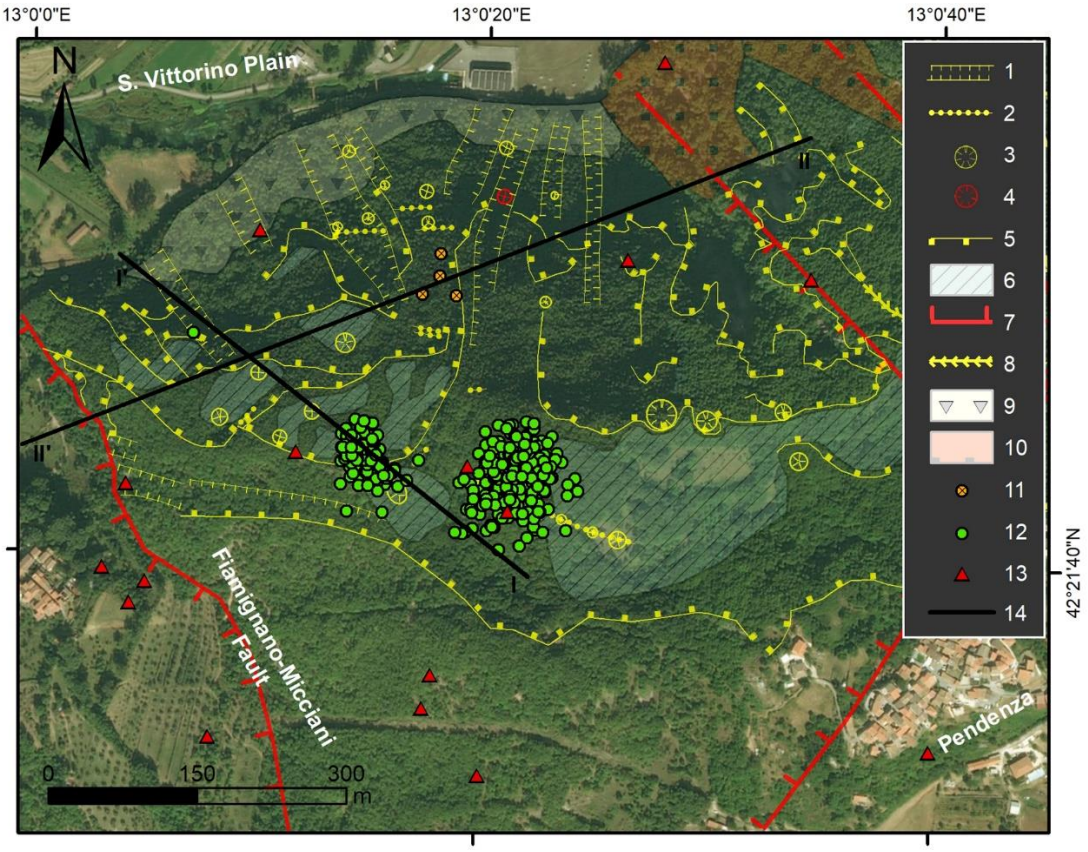

Fig. 4.15. Satellite view of the Peschiera Springs Slope showing: 1) trench; 2) tension crack; 3) sinkhole; 4) 1997 collapse of sinkhole; 5) scarp; 6) karstified flat; 7) fault; 8) gully; 9) slope debris; 10) debris fan deposit; 11) underground SNS array station; 12) collapse epicentre; 13) failure epicentre; 14) cross-section (see Fig. 4.16).

According to Walter *et al.* (2012b), for microseismic events the accuracy of hypocentre localisation can be assumed as about 10% of the epicentral distance. Since the hypocentral uncertainty depends to the distance from the origin to the array stations, it varies from 5 up to 25 m for collapse events but it can also exceed 40 m for the fairest failures.

Figure 4.16 reports the hypocentres of microseismic events projected in two geological cross-sections (see Fig. 4.15) and in a 3D model of the Peschiera Spring Slope derived by the LIDAR radar remote survey of 2007. Several observations can be possible by analysing the distribution of the hypocentre depths respect to the groundwater level, that had a mean quote of about 420 m a.s.l. during the analysed period. Failure hypocentres were obtained between 460 and 290 m a.s.l., with a mean quote at about 350 m a.s.l.; however, only 3 events occurred above the groundwater level against the other 13 ones that had origin below the groundwater level. On the other hand, all the collapses hypocentre resulted below the groundwater level. As a matter of fact, the origin point of collapses were assessed at a depth between 420 and 360 m a.s.l., with a mean quote at about 375 m a.s.l.

Such a hypocentre variation evidenced as collapses occurred in a concentrated layer below the groundwater level, other than in specific zones of the rock mass, while failure occurrence seems not to be directly related to the karsts aquifer hosted into the Peschiera Spring Slope. As shown in Subparagraph 3.3.2, a direct relationship between the groundwater level variations and the collapse occurrence were already evidenced by Fiorucci *et al.* (2017). As a matter of fact, the accelerometric network detected the most of the collapse crises and, therefore, the maximum number of collapses during the period in which the Peschiera Springs discharged the maximum daily total values of water (i.e. September 2011, June-July 2014 and June-July 2015). The high values of water discharge probably reflect an increase of the pore water pressures into the karst aquifer hosted into the slope, that can influenced the stress field in the rock mass. The hypocentre depths of the recorded collapses are localised in a depth in which Maffei *et al.* (2004) evidenced the presence of tensile stresses into the aquifer, that aid karst dissolution and induce the formation of cavities. In summary, the results obtained by the SNS array in this Ph.D. thesis confirm the hypothesis of a strict relation between the occurrence of collapses and the groundwater action into the rock mass.

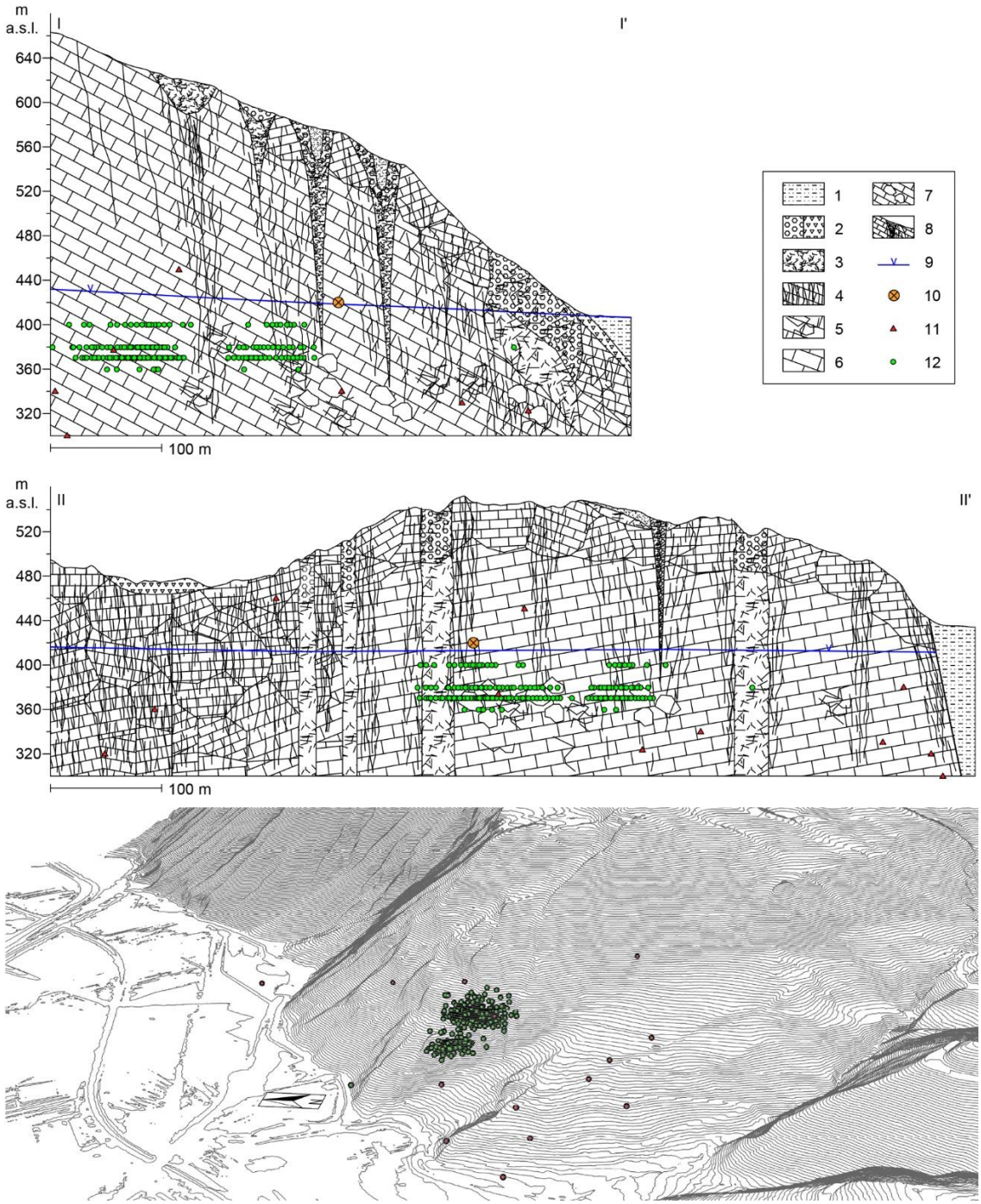

Fig. 4.16. Location of event hypocentres at the Peschiera Spring Slope: **top** geological cross-sections (see Fig. 4.15): 1) alluvial deposits of the San Vittorino plain; 2) trench and slope debris; 3) intensely jointed rock mass; 4) concentration of failures in the rock mass; 5) dislodged rock mass; 6) rarely jointed rock mass; 7) underground caves in the aquifer; 8) sinkhole; 9) groundwater level; 10) central station of the SNS array; 11) failure; 12) collapse; **bottom** 3D view with hypocentres of failures (red dots) and collapses (green dots).

4.2.2. Clustering of microseismic events

As evidenced in the section focused about the experimented methodology (Paragraph 3.1), a study about the spatial distribution of the hypocentre of the analysed events was carried out for trying to define clusters of microseismic events into the investigated rock masses. By assuming that all microseismic events within a cluster are originated by a same rock mass volume within the slope and, therefore, that they are related to a specific deformation process occurring at that location, each cluster can be treated as microseismic sources and characterised in terms of event magnitude and frequency. As already evidenced in Subparagraph 2.3.2, Hudyma & Potvin (2010) proposed a process of spatial clustering in deep mines of Australia and Canada for studying microseismic events induced by mining activities and their related microseismic sources.

Operatively, a first single event was taken into account and its hypocentre coordinates were compared to those of all the other events originated within the rock mass. Only the events having a hypocentre position proximal to the starting event were assigned to the same specific cluster of that microseismic event. Such a spatial clustering analysis allowed to exclude single and isolated events originated in other portions of the rock mass.

For the Selmun case study, the origin points of the analysed collapses are focused along the unstable NW edge of the cliff slope, but unfortunately the availability of only 17 collapse hypocentres did not allow to carry out a spatial clustering analysis of the recorded microseismic events.

On the other hand, for the Peschiera site the hypocentre coordinates were defined for a larger number of microseismic events, i.e. 16 failures and 381 collapses. However, failures and collapses were treated separately for the spatial clustering analysis since their different mechanisms of origin into the rock mass. Unfortunately, failures did not formed clusters due to their low number and their hypocentre dispersion into the slope. On the other hand, the clustering process of collapse hypocentres outputs a considerable result in terms of definition of clusters. As a matter of fact, 2 different clusters of microseismic events (S1 and S2) were defined into the rock mass by applying the spatial clustering analysis on the collapses occurred at the Peschiera Spring Slope during the analysed period. Figure 4.17 shows the location of both microseismic event clusters on a satellite

view of the Peschiera Springs Slope, while Figure 4.18 reports their projection in two geological cross-sections (see Fig. 4.17) and in the 3D model of the slope

Cluster S1 was defined by 278 collapses and is located in the Southern part of the slope, a zone characterised by very few landforms and, therefore, still in an early stage of deformation process. Cluster S2 was obtained by 102 collapses and its location is in the same Southern part of the slope but in a zone partially already involved in the deformation process at a mature stage, characterised by an average steady strain rate of 1 mm/y.

By considering the temporal occurrence of the analysed events, it was possible to observe a different and distinct period of microseismic activity between the two identified clusters. As a matter of fact, the collapses referred to cluster S1 occurred in five different crises between May and June 2015, while those grouped in cluster S2 in two crises on July 2015.

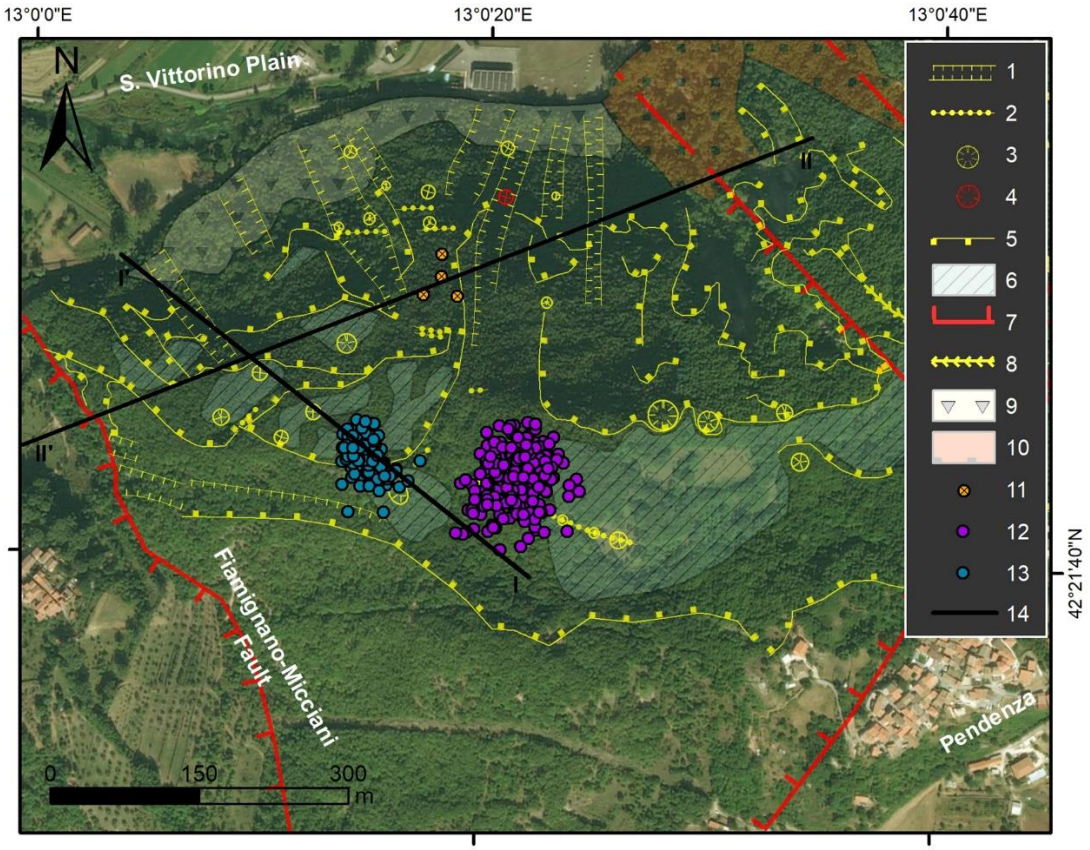

Fig. 4.17. Satellite view of the Peschiera Springs Slope showing: 1) trench; 2) tension crack; 3) sinkhole; 4) 1997 collapse of sinkhole; 5) scarp; 6) karstified flat; 7) fault; 8) gully; 9) slope debris; 10) debris fan deposit; 11) underground SNS array station; 12) collapse related to cluster S1; 13) collapse related to cluster S2; 14) cross section (see Fig. 4.18).

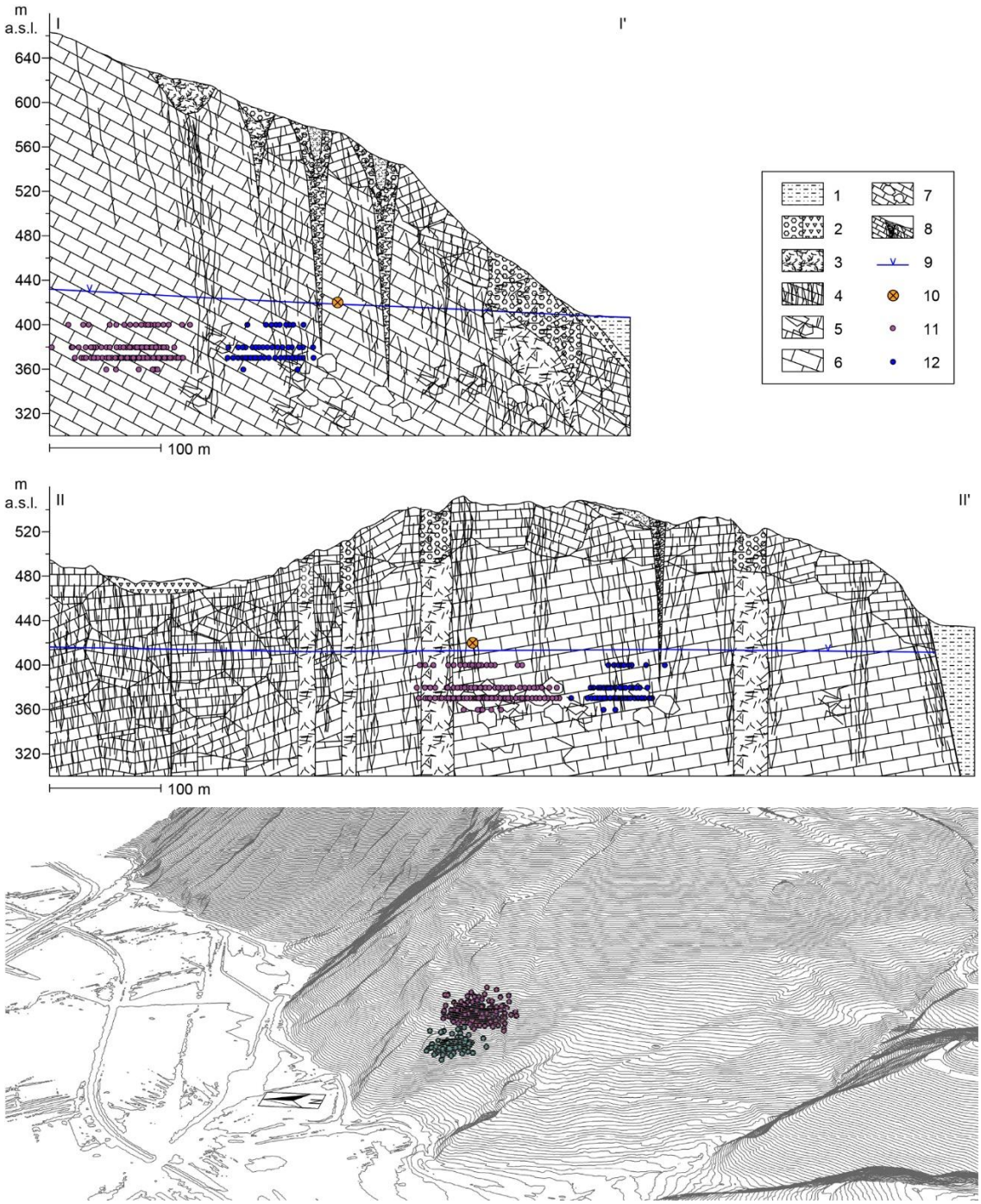

Fig. 4.18. Location of clustered collapse hypocentres at the Peschiera Spring Slope: **top** geological cross-sections (see Fig. 4.17): 1) alluvial deposits of the San Vittorino plain; 2) trench and slope debris; 3) intensely jointed rock mass; 4) concentration of failures in the rock mass; 5) dislodged rock mass; 6) rarely jointed rock mass; 7) underground caves in the aquifer; 8) sinkhole; 9) groundwater level; 10) central station of the SNS array; 11) collapse of cluster S1; 12) collapse of cluster S2; **bottom** 3D view with hypocentres of collapses related to cluster S1 (purple dots) and cluster S2 (blue dots).

Finally, the two clusters were treated as two different microseismic sources and for each of them characteristic relationships between occurrence, magnitude, acceleration and energy of collapses were defined. Figures 4.19 and 4.20 show such relationships, respectively for cluster S1 and cluster S2.

First, a relationship between frequency of events and their M_L was produced, according to the Gutenberg & Richter (1954) power law, introduced in Subparagraph 2.3.2, that considers the cumulative number of events having M_L value higher than a certain M_L. By comparing the curves obtained for cluster S1 (Fig. 4.19a) and cluster S2 (Fig. 4.20a), it is possible to observe a marked different distribution of events. As a matter of fact, cluster S1 seems to be characterised by a higher probability of occurrence of events with larger M_L than cluster S2. By shaping a linear projection of the curve from frequency-magnitude graphs for each curves, cluster S2 seems to be able to produce a collapse having M_L up to -2.0, while the already occurred single event with M_L -0.3 can be considered as the largest event that can be produced by cluster S1. However, both curves seem not to be defined enough for evaluating a stable *b* value. In particular, cluster S1 evidences a lack of events having M_L between -1.0 and -0.3 that made difficult to shape a highly reliable linear projection of the frequency-magnitude curve.

A comparison between values of M_L assessed at the origin and PGA_h recorded at the SNS array was carried out for the different events occurred both in cluster S1 (Fig. 4.19b) and cluster S2 (Fig. 4.20b). The curve related to cluster S1 evidenced that most of the recorded events are characterised by low values of M_L and PGA_h, with few and rare collapses having higher values and the exception of a single event with M_L -0.3 that produce a PGA_h at the array in the order of 10^{-2} m/s^2. On the other hand, events produced by cluster S2 are grouped almost exclusively in the field characterised by low values of both parameters.

Similar deductions can be done also by considering the comparison between PGA_h and AI_h values recorded at the SNS array for cluster S1 (Fig. 4.19c) and cluster S2 (Fig. 4.20c). Both clusters are mainly characterised by events producing low values of PGA_h and AI_h, even though cluster S1 shows few energetic events and the single more-energetic collapses characterised by PGA_h of 10^{-2} m/s^2 and AI_h of 10^{-7} m/s. In general, the most of the analysed collapses are characterised by low values of M_L at the origin that produce low values of acceleration and energy at the SNS array.

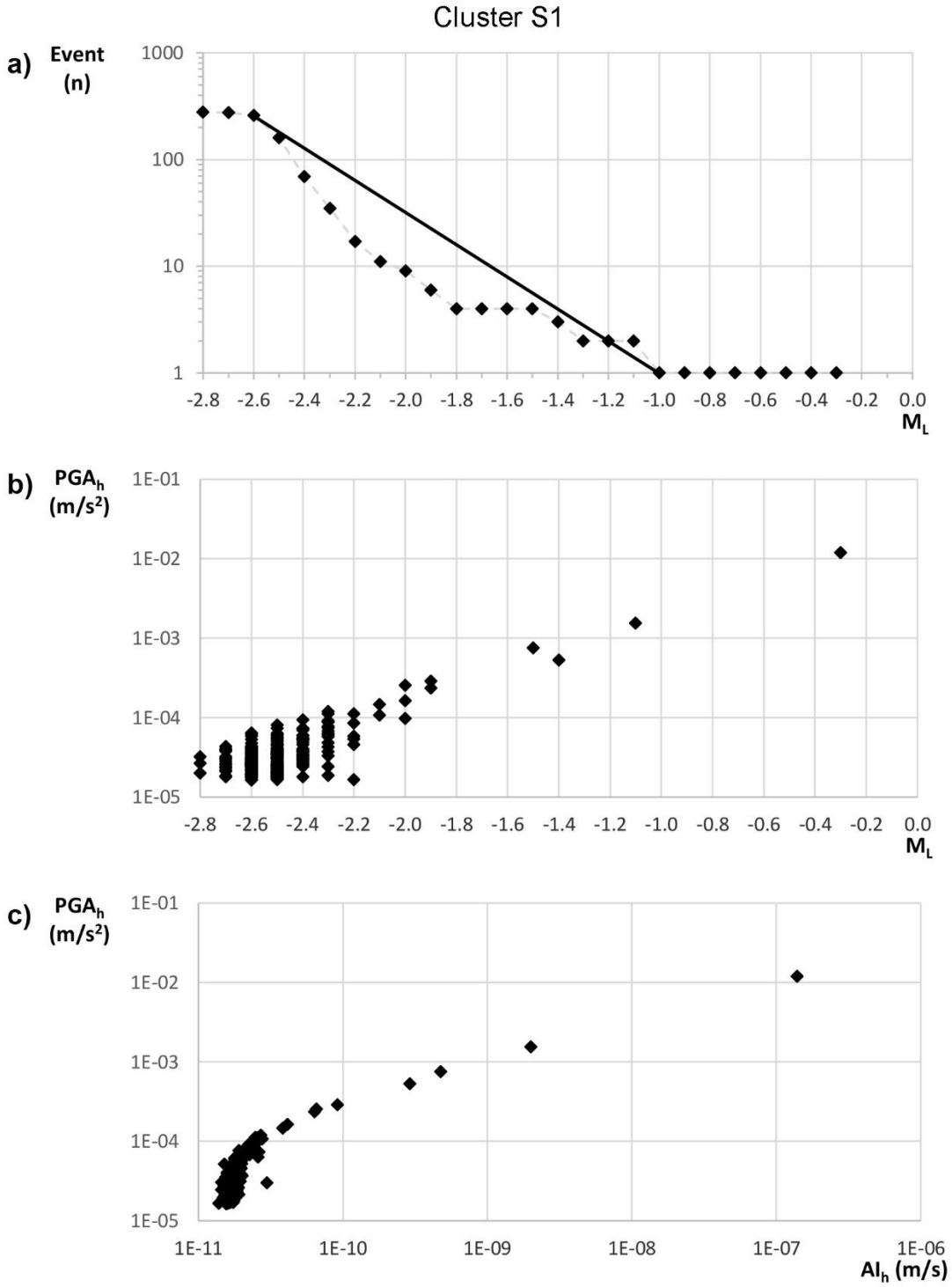

Fig. 4.19. Comparisons between event occurrence, magnitude, acceleration and energy for cluster S1 of the Peschiera Spring Slope: **a** M_L vs. number of events, according to the Gutenberg & Richter (1954) power law relation; **b** M_L vs. PGA_h; **c** AI_h vs. PGA_h.

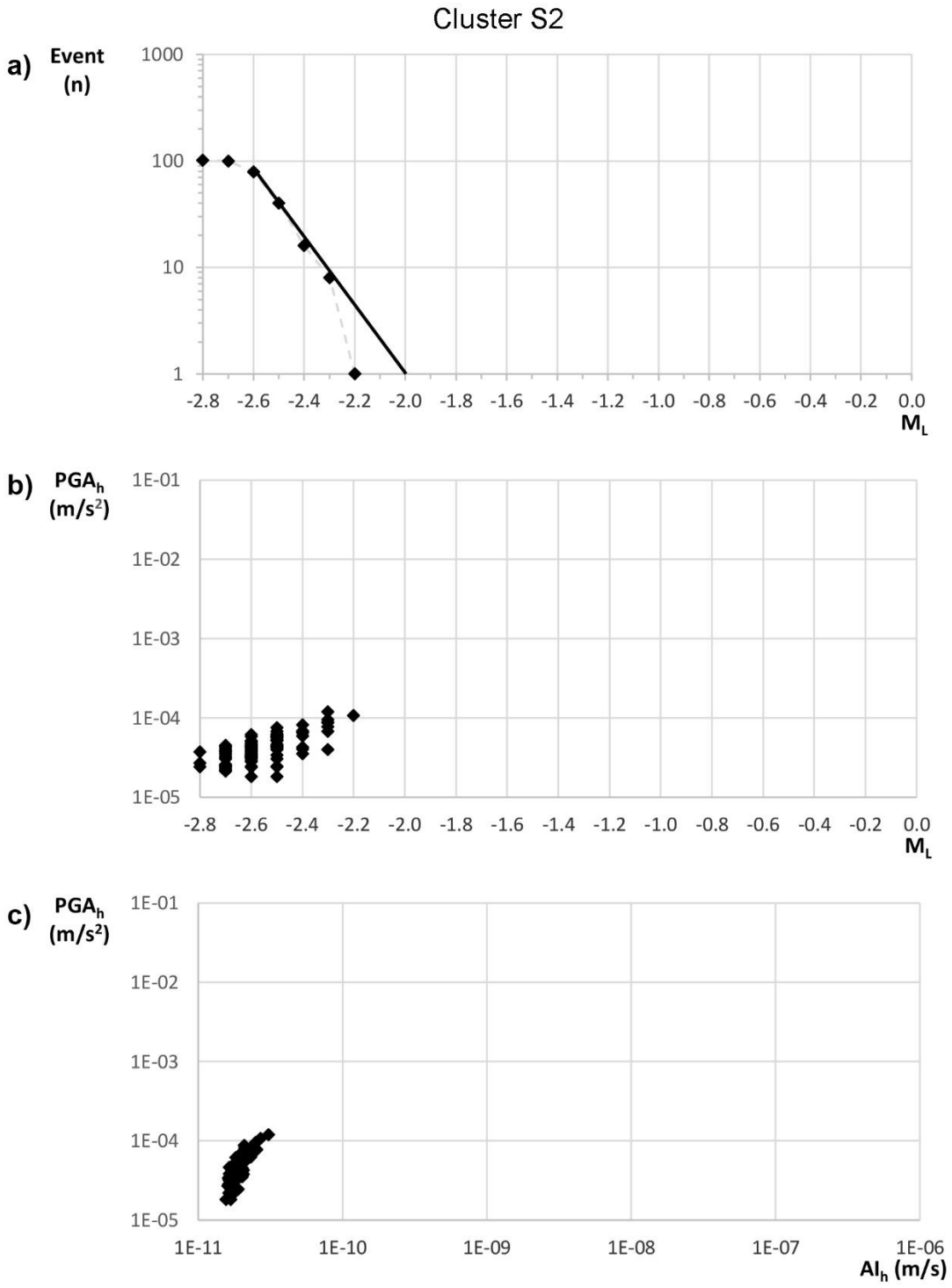

Fig. 4.20. Comparisons between event occurrence, magnitude, acceleration and energy for cluster S2 of the Peschiera Spring Slope: **a** M_L vs. number of events, according to the Gutenberg & Richter (1954) power law relation; **b** M_L vs. PGA_h; **c** AI_h vs. PGA_h.

5. Applications of passive seismic for landslide risk management

5.1. Preliminary study of seismic noise for monitoring a rock block

In the framework of strategies devoted to ensure safety of tourists, the results obtained at the Selmun Promontory can be the basis for designing a monitoring network for early warning. In this regard, the installation of permanent seismic sensors can allow to identify incipient failures that can be precursors for the collapse of some portions of the cliff slope. As a matter of fact, the analysis of continuous records of ambient seismic noise can be able to capture anomalies of the noise parameters in specific frequency ranges that could be related to an incoming detachment of the unstable rock block. Such an approach can be borrowed by earthquake engineering, where the monitoring of the main resonance frequencies of buildings and civil structures was already experimented for detecting changes in stiffness during their progressive damage (Doebling *et al.*, 1996; Kim & Stubbs, 2003; Clinton *et al.*, 2006).

As already evidenced in Paragraph 2.2, at the test site of Chamousset (Vercors Massif, French Alps) significant changes were observed in the resonance frequency of a rock block approaching to the collapse, i.e. a drop in the value of the resonance frequency (Lévy *et al.*, 2010) and a decrease in the amplitude of the base noise level (Got *et al.*, 2010). Even if it presents positive future potentialities, such a monitoring approach is still under study in the scientific community to identify and calibrate the parameters that could help to evaluate an aggravation of the stability conditions and an incipient failure of an unstable mass. An important issue is the need to filter these parameters respect the environmental conditions. In this regards, Valentin *et al.* (2017) evidenced a tremendous sensitivity of the ratio amplitude parameters of the first eigenmode frequency of an unstable rock block respect to wind conditions at the test site of Les Arches (Vercors Massif, French Alps). Instead, Bottelin *et al.* (2017) observed a variation of the amplitude peaks of the fundamental frequencies of a reinforced rock block related to temperature variations at the La Bourne test site (Vercors Massif, French Alps).

In this Ph.D. thesis, a preliminary study of long records of seismic ambient noise was carried out in the stable and unstable zones of Selmun, to evaluate the applicability of a future permanent monitoring system based on a similar approach. The aim of this preliminary study was evaluated the perspective of an approach based on the analysis of

specific seismic noise parameters in the frequency range of the eigenmode frequency of the unstable block of zone B, that could indicate changes in the vibrational behaviour of the rock block and/or to an incoming general collapse.

For this purpose, 4 stations that recorded seismic noise in continuous mode were deployed on the Selmun Promontory: 1 on the unstable block composed by zone B (SEL101) and 3 on the stable plateau area of zone A (SEL102, SEL103 and SEL104), at progressively major distance from the zone B (see Figure 3.9 for station locations). Each station was equipped by one 3-component LE-3D/5s seismometer by Lennartz and one REFTEK 130-01 datalogger set at 250-Hz sampling rate. The seismic ambient noise was recorded for about 114h, distributed in 3 different periods in 2016: i) from 15:00 UTC of September 24th to 08:30 UTC of September 26th; ii) from 09:00 UTC of September 28t^{h} to 14:30 UTC of September 29th; iii) from 16:30 UTC of October 6th to 13:30 UTC of October 8th. Different weather conditions occurred during the recording: the first campaign was characterised by weak wind in the first half and by strong wind in the second half; instead, the second campaign was characterised by strong wind and the third campaign by weak wind. Unfortunately, no quantitative weather data are available. Based on the method proposed by Got *et al.* (2010), an automated procedure was implemented on Unix platform for computing the average and the base noise level in different frequency range for each component of each records. Such a procedure is based on the use of Fortran77 and SAC codes and was designed and developed in cooperation with Antonella Paciello, researcher at Research Centre Casaccia of ENEA.

Such an automated procedure works in the time domain. After a pre-processing step in which the records are converted in nm/s, each time history is filtered by a band-pass filter in some specific defined frequency ranges. Then, both the average amplitude value and the minimum amplitude value are computed on 20-s time windows for each filtered time history. Finally, the values of both parameters are averaged on 1-h windows and plotted respect the time for obtaining a rate and analysing their variations.

For the Selmun Promontory, four frequency ranges were chosen based on the results obtained by the 1-h seismic ambient noise measurements: 1-2 Hz, 2-5 Hz, 5-10 Hz and 10-30 Hz. The first frequency range (1-2 Hz) is focused on the stratigraphic resonance frequency of the site (f_0). On the other hand, the second frequency range (2-5 Hz) comprises the eigenmode frequency of zone B (3.3-3.5 Hz) and could be useful for

monitoring the vibrational behaviour of the unstable block. Finally, the last frequency ranges (5-10 and 10-30 Hz) contains the medium-high frequencies.

Figures 5.1 and 5.2 show the results obtained respectively at the station on the unstable block (SEL101) and at the nearest station on the stable plateau (SEL102). First, it is possible to observe in both cases a directly variation of both noise parameters with the weather conditions, that tend to increase their values with the wind increase. Then, the frequency range 1-2 Hz seems to be the more stable than the other three frequency ranges, in both base and average seismic noise. Only at station SEL101 (Fig. 5.1), located on the unstable rock block of zone B, the frequency range 2-5 Hz shows systematically higher values in both noise parameters (i.e. minimum and average), in particular for the horizontal components. Such a result confirm the hypothesis that the polarized frequency at 3.3-3.5 Hz is related to the vibrational behaviour of the rock block and that rock block is characterised by a prevalent sub-horizontal oscillation.

The results obtained by this preliminary study of long seismic noise measurements at the Selmun Promontory seem to confirm the opportunity to monitor an unstable block by analysing the time variation of noise parameters in the frequency range of its eigenmode. In particular, the performed analysis confirmed the sensitivity of the first eigenmode frequency of an unstable rock block respect to wind conditions, already observed by Valentin *et al.* (2017). Such a result evidences the importance of test sites at real scale of unstable rock slope and, in this regard, the Selmun Promontory can represent a significant site where a similar monitoring approach can be tested starting from the consistent results obtained by this preliminary analysis.

In future perspective, several improvements could be needed before carrying out a permanent monitoring at the Selmun Promontory, as the implementation of an analysis devoted to obtain noise parameters in the frequency domain and the addition of a system aimed to record weather parameters to measure the variations of the environmental acting forces (i.e. wind, temperature and rain). After that, a detailed study about the time variation of noise parameters in time and frequency domains can be carried out to define their rates evidencing changes in the vibrational behaviour of the unstable rock block, that could be precursors of collapse. However, the obtained v values of the base noise level will be used for trying to assess the landslide hazard in terms of probability of exceedance and implement a landslide hazard matrix for the Selmun case study (Chapter 6).

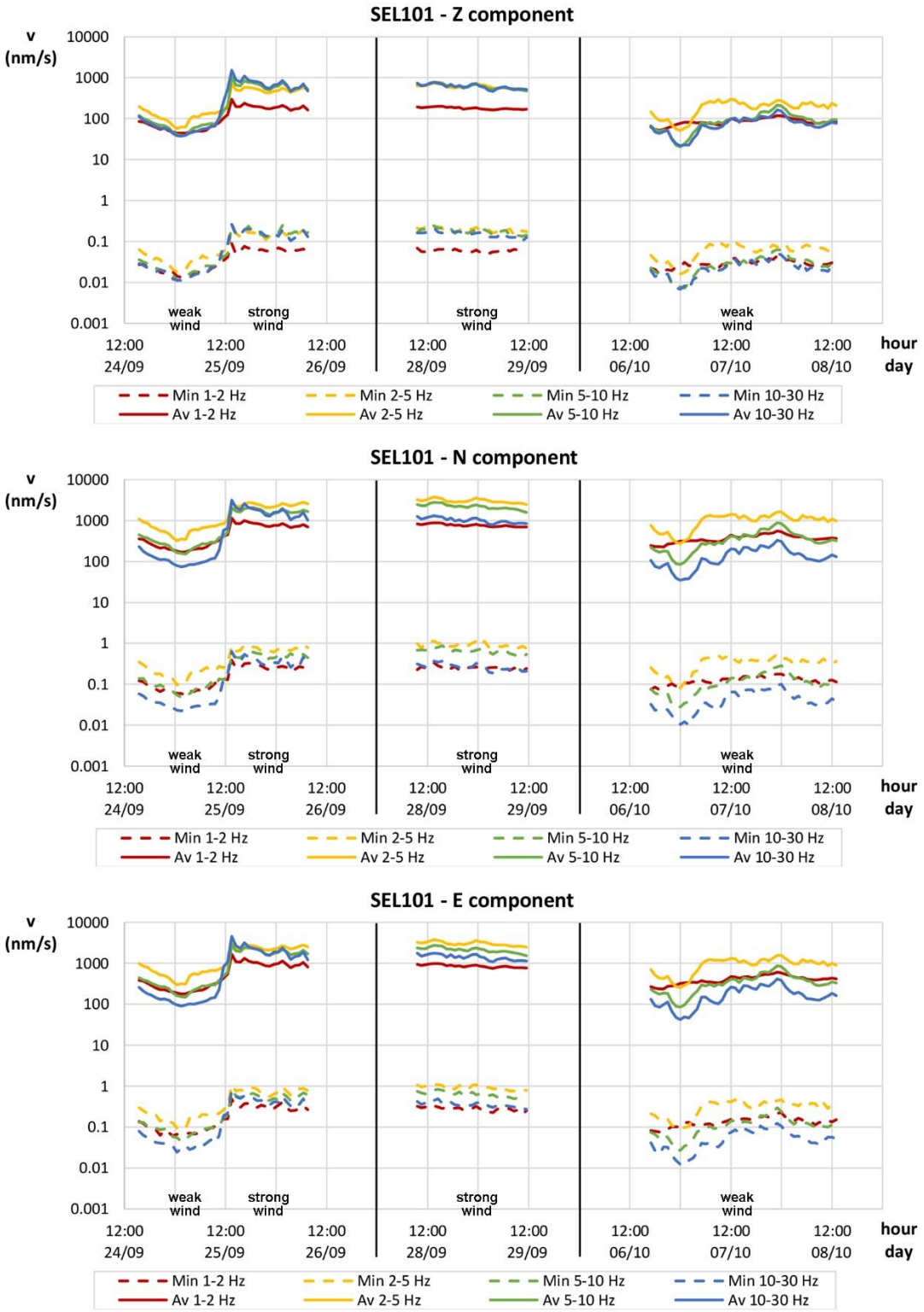

Fig. 5.1. Variation of base seismic noise level and average seismic noise level for four frequency ranges at station SEL101 (see Figure 3.9 for location) of the Selmun Promontory.

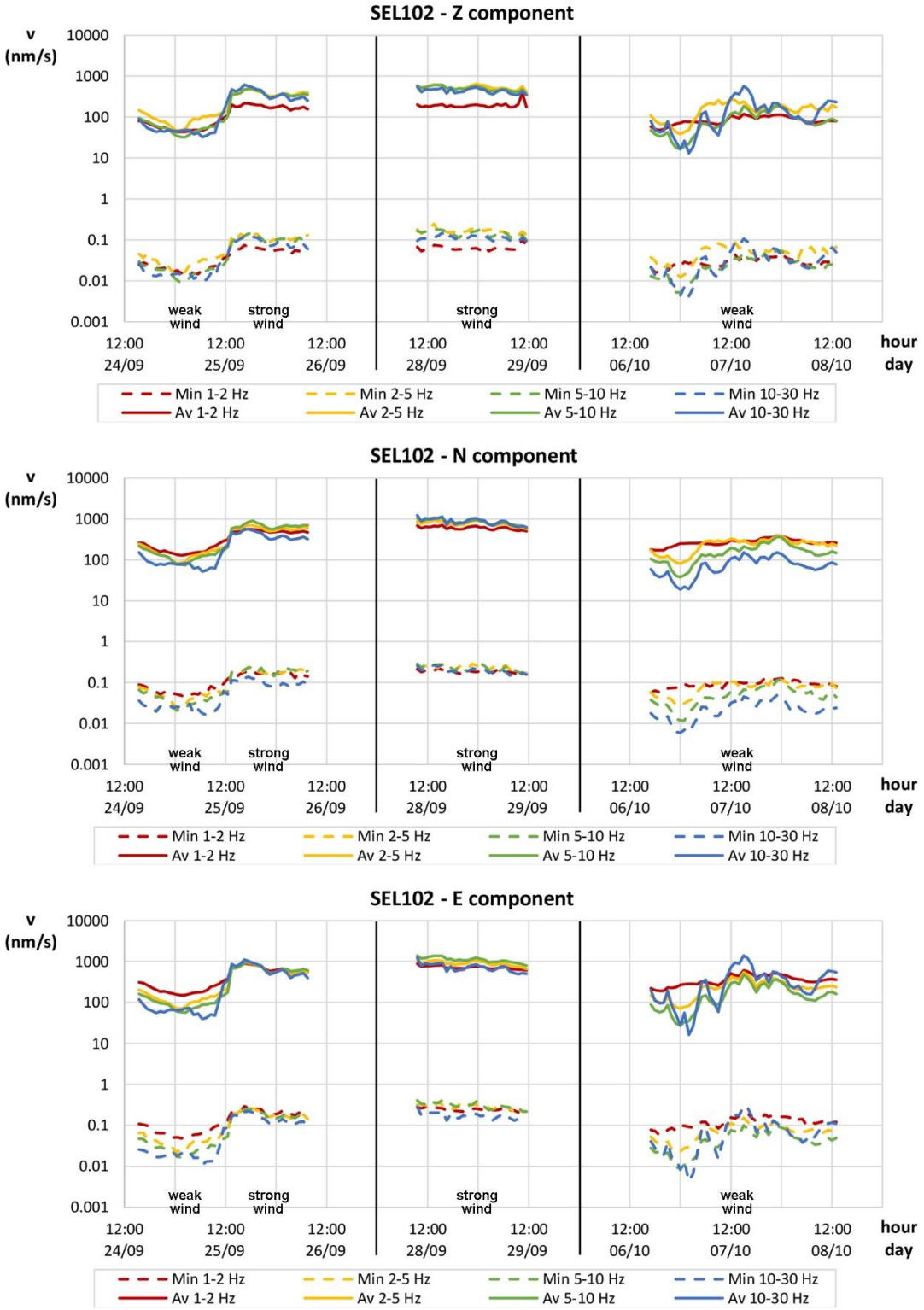

Fig. 5.2. Variation of base seismic noise level and average seismic noise level for four frequency ranges at station SEL102 (see Figure 3.9 for location) of the Selmun Promontory.

5.2. Monitoring of microseismic events by a 3D seismic network

As evidenced in the previous Subparagraphs 4.2.1 and 4.2.2, the nanoseismic monitoring technique resulted a very important tool for investigating gravity-induced instability in terms of definition of active rock mass volumes that originate microseismic events. The main advantage of nanoseismic monitoring is that it allows to detect and to locate also very weak events, providing the most-complete characterisation of microseismic events produced by a single source. On the other hand, the event characterisation is a very time-consuming procedure because each microseismic event have to be manually located by an operator after a visual screening of long continuous-recording seismic data, therefore it cannot be automated. Such a disadvantage is an important limit for applying nanoseismic monitoring in a context in which an early warning is required, as for managing the landslide risk in a strategic infrastructure as the drainage plant hosted into the Peschiera Spring Slope.

In the light of the obtained results and by considering the different seismic monitoring systems installed at the Peschiera site, a procedure for managing the landslide risk threating the drainage plant was implemented in the framework of this work. Such a procedure is devoted to integrate the methods of analysis provided by the two independent available seismic monitoring systems: the SNS array and the accelerometric network, that is composed of 7 sensors of which 4 underground (C6, F1, C1 and GA) and 3 on the slope surface (VC6, VC1 and VGA). Contrary to the SNS array, the accelerometric network is not able to detect also the weakest events but is already automated for detecting and characterising of microseismic events as well as for computing a control index based on the events recorded by the 4 underground stations. As already explained in Subparagraph 3.3.2, this procedure was implemented by Lenti *et al.* (2012) and represents a fundamental tool for managing the landslide risk and controlling the safety of the drainage plant (Fiorucci *et al.*, 2015, 2016a).

The Ph.D. student developed the here-presented procedure during the six-month period (February-July 2016) that he spent at French Institute for Sciences and Technology for Transport, Development and Networks (IFSTTAR) of Marne-la-Vallée (Paris, France) in the context of the Erasmus+ Programme. The procedure is based on the one implemented by Lenti *et al.* (2012), but considering also the 3 accelerometric stations installed on the slope surface and the results obtained by the SNS array about the landslide

hazard characterisation. The final aim of such a procedure is to evaluate quickly the active volume of rock mass after the record of each microseismic event.

The use of the surface accelerometric station (VC6, VC1 and VGA) required a preliminary evaluation of their site amplification effects, evidenced also by the seismic noise measurements whose results were exposed in Subparagraphs 4.2.1 and 4.2.2. The evaluation of the amplification effects was carried out by selecting a set of 15 earthquakes with origin far than 40 km from the slope between all the events recorded by the network (Tab. 5.1). Such earthquakes were chosen because their attenuation inside the slope is negligible than the attenuation in the path between the origin and the slope.

Day	UTC time	Source	Lat	Long	Depth (km)	M	Distance (km)
26/03/2014	02:59:17	Martani	42.789	12.536	6.7	3.0	60.9
01/04/2014	22:51:10	Martani	42.781	12.544	7.2	3.1	58.9
02/04/2014	02:10:48	Martani	42.789	12.527	6.7	3.1	61.3
15/04/2014	08:10:34	Colfiorito	42.975	12.912	9.1	3.3	68.1
19/04/2014	21:28:00	Gubbio	43.349	12.534	7.9	3.7	116.2
14/06/2014	08:51:50	Martani	42.669	12.548	7.2	3.5	50.9
18/09/2014	21:46:35	Norcia	42.769	13.103	9.9	2.7	46.0
24/12/2014	11:40:40	Frentani	41.707	14.956	18.0	4.0	177.4
28/02/2015	03:16:01	Fucino	41.950	13.534	10.6	4.1	63.5
18/03/2015	04:03:40	Norcia	42.718	13.048	9.9	2.5	40.0
07/04/2015	07:45:25	Tivoli	41.923	12.715	15.7	2.5	55.1
08/04/2015	14:30:13	Sibillini	42.875	13.290	7.8	3.2	61.4
08/05/2015	04:58:25	Laga	42.781	13.539	20.4	3.0	63.7
21/05/2015	09:42:11	A. Piceno	43.044	13.314	21.5	3.4	79.5
19/09/2015	07:22:00	Urbino	43.628	12.335	7.1	3.7	150.7

Tab. 5.1. Set of 15 earthquakes recorded by the accelerometric network having epicentre far than 40 km from the Peschiera Spring Slope; hypocentre, epicentre and M values were obtained by the INGV web site (http://cnt.rm.ingv.it/).

By analysing the PGA values computed through SAC for these far-field earthquakes (Fig. 5.3), it was possible to observe that the stations installed on the slope surface (VC6, VC1 and VGA) show systematically higher PGA values then the underground stations installed inside the drainage plant (C6, F1, C1 and GA).

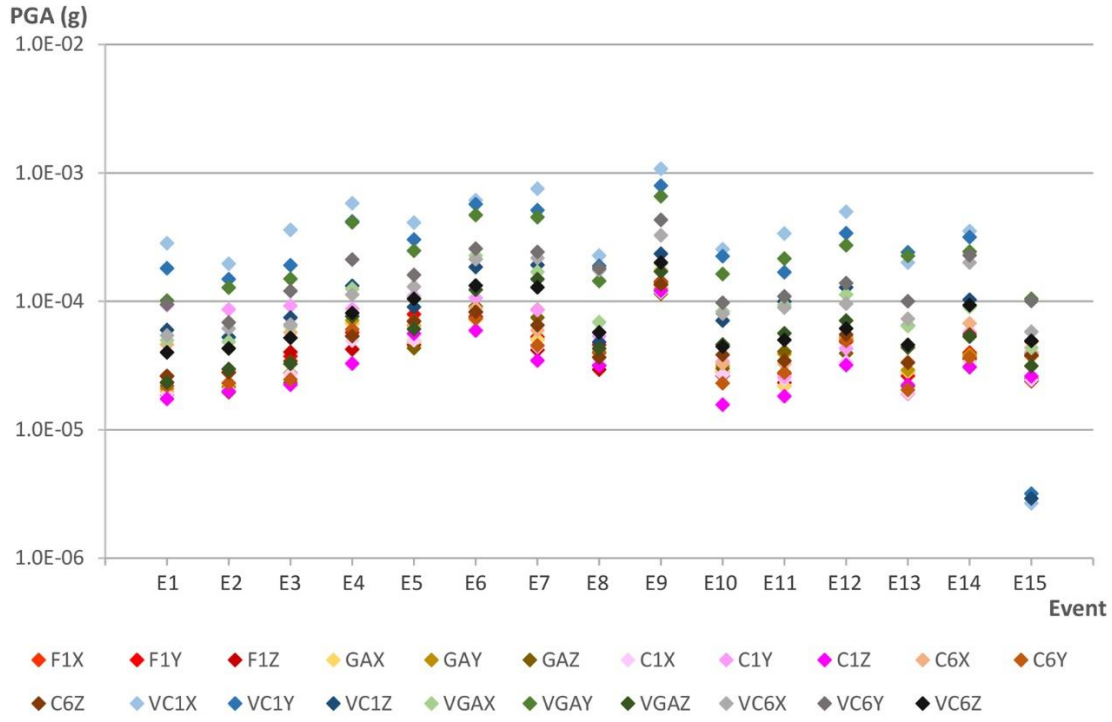

Fig. 5.3. PGA values of the 15 far-field earthquakes recorded by the accelerometric network of the Peschiera Spring Slope.

To evaluate the amplification effects, the parameter E_r was defined according to the follow equation [Eq. 5.1]:

$$E_r = \frac{PGA_{STA} - PGA_{REF}}{PGA_{REF}} \cdot 100 \qquad [5.1]$$

where PGA_{STA} represents the PGA value recorded at the considered station and PGA_{REF} the PGA value recorded at the reference station. Such parameter quantifies the percentage difference of PGA values between each station and a reference station. The term of reference station has not a seismological meaning, but here it is referred to a station that does not evidence marked amplification effects and is located in a central position of the slope. Station F1 was chosen as reference and E_r was computed for all the far-field earthquakes on homologous spatial components.

Figure 5.4 shows the variation of the E_r parameters between the several stations of the network, evidencing a not negligible PGA amplification for the stations on the slope surface and for station C1Y respect to the reference.

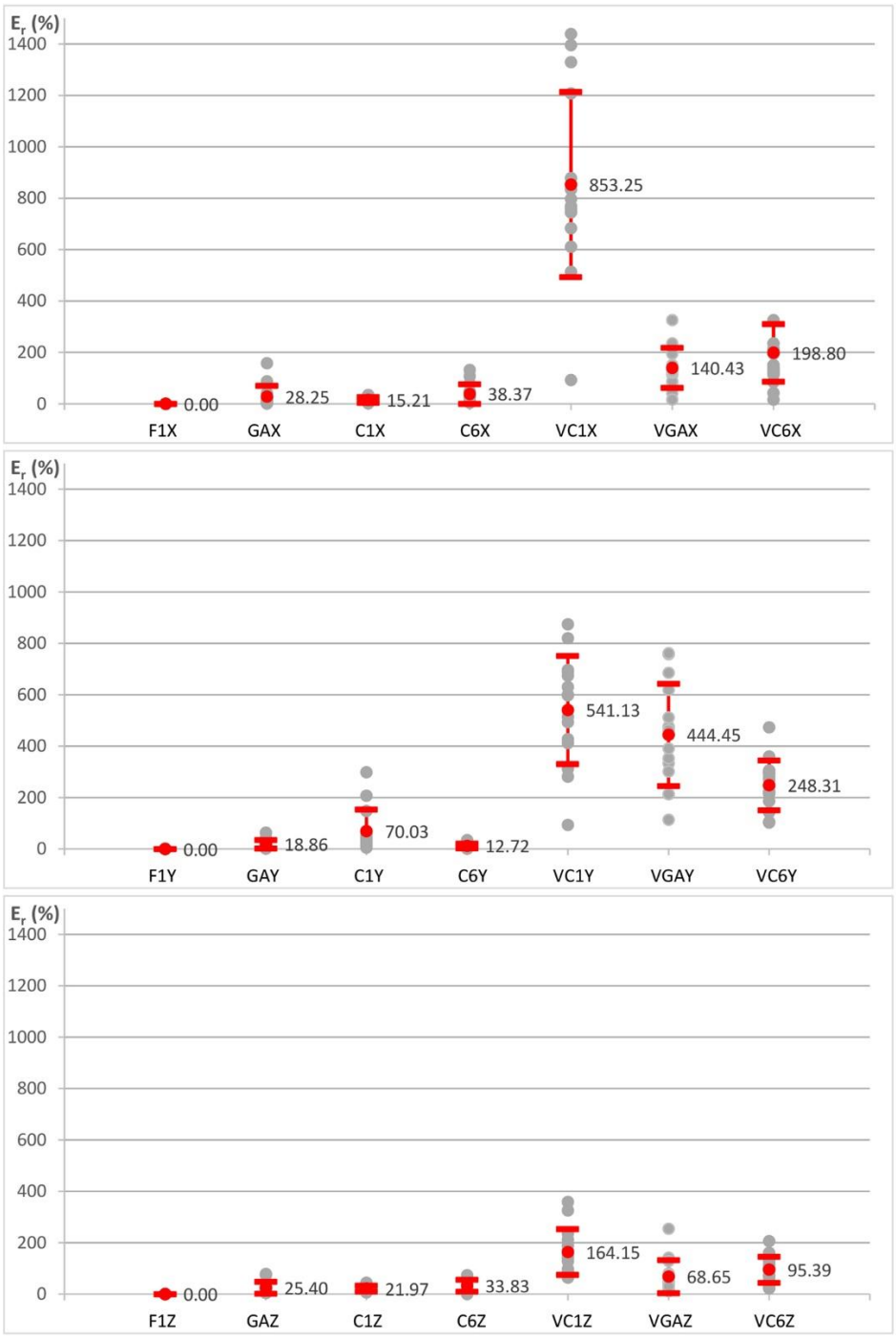

Fig. 5.4. Values (grey dots), average value (red dot) and standard deviation (red bar) of E_r computed on the 15 far-field earthquakes recorded by the accelerometric network of the Peschiera Spring Slope.

For the surface stations (VC6, VC1 and VGA), the amplification effects seem to be major for the horizontal components than the vertical ones. In fact, the mean E_r value results between 68.65% and 164.15% for the vertical components and between 140.43% and 853.25% for the horizontal components. For the underground stations (C6, F1, C1 and GA), it is possible to observe that mean E_r varies between 21.97% and 33.83% for the vertical components and between 12.72% e 38.37% for the horizontal components, except for C1Y that shows an average E_r value of 70.03%. The observations about the E_r variation confirm that the amplification affects interest mainly the surface stations, while they are negligible for the stations installed within the drainage plant.

For removing the amplification effects, a complex function called R was defined according to Equation 5.2:

$$R(\omega) = \frac{STA(\omega)}{REF(\omega)} \quad [5.2]$$

representing the ratio between the Fourier Transform of a signal recorded at a given station STA and the same signal recorded at the reference REF.

By considering a specific R_m function for each component of each station, it is possible to report to the reference station any event recorded in the considered station by the following equation [Eq. 5.3]:

$$STA_{CONV}(\omega) = \frac{STA(\omega)}{R_m(\omega)} \quad [5.3]$$

in which STA_{CONV} represents the signal reported to the reference REF by applying, in the frequency domain, the ratio between the original signal recorded at the considered station STA and its own function R_m.

By using SAC, the different R_{eq} functions were computed for each far-field earthquakes recorded at a given station [Eq. 5.4]:

$$R_{eq}(\omega) = \frac{STA_{eq}(\omega)}{REF_{eq}(\omega)} \quad [5.4]$$

and the resulted Fourier Transform were expressed as amplitude and phase [Eq. 5.5]:

$$R_{eq}(\omega) = \frac{A_{eq,STA}(\omega) \cdot e^{i\varphi_{eq,STA}(\omega)}}{A_{eq,REF}(\omega) \cdot e^{i\varphi_{eq,REF}(\omega)}} \quad [5.5]$$

that are solvable in the following form [Eq. 5.6]:

$$R_{eq}(\omega) = \left(\frac{A_{eq,STA}(\omega)}{A_{eq,REF}(\omega)}\right) \cdot e^{i\left(\varphi_{eq,STA}(\omega) - \varphi_{eq,REF}(\omega)\right)} \quad [5.6]$$

Finally, the mean R_m complex function was computed by averaging the different R_{eq} related to the 15 far-field earthquakes recorded at the station STA by the following equation [Eq. 5.7]:

$$R_m = \frac{\sum_{i=1}^{15} R_{eq,i}}{15} \quad [5.7]$$

Then, the R_m complex functions, obtained for each component of each station, were applied by a deconvolution operation to report the far-field earthquakes to the reference, according to Equation 5.3. The deconvolution operation was applied only on the signals recorded by the surface stations and for component C1Y. Figure 5.5 shows the PGA values computed by SAC on the deconvoluted time histories.

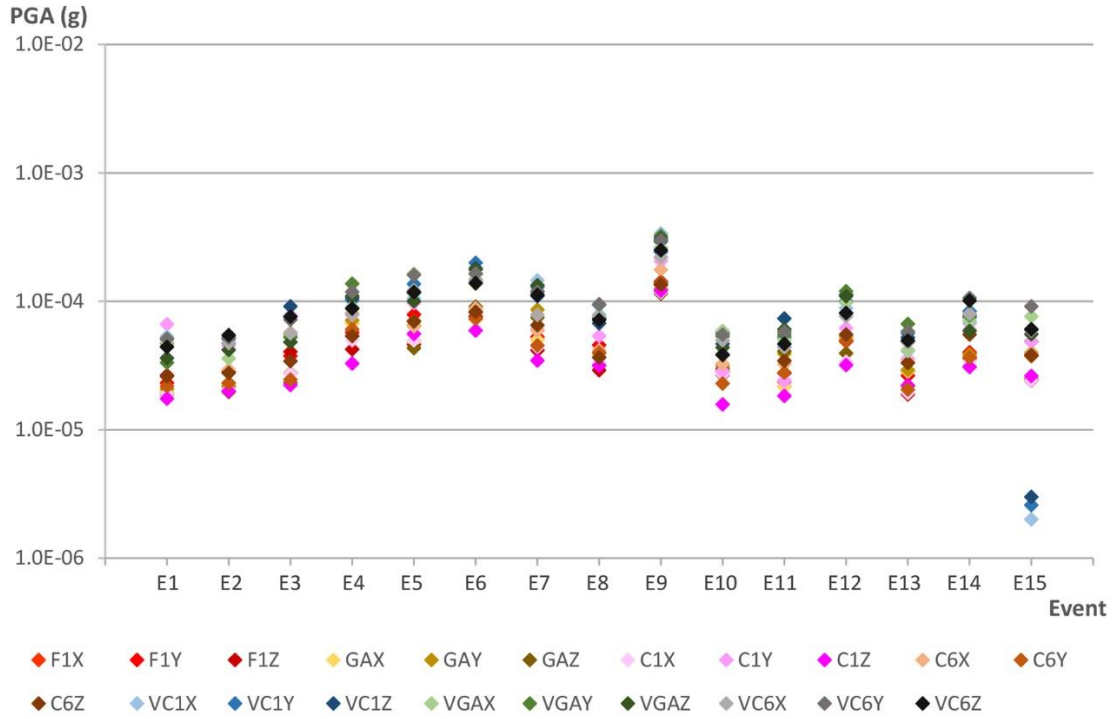

Fig. 5.5. PGA values computed after the deconvolution operation on the time histories of the 15 far-field earthquakes recorded by the accelerometric network of the Peschiera Spring Slope.

By comparing the PGA values before (Fig. 5.3) and after (Fig. 5.5) the deconvolution, it possible to observe a reduction of the amplification effects. As a matter of fact, the stations installed on the slope surface after the deconvolution show PGA values very similar to the station inside the drainage plant. In addition, the variation of the E_r parameter, defined according to Equation 5.1, seems to be very similar for all the stations after the deconvolution (Fig. 5.6), especially if compared with the values

computed on the original time histories (Fig. 5.4). As a matter of fact, for surface stations the mean E_r value computed after the deconvolution operation results between 115.45% and 130.65% for the vertical components and between 83.07% and 145.65% for the horizontal ones. Even component C1Y shows less dispersion of its mean E_r value.

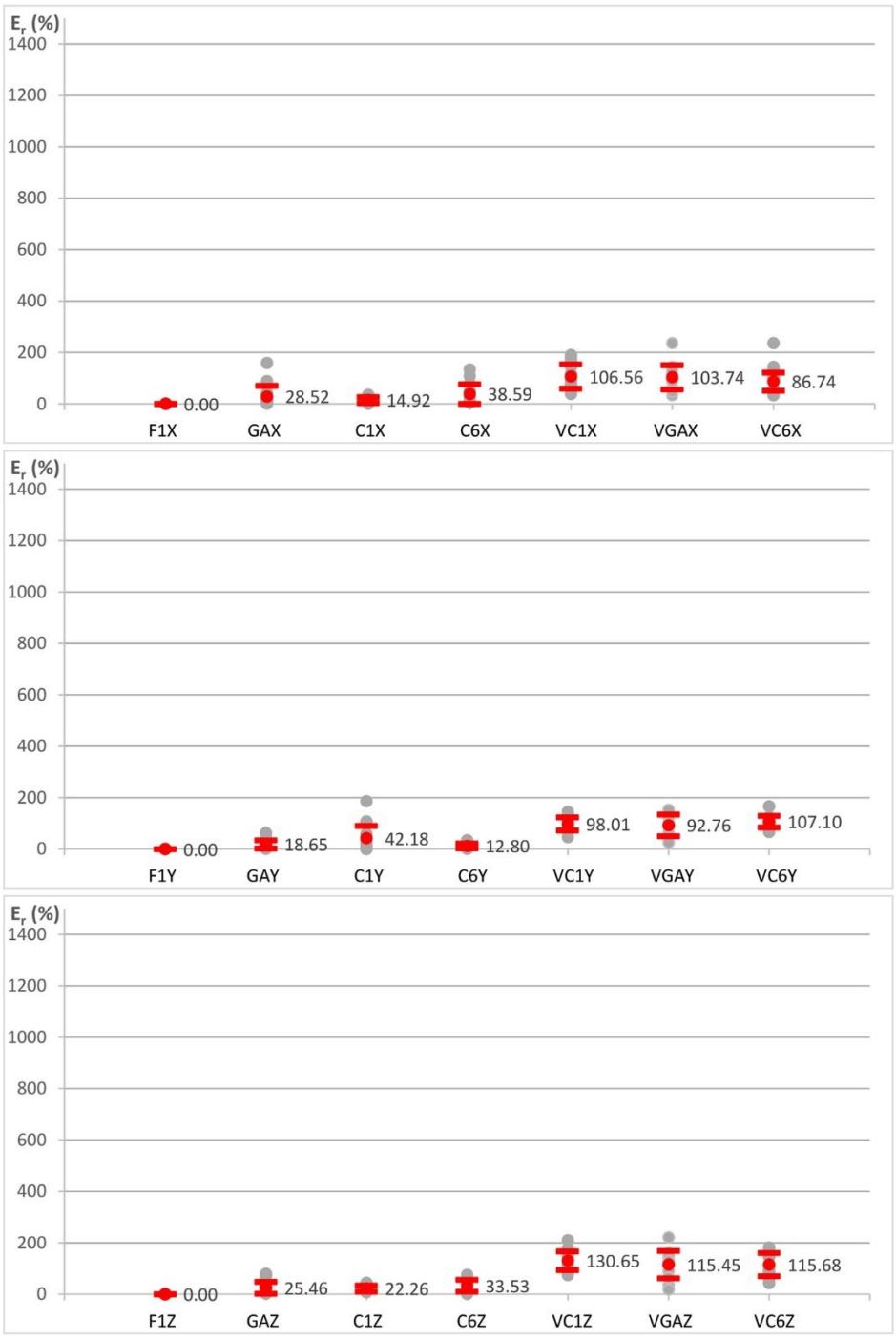

Fig. 5.6. Values (grey dots), average value (red dot) and standard deviation (red bar) of E_r computed after the deconvolution operation on the time histories of the 15 far-field earthquakes recorded by the accelerometric network of the Peschiera Spring Slope.

In the light of the positive results obtained on the analysed far-field earthquakes, the computed R_m complex functions were applied for carrying out a deconvolution on the time histories recorded by the surface accelerometric stations and by component C1Y of different types of events, e.g. near-field earthquakes, collapses and failures, obtaining not-perturbed time histories.

After the definition of functions for correcting the amplification effects at the surface stations, a procedure for evaluating the source of the events recorded by the accelerometric network was designed. Such procedure does not allow to obtain the hypocentre of the event but only the volume of rock mass from which it is originated. The procedure, implemented on Unix platform through specific scripts for SAC, MATLAB and Fortran codes, is able to distinguish the type of event and associate it with a volume of the slope based on the maximum value of PGA obtained after the deconvolution. A cross-correlation between the first-arrival times of a set of collapses did not output reliable results, probably due to the use of sensors not-aimed to record very weak events, joined to a not-sufficient sampling rate frequency of the datalogger (250 Hz) compared to the seismic wave velocity value of the rock mass (2.6 km/s for P-waves).

The procedure is explained by the flow chart of Figure 5.7. Each block has a code and its shape indicates a different kind of operation:

- rectangle for the start and the end of the procedure;
- ellipse for reading and/or writing operations;
- parallelogram for analysis process;
- rhombus for control and/or choice operations.

The input (L1) is represented by a list of *N* events recorded by the accelerometric network. The procedure starts a main cycle on the list of events for analysing each event at time. Since each event consists of 21 time histories (3 components for 7 stations), the procedure analyses one time history at time. In block A1, the amplification effects are removed by applying the previous defined R_m complex functions and three values are computed:

- PGA_{or}, representing PGA on the original time history;
- PGA_{head}, representing PGA on the original time history between 2 and 12 s;
- PGA_{conv}, representing PGA on the convoluted time history.

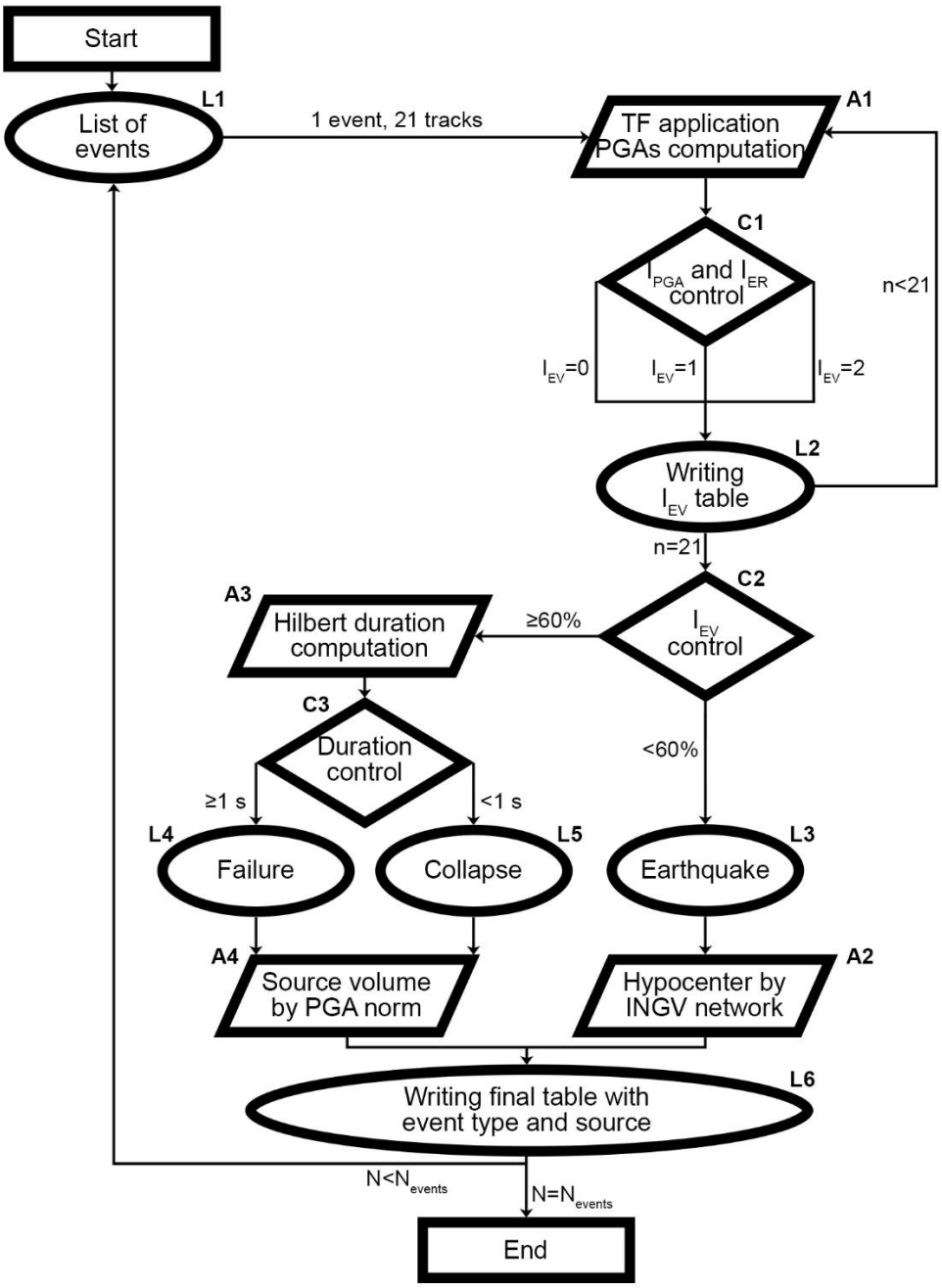

Fig. 5.7. Flow chart explains the procedure of definition of source for the events recorded by the accelerometric network of the Peschiera Spring Slope.

Based on the PGA values, two control index are assigned to the analysed time history. Index I_{PGA} depends by the ratio R_{PGA}, defined as [Eq. 5.8]:

$$R_{PGA} = \frac{PGA_{or}}{PGA_{head}} \qquad [5.8]$$

Since typically collapses are not recorded by all the accelerometric station, R_{PGA} allows to define if an event exists in the time history (I_{PGA}=1 when R_{PGA}≥1.5) or if the

time history contains only seismic ambient noise (I_{PGA}=0 when R_{PGA}<1.5). In the latter case, the time history is excluded by the subsequent analysis.

Index I_{ER} is assigned based on the parameter E_r, already defined by the Equation 5.1. Parameter E_r is computed on the time history after the deconvolution operation and indicates the difference between PGA_{conv} at that considered station and PGA_{conv} at reference station. Then, this value is compared with those obtained on the far-field earthquakes (Fig. 5.6): I_{ER} is equal to 0 if the obtained E_r value is comprised between the standard deviation range of E_r computed on far-field earthquakes, I_{ER} is equal to 1 if the obtained E_r value is not comprised.

In block C1, a value of index I_{EV} is assigned based on the other two previous indexes:

- I_{EV}=0 when I_{PGA}=0, the time history contains only seismic ambient noise;

- I_{EV}=1 when I_{PGA}=1 and I_{ER}=0, the time history is statistically in the range of E_r related to earthquakes and can be an earthquake;

- I_{EV}=2 when I_{PGA}=1 and I_{ER}=1, the time history is statistically outside the range of E_r related to earthquakes and can be an event originated within the slope.

This distinction is possible because events originated within the slope (i.e. collapses and failures) are characterised by a fast attenuation into the slope and therefore produce PGA values different between the 7 accelerometric stations. On the contrary, earthquakes are originated at distance larger than the slope dimensions, therefor their attenuation into the slope can be considered negligible compared to the attenuation occurred in the path between the origin and the slope.

The procedure carries out the previous analyses on the 21 time histories of the event, then it entries in block C2 in which all the 21 values of index I_{EV} are considered and the parameter R_{EV} is defined according to the following equation [Eq. 5.9]:

$$R_{EV} = \frac{\#2}{\#T} \cdot 100 \qquad [5.9]$$

where $\#2$ represents the number of time histories having I_{EV} equal to 2 and $\#T$ the numbers of time histories having I_{EV} equal to 1 or 2. Parameter R_{EV} allows to identify the event based on a statistic on all the 21 time histories of the event. The event is originated within the slope if R_{EV} is equal or bigger than 60%, therefore it is a collapse or a failure; the event is an earthquake if R_{EV} is less than 60%. The threshold value of 60% was tested

on a set of 15 far-field earthquakes (epicentre farther than 40 km), 16 near-field earthquakes (epicentre nearer than 40 km), 15 collapses e 16 failures, outputting a wrong solution only for 3 weak earthquakes having epicentre nearer than 5 km to the slope.

If R_{EV} is less than 60%, the procedure entries in block L3 and the event is defined as an earthquake, whose features (e.g. epicentre, hypocentre, magnitude) can be obtained by the INGV web site.

If R_{EV} is at least 60%, the procedure performs the Hilbert Transform in analysis block A3 and, then, entries in control block C3 for evaluation its duration: the event is classified as a collapse if duration is less than 1 s, while the event is classified as a failure if duration is more than 1 s. In both cases, the procedure passes to analysis block A4 for assessing the station in which occurred the greatest resentment. In such a block, the norm of the PGA_{conv} values is computed as [Eq. 5.10]:

$$PGA_{conv,NOR} = \sqrt[2]{(PGA_{conv,NS})^2 + (PGA_{conv,EW})^2 + (PGA_{conv,Z})^2} \quad [5.10]$$

where $PGA_{conv,NOR}$ the PGA norm at the station and $PGA_{conv,NS}$, $PGA_{conv,EW}$ e $PGA_{conv,NS}$ the three values of PGA_{conv} computed for the three component of motion.

At the end, the procedure writes one line on a table of output with (Fig. 5.8): i) ID of the event; ii) type of event, i.e. “ERQ” for earthquake, “COL” for collapse and “FLR” for failure; iii) source of the event, i.e. the code of the station with the maximum PGA norm or “INGV” in case of earthquake. The procedure comes back to the block L1 and re-starts the whole cycle of analyses for all the *N* events in the input list.

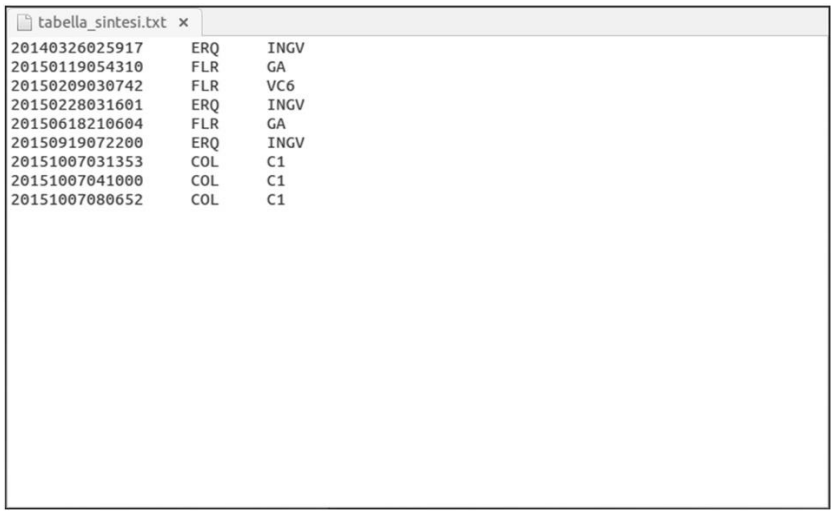

Fig. 5.8. Example of output table of the automated procedure implemented for analysing the events recorded by the accelerometric network of the Peschiera Spring Slope.

Finally, a volume of rock mass was assigned to each accelerometric station. The division of the slope in different volumes was carried out by conjoining the adjacent accelerometric stations and considering the middle point to shape a separation plane. Such rock mass volumes will be used with the hazard features of the microseismic sources to implement a landslide hazard matrix (Chapter 6) for the Peschiera Spring Slope.

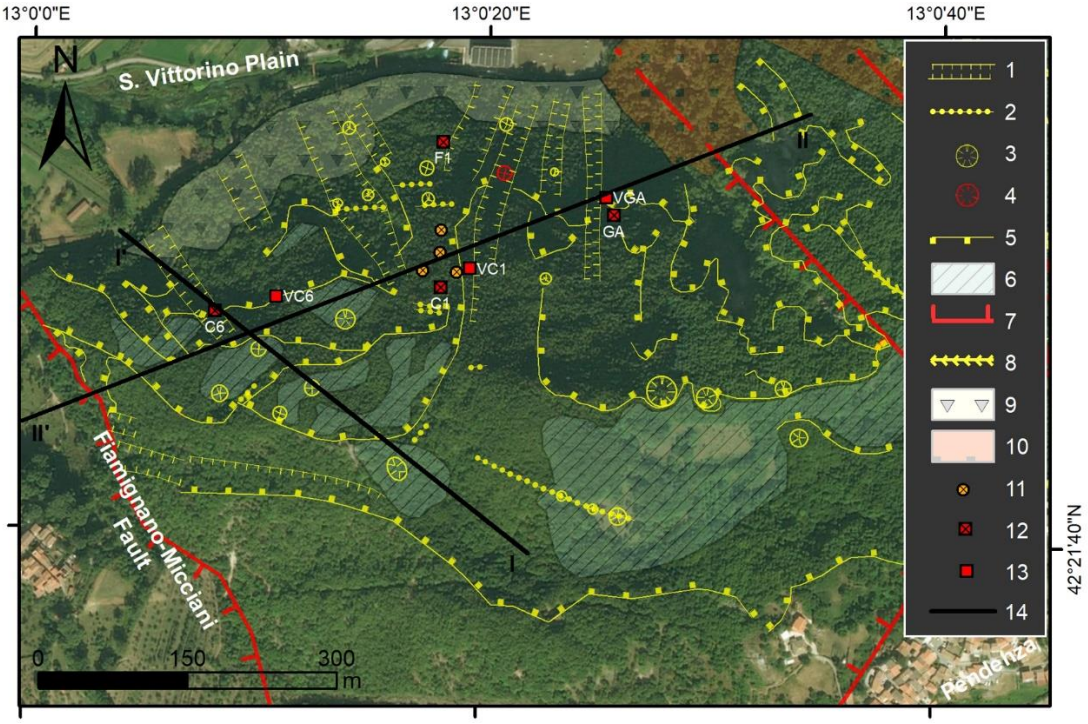

Fig. 5.9. Satellite view of the Peschiera Springs Slope showing: 1) trench; 2) tension crack; 3) sinkhole; 4) 1997 collapse of sinkhole; 5) scarp; 6) karstified flat; 7) fault; 8) gully; 9) slope debris; 10) debris fan deposit; 11) underground SNS array station; 12) underground and 13) surface accelerometric network station (with ID); 14) cross-section (see Fig. 5.10).

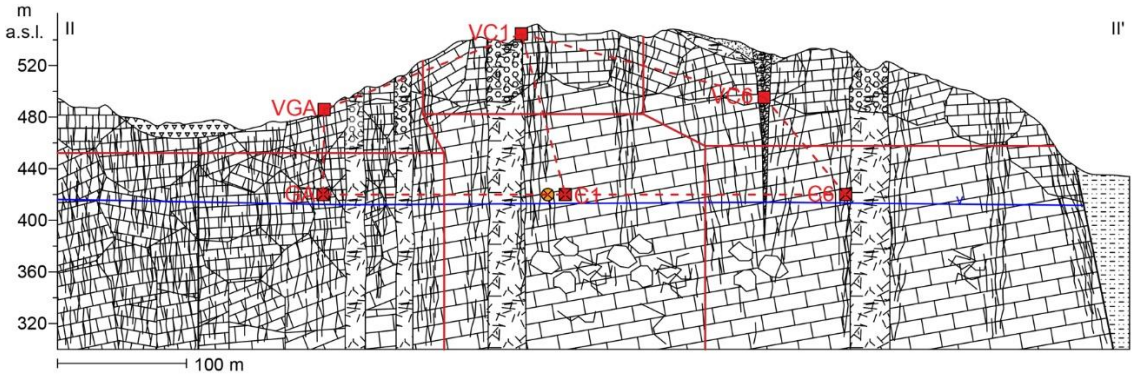

Fig. 5.10. Geological cross-section of the Peschiera Spring Slope (see Fig. 5.9) with seismic stations. The dashed red lines conjoin the different accelerometric stations, the solid red lines separate the different rock mass volumes associated to each station.

6. Discussion

6.1. Considerations about the obtained results

The present section focuses on the discussion of the results obtained in the two case studies (Chapter 4) by the experimental approach proposed by this Ph.D. thesis and their application for monitoring an instability process and managing the related risk (Chapter 5). Both in the Selmun and in the Peschiera case study the two different seismic passive approaches outputted consistent results that allow to characterise the gravity-induced slope instabilities and define some important specific features from which beginning to design strategies for managing the related geological risk. At the same time, the research evidenced some limits encountered during the application of the two geophysical approaches, related to the actuated experimentation as well as to the different geological contexts in which the landslide processes occur. As a matter of fact, the different scales of the instability processes in the two case studies played a key role to obtain or not consistent results by the employed geophysical techniques. However, the experimentation was carried out in two sites having marked different dimensions of instability processes in order to have a feedback of which approach could be more suitable for investigation and/or monitoring of landslides. In parallel, another issue to discuss is surely how much the amount of available seismic data may have influenced the obtained results. The availability of seismic data can be considered in terms of number of 1-h records for seismic ambient noise measurements and hours of continuous records for monitoring of microseismic events.

For the seismic ambient noise measurements, the number of measurements performed at the Selmun Promontory (i.e. 116) resulted more than enough to characterise the seismic response of an area having that dimension and some stations resulted rather redundant, especially in the unstable zones. On the other hand, the number of measurements carried out on the surface of the Peschiera Spring Slope (i.e. 8) seems not to be sufficient to obtain a reliable seismic response characterisation of the whole rock mass composing the slope, even though some important observations were made about the different features of the seismic response of the investigated zones. The deployment of seismic sensors at the Selmun site was favoured by the visibility and the accessibility of the landforms related to the instability process involving the cliff slope. As a matter of

fact, the presence of open and sub-vertical fractures on a flat morphology characterised by poor vegetation as the UCL plateau top was the best context for distributing the seismic ambient noise measurement stations. On the other hand, the environmental conditions were absolutely unfavourable for the sensor deployment on the Peschiera Spring Slope surface. Indeed, the Peschiera Spring Slope is involved in a larger and complex landslide process whose landforms are not easily visible due to the dense vegetation cover. In addition, the movement along the slope and the transport and installation of seismic sensors are made difficult due to its steep sharp, that limits the deployment of seismic noise measurement stations.

Even if at very different levels, seismic ambient noise measurements allowed to obtain remarkable outputs in terms of stability level of the several unstable zones in both case studies. The obtained results suggest to apply the seismic ambient noise measurement approach as tool for evaluating the different landslide susceptibility of the different unstable zones (Brabb, 1984), towards the definition of a landslide hazard zonation (Varnes & IAEG, 1984). At the Peschiera case study, the obtained results can be considered as preliminary and encourages future field activities to add new single-station measurements of seismic noise on the slope surface.

On the other hand, a consistent contribution to the direction of landslide hazard zonation was obtained at the Selmun Promontory. The results obtained by seismic noise measurements resulted in good agreement with a zonation carried out based on geological engineering surveys of fractures; in addition, they allowed to evaluate specific features of the vibrational behaviour of the unstable zones. In particular, despite a dense net of open fractures, zone B can be considered as a unique unstable rock block since its uniform seismic response. Therefore, the maximum landslide event have to be evaluated as related to the movement of the whole zone, producing an event having higher intensity than the detachment of a single rock block from the UCL plateau edge. For this unstable zone, the seismic ambient noise measurements evidenced also an eigenmode frequency at 3.3-3.5 Hz. Such a parameter has to be taken into account for evaluating the landslide triggering in case of seismic shaking, as already occurred with the Crete earthquake on 1856 that induced movements along the joints and the damage of the historical Għajn Ħadid watchtower. The preliminary results obtained by studying specific parameters of seismic noise in the eigenmode frequency range seem to evidence as an approach based on

continuous recording of seismic ambient noise can be a reliable way for monitoring of changes in the vibrational behaviour of the unstable slope, that could be possible precursors of a generalised collapse. However, in the next sections (Subparagraphs 6.2 and 6.3) the values obtained by the analysis of the long seismic noise measurements will be used for implementing a landslide hazard matrix for the Selmun Promontory.

Also the results obtained by analysis of seismic data recorded in SNS array configuration and processed by NanoseismicSuite software were conditioned by the different geological contexts involved by the two gravity-induced slope instability process as well as by the data availability. The different knowledge of the microseismic activity of the two landslide processes also played a key role.

At the beginning of this work, the knowhow on the gravity-induced processes involving the Peschiera Spring Slope landslide was already in a very advanced stage. The SNS data at Peschiera case study were recorded by a permanent array installed after 20 years of investigation of the instability process and almost 10 years of monitoring of microseismic events by a traditional accelerometric network. The permanent SNS array allowed to record several months of continuous seismic data. The array is installed within the drainage plant, where the noise conditions are very favourable because the records cannot be disturbed by external factors e.g. human activity, machinery, cars and wheatear conditions. On the other hand, the investigation of the landslide involving the Selmun Promontory started with this Ph.D. thesis and the microseismic activity of such a landslide was totally unknown before. As a matter of fact, as evidenced by the obtained results, the first position in which the SNS array was located did not allow to detect microseismic events, therefore a second SNS array location was experienced in a zone closer to the unstable cliff edge. Even if both SNS array recorded seismic data only for few hours in some dedicated measurement campaigns, the obtained results evidenced as the position of the array SNS2 was better than the one of the SNS1 for detecting microseismic activity related to the Selmun instability process. Another issue to consider is the less favourable noise condition of the Selmun Promontory compared to the Peschiera SNS array installation. As a matter of fact, the instruments were installed on the plateau top and recorded the vibrations produced by the different external sources that can masked possible microseismic events. In general, in the light of the obtained results, the monitoring of microseismic events at the Selmun Promontory seems to require the

installation of sensors in a position rather close to the unstable edge and such a deduction can be justified with the fast attenuation into the rock mass of the weak microseismic events originated by the unstable zone.

At the Peschiera Spring Slope, the data of the SNS array outputted very remarkable results, also considering all the above-mentioned favourable factors. The results obtained by the nanoseismic monitoring technique (Joswig, 2008) allowed to define two different microseismic sources related to the gravity-induced slope instability process involving the slope. A characteristic distribution curve related to frequency and magnitude of events, based on the Gutenberg & Richter (1954) power law, was defined for both sources. In the next sections (Subparagraphs 6.2 and 6.3), such curves will be used for assessing the hazard of the two microseismic sources and for implementing a landslide hazard matrix for managing the landslide risk at the drainage plant of the Peschiera Spring Slope.

In summary, the two experimented geophysical approaches allowed to obtain results at different levels in the two case studies. The analysis of seismic ambient noise measurements at single-station configuration outputs consistent results at the scale of a landslide involving a limited-size cliff slope and characterised by a clear pattern of fractures. The definition of the eigenmode frequency of an unstable rock block can be a useful base for designing a permanent monitoring system based on variations of specific parameters computed on continuous recording of seismic ambient noise. Seismic ambient noise measurements did not allow to obtain results at the same level in case of a large landslide involving an entire mountainous slope.

On the contrary, the monitoring of microseismic events produced by an instability process through the nanoseismic monitoring approach allowed to obtain remarkable results in case of large landslide involving an entire mountainous slope. In case of a landslide involving a limited-size cliff slope, nanoseismic monitoring seems not to be the best monitoring solution. Probably, a traditional microseismic monitoring carried out by deploying sensors directly on the unstable zone could be the best solution for monitoring of microseismic events related to gravity-induced instability process in such a context.

6.2. Assessment of the landslide hazard

In the light of the results obtained (Chapter 4) by the experimental approach proposed by this work and their application for monitoring an instability process (Chapter 5), in the present section an assessment of the hazard for the two analysed landslide process was carried out. As already exposed in Chapter 1, the hazard indicates the probability of occurrence within a specific period of time and within a given area of a potentially damaging phenomenon having a given magnitude. In case of earthquakes, the probability of occurrence of events is computed by using a probabilistic model based on the Poisson distribution of their magnitude jointed with their statistical distribution during time (Cornell, 1968; Bullen & Bolt, 1985). The following equation [Eq. 6.1]:

$$P_{n\geq 1} = 1 - e^{-\lambda V_R} \qquad [6.1]$$

represents the possibility of occurrence during a reference period V_R of at least one event ($n \geq 1$) having a given magnitude and a frequency λ, that is expressed as [Eq. 6.2]:

$$\lambda = \frac{1}{T_R} \qquad [6.2]$$

where T_R is the statistical return period of the given-magnitude event.

Figure 6.1 represents the $P_{n\geq 1}$ functions obtained by varying λ for specific values of V_R. The maps of earthquake hazard, e.g. Montaldo *et al.* (2007) for Italy, are produced by fixing a $P_{n\geq 1}$ value related to specific T_R and V_R values (commonly 475 and 50 years) and computing the expected acceleration or magnitude related to that $P_{n\geq 1}$ value.

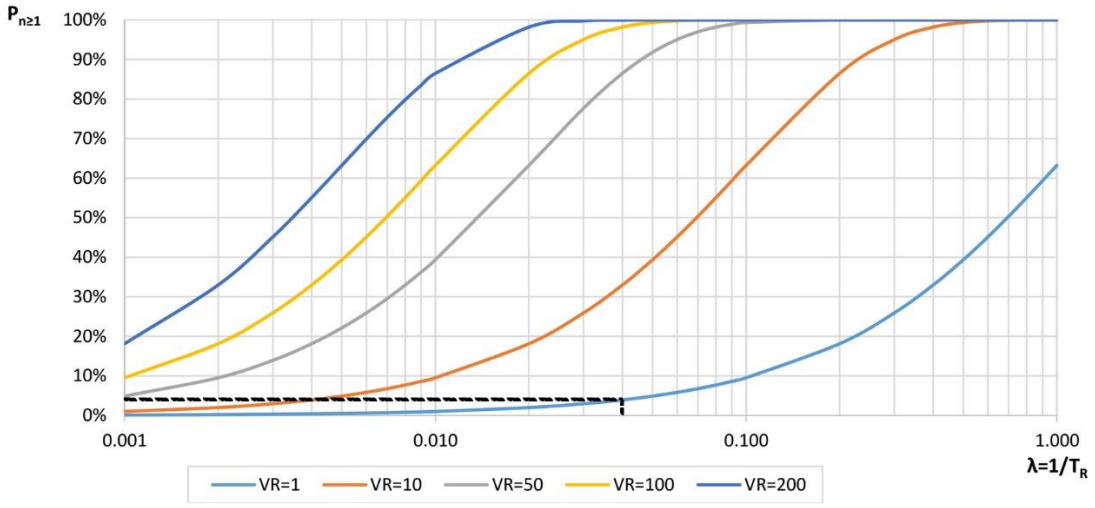

Fig. 6.1. Standard curves of variation of $P_{n\geq 1}$ for different values of V_R; the dashed black line indicates the $P_{n\geq 1}$ value considered for this work.

In this work, a similar approach was applied for evaluating the hazard of the two microseismic source identified within the Peschiera Spring Slope. A function with V_R equal to 1 year was considered due to the limited time observation for the analysed instability process (Fig. 6.1); then, a value of $P_{n\geq1}$ equal to 4% was achieved by fixing a T_R value of 25 years. The frequency-M_L curves obtained by the SNS array (Figs 4.19 and 4.20) are shaped by cumulating the number of events having at least a given value of M_L, therefore they can be considered in terms of probability of exceedance by normalising the cumulative numbers of events (Fig. 6.2). By considering a $P_{n\geq1}$ value of 4%, source S1 resulted characterised by a M_L equal to -1.7 while a M_L equal to -2.2 was obtained for source S2.

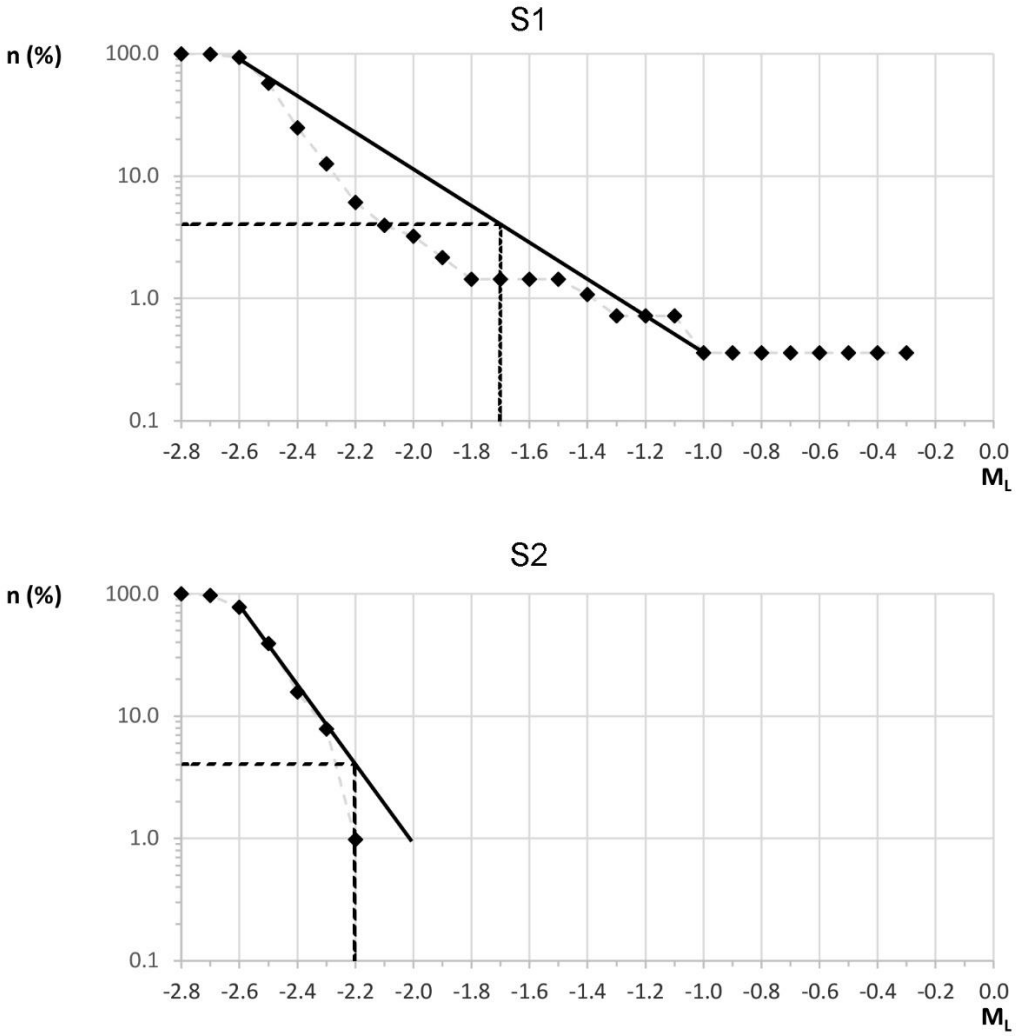

Fig. 6.2. Curves of $P_{n\geq1}$ for microseismic sources S1 and S2 at the Peschiera Spring Slope; the dashed black line indicates the considered $P_{n\geq1}$ value and the related value of M_L.

To apply the same probabilistic approach, the v value obtained by the analysis of the long seismic noise measurement at the Selmun Promontory (Figs 5.1 and 5.2) were used for trying a preliminary hazard evaluation. First, it was decided to analyse the base noise level values because they are more sensible to changes of the vibrational behaviour of the unstable blocks (Got *et al.*, 2010) and, in particular, in the frequency range between 2 and 5 Hz because they are related to the eigenmode frequency of the unstable block of zone B. By considering the sub-horizontal oscillation of a block, the mean horizontal v value was computed for each time step and, finally, its normalised distribution was obtained (Fig. 6.3). By considering a $P_{n\geq 1}$ of 4%, zone B (unstable) resulted characterised by a *v* equal to 1.05 while a *v* value equal to 0.45 was obtained for zone A (stable).

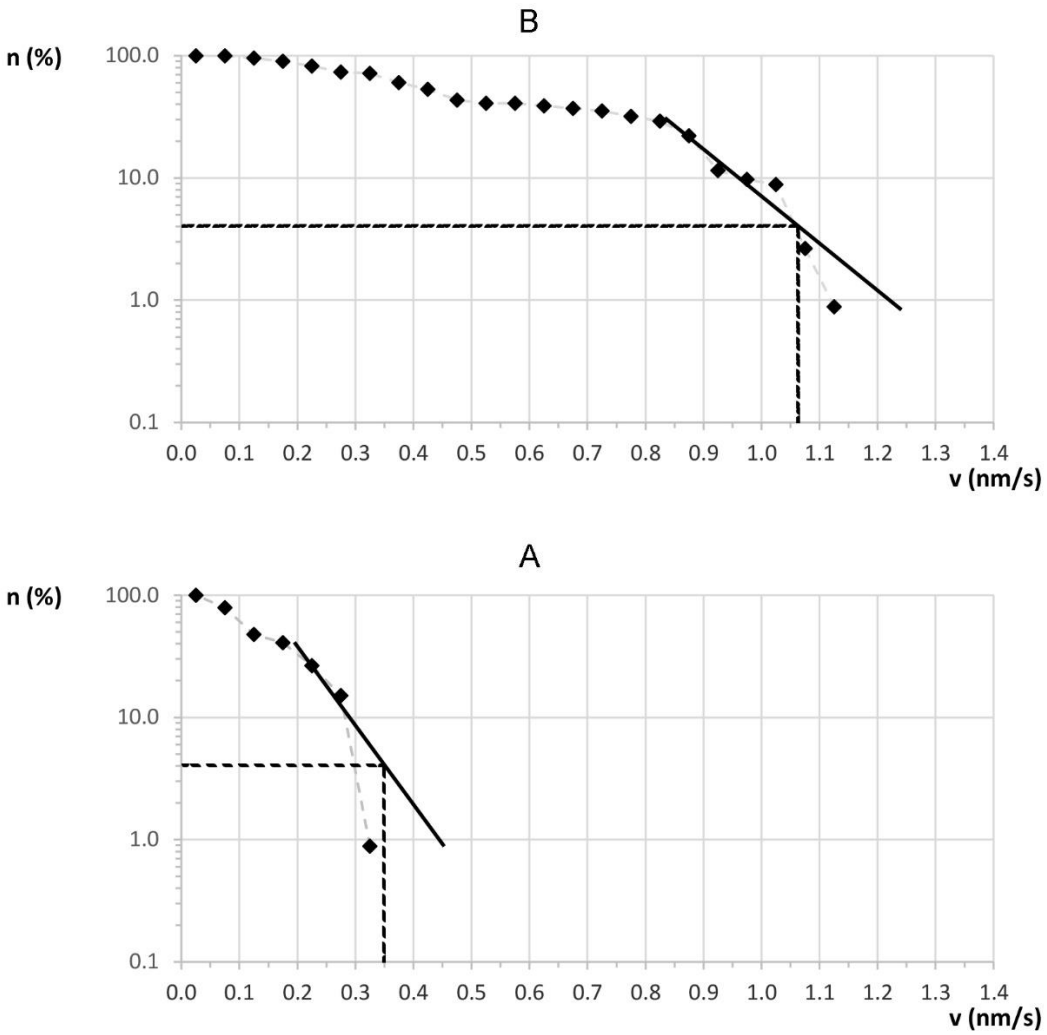

Fig. 6.3. Curves of $P_{n\geq 1}$ for zones A (stable) and B (unstable) at the Selmun Promontory; the dashed black line indicates the considered $P_{n\geq 1}$ value and the related v value.

6.3. Implementation of a landslide hazard matrix

According to the procedure for producing the maps of earthquake hazard, a hazard matrix was implemented to express the landslide hazard in each case study of this Ph.D. thesis. Such a hazard matrix was designed to represent all the aspect of the landslide hazard. As a matter of fact, the x-axis represent the zonation of the hazard while the y-axis the element of hazard in that zone; in addition, a colour scale is applied for showing the different values of intensity of the expected event at a given $P_{n\geq 1}$ value, that was fixed at 4% in 1 year as already explained in the previous section (Paragraph 6.2).

Figure 6.4 shows the landslide hazard matrix for the Peschiera Spring Slope. The zones of the x-axis were obtained by the rock mass volumes defined for the procedure for quickly evaluating the source of the events recorded by the accelerometric network (see Paragraph 5.2). Then, three hazard elements were defined for the y-axis: sources S1, falling in the volume related to station C1, and source S2, assigned to stations C6 and C1 since it lies in both volumes; in addition, a hypothetical source S3 was defined to cover other possible sources originated in the other zones of the slope. Finally, the values of the expected M_L for $P_{n\geq 1}$ of 4% in 1 year were obtained from the normalised frequency-M_L curves (Fig. 6.2); the minimum value of M_L was hypothesised to the hypothetical source S3 for representing the rest of the slope where no microseismic sources were found.

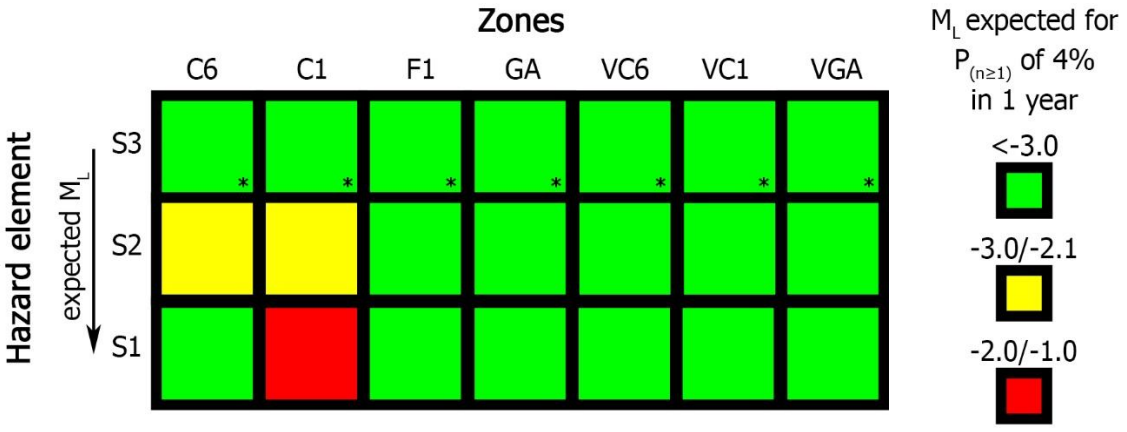

Fig. 6.4. Landslide hazard matrix proposed for assessing the landslide hazard at the Peschiera Spring Slope; the asterisks indicate hypothesised values.

Figure 6.5 shows the landslide hazard matrix implemented for the Selmun Promontory. The zones of the x-axis were defined based on engineering geological surveys and on the features of the seismic response (see Paragraph 4.1). Then, four hazard elements were considered for the y-axis: element A in the stable zone A and element B representing the unstable rock block in zone B; in addition, the elements Din and Dex were defined for representing the internal and external unstable rock block existing in zone D. Finally, the values of the expected v for $P_{n\geq 1}$ of 4% in 1 year were obtained from the normalised curves of frequency and v (Fig. 6.3). An intermediate value of v was hypothesised for elements Din and Dex because such blocks show less marked features of ellipticity and polarization of the particle motion then block in zone B but no long seismic ambient noise measurements were available for carrying out a computation of the v values for these hazard elements.

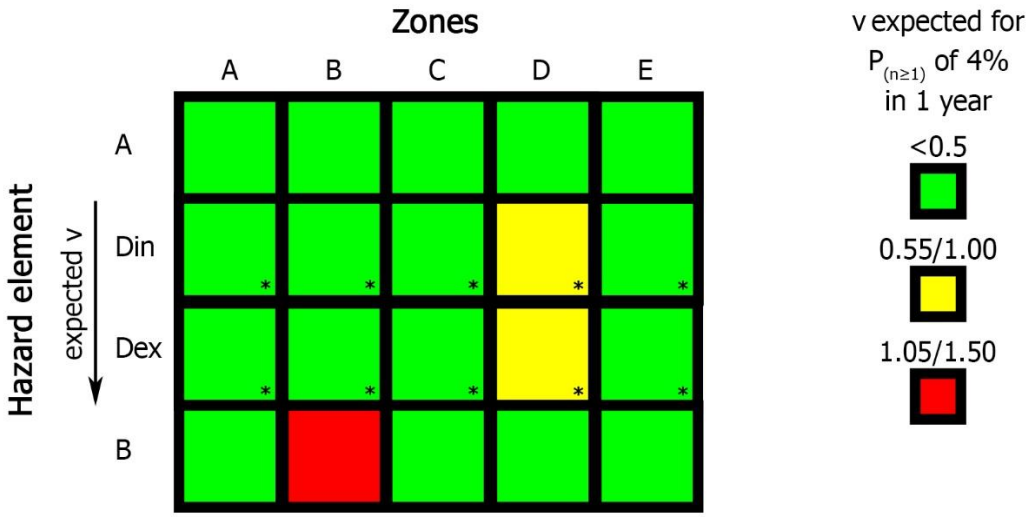

Fig. 6.5. Landslide hazard matrix proposed for assessing the landslide hazard at the Selmun Promontory; the asterisks indicate hypothesised values.

7. Future perspectives

In the light of the results obtained by the proposed methodology (Chapter 4) and by their possible applications (Chapter 5) as well as the advantages and disadvantages highlighted by the experimentation for each geophysical approach and by the implemented hazard matrix (Chapter 6), different solutions can be evaluated for managing the landslide risk in the two case studies. This section of the Ph.D. thesis is focused about the future perspectives that could be performed in the two case studies for improving the characterisation of the landslide processes as well as for monitoring the instabilities and managing the related risk.

For the Selmun case study, currently the installation of a permanent monitoring system is not planned despite the consistent results obtained by the analysis of passive seismic measurements. A SNS array cannot not be considered as the best monitoring solution because it should be installed with a reduced aperture and in a position close to the unstable cliff edge due to the fast attenuation of the microseismic events. Both constrains would represent not-favourable conditions for the application of nanoseismic monitoring, that requires a larger array aperture for appreciating the different first arrival times of seismic waves among its stations and a distance between the array and the source at least 5 times the SNS array aperture for obtaining a perfectly reliable waves phase picking. On the contrary, the best monitoring solution for the Selmun Promontory seems to be represented by a system composed of seismic sensors directly installed on the unstable zones. Such a system could be applied for performing a monitoring that joints the detection of microseismic events and the computation of seismic noise amplitude in the frequency range of the eigenmode frequency of the unstable block, in both time and frequency domains. By observing variation of both parameters during time could be possible to individuate anomalies in rate of event number and/or in rate of seismic noise amplitude that can be indicative of an incoming general collapse. In addition, further long measurements of seismic noise should be carry out for improving the landslide hazard matrix proposed in Paragraph 6.3.

For the Peschiera case study, the application of the hazard matrix proposed in Paragraph 6.3 seems to represent a reliable tool for designing the management in quasi-real-time of the landslide risk threating the drainage plant. Unfortunately, both the accelerometric network and the SNS array have been switched off for a significant

refurbishment work that involves the drainage plant, therefore the hazard matrix was tested only theoretically in the aftermath on a set of events related to the period in which they were working together. The hazard matrix could be applied for management purposes after a first experimental period that will carry out after the re-start of both systems. In the meanwhile, several activities can be performed for obtaining some improvements to characterise the gravity-induced instability process. On one side, a field campaign could be planned with the aim to complete the cover of single-station seismic noise measurements on the slope surface and better define the seismic response of the different landslide zones. On the other side, the frequency-magnitude event curves of the microseismic sources identified within the slope can be implemented with the analysis of remaining microseismic events recorded by the SNS array. Such a progress in the event analysis could be useful for obtaining better-defined frequency-magnitude curves and, therefore, for evaluating a stable *b* value for the two microseismic sources. In particular, a similar progress would be important for obtaining a reliable linear projection of the frequency-magnitude curve for cluster S1 because the current curve evidences a lack of events having M_L between -1.0 and -0.3.

In general, both geophysical approaches outputted consistent results that seem to be recommend the use of such techniques for characterising and monitoring landslide processes involving rock masses. As a matter of facts, the results obtained in this work suggest to carry out an extensive experimentation, also in other case studies, that could provide additional elements for verifying the applicability of such techniques. The Ph.D. student himself performed several measurements in some other sites (Iannucci *et al.*, 2016) and obtained preliminary results that confirmed the main output obtained by this work. Probably, more efforts should be done in future to speed up and automate the analysis stages of these approaches, for making them usable in the context of the early warning systems.

8. Conclusions

Assessment of landslide hazard and managing the related risk have always been widely studied topics in the scientific community due to the presence of populated settlements as well as tourist and cultural heritage sites threated by slope instability processes. In the last decade, geophysical techniques have been integrated in multidisciplinary approaches to study propagation of gravity-induced slope instability processes as well as to design monitoring systems devoted to manage infrastructures.

In this Ph.D. thesis, several geophysical measurements were carried out in two case studies of rock masses interested by gravity-induced slope instability processes to test as these techniques can be a useful support for applied geology towards the evaluation of landslide hazard as well as the management of related risk, by integrating the traditional engineering geological surveys. Among the available geophysical techniques, two approaches of passive seismic were chosen due to their capability to be used for observing variations of specific effects or parameters during time: i) analysis of seismic ambient noise measurements; ii) monitoring of microseismic events produced by the slope instability process.

The two case studies were selected by considering the variation of the scale of the landslide process as well as the natural environment interested by the instability. In both cases the landslide involved a rock mass: i) Selmun case study, one cliff slope North Western coast on the island of Malta (Central Mediterranean Sea); ii) Peschiera case study, one slope in mountainous area of Central Apennines (Italy) interested by a large instability process.

At the Selmun case study, the seismic noise measurements allowed to obtain remarkable outputs in terms of stability level of the several unstable zones and, therefore, to evaluate their different landslide susceptibility in the framework of a landslide hazard zonation. In particular, it was possible to observe the uniform seismic response of one unstable zone characterised by a dense net of open fractures and to assess its eigenmode frequency. A preliminary study evidenced the capability of continuous seismic ambient noise measurements to be applied for monitoring the changes in the vibrational behaviour of the unstable zone, that could indicate an incoming general collapse. On the other hand, the installation of a SNS array allowed to detect and locate few microseismic events produced by the unstable cliff.

At the Peschiera site, the seismic noise measurements evidenced the different seismic response of different zones of the slope involved in the complex landslide process. On the other hand, the SNS array allow to locate 397 events related to the slope instability, distinguished in two different types having different waveforms: 16 failures and 381 collapses. While the failures resulted distributed into the whole slope, the collapses focused in two different spatial clusters below the groundwater level, at a depth in which karst processes produce cavities. The clusters were treated as two distinct microseismic sources and a frequency-magnitude curve of events was produced for each one. Such curves allowed to define the attitude to produce events having different values of magnitude and to assess the magnitude of the maximum expected event, giving therefore information about the different hazard of the two clusters. Then, an automated procedure for analysing events recorded by another seismic network (i.e. accelerometric network) installed within the slope was developed.

Finally, the implementation of a landslide hazard matrix was proposed for the both case studies. Such matrixes were implemented by jointing the hazard zonation and the hazard elements defined for each site, characterised by deterministic approaches, with their attitude to produce events having a given magnitude, assessed by a probabilistic approach. As a matter of fact, each landslide hazard matrix is based on the statistic frequency of the occurred events (i.e. signal amplitude values of long seismic noise for the Selmun case study and M_L values of collapses for the Peschiera case study) and their probability of exceedance in a fixed period and can be used as a tool for managing the related risk.

In conclusion, even if with different levels of results obtained for the two case studies, this Ph.D. thesis evidenced as passive seismic represents a useful tool for investigating and monitoring gravity-induced slope instability processes since it allows to achieve the different initial objectives: i) evaluate the landslide susceptibility and produce a landslide hazard zonation; ii) characterise the landslide hazard; iii) give a contribution for managing the landslide risk.

Ringraziamenti

Al termine di questa tesi (che è veramente l'ultima, promesso) mi prendo la libertà di abbandonare il linguaggio tecnico-scientifico e l'inglese per dedicare qualche riga a chi ha contribuito, in maniera più o meno consapevole, alla riuscita di questi tre lunghi anni di ricerca.

Ringrazio innanzitutto il mio tutor, il Prof. Salvatore Martino, per avermi, per la terza volta, guidato e seguito con costanza durante tutto il lavoro di tesi, dandomi l'opportunità di rendere il Dottorato interessante sia nei modi che nei luoghi in cui ho svolto la mia ricerca. Un ringraziamento va ai miei due co-tutor, il Dott. Luca Lenti ed il Dott. Sebastiano D'Amico, per aver messo a disposizione le loro competenze ed avermi ospitato nelle due strutture di cui fanno parte, il Dipartimento GERS dell'IFSTTAR di Champs-sur-Marne ed il Dipartimento di Geoscienze dell'Università di Malta; se il Dottorato si è rivelato un'esperienza di formazione personale, oltre che professionale, è stato sicuramente anche grazie ai tanti mesi che avuto l'opportunità di trascorrere all'estero. Ringrazio poi i miei due co-tutor non ufficiali, la Dott.sa Antonella Paciello ed il Dott. Stefano Rivellino, per i tanti consigli e gli aiuti pratici che mi hanno dato durante lo svolgimento di questa ricerca.

Desidero ringraziare il Dott. Jan Burjánek per aver messo a disposizione i propri codici di analisi e l'Ing. Giorgio Martino di ACEA-Ato2 ed il Dott. Carlo Romagnoli di ACEA-Elabori per avermi permesso di utilizzare i dati del sistema di monitoraggio del Versante delle Sorgenti del Peschiera. Un ringraziamento va anche a Fabio Martorelli, Marisa Regina e Gianmarco Rea che mi hanno dato un aiuto fondamentale nelle attività di campagna e di laboratorio durante le loro tesi di laurea.

Ringrazio gli amici di sempre che mi hanno pazientemente atteso mentre ero in giro per l'Europa. Ringrazio Martina che mi ha accompagnato nel corso di questi tre anni di Dottorato. Ringrazio i miei genitori, Dina e Nicola, che mi hanno sempre lasciato la libertà di scegliere di fare ciò che mi piaceva fare. Ringrazio Giulia perché c'è sempre e, visto che ha scelto anche lei di intraprendere questo percorso, le auguro di poter svolgere un Dottorato interessante e formativo almeno quanto il mio.

Ringrazio infine, sempre pur sapendo che non lo saprà mai, la tanta musica che mi ha tenuto compagnia durante le miei giornate e che continuerà sempre a farlo.

References

Aki K. (1957). Space and time spectra of stationary stochastic waves, with special reference to microtremors. *Bulletin of the Earthquake Research Institute, University of Tokyo*, **35**, 415-457.

Aki K. (1965). A note on the use of microseisms in determining the shallow structures of the earth's crust. *Geophysics*, **30** (4), 665-666.

Alber M., Fritschen R., Bischoff M. & Meier T. (2009). Rock mechanical investigations of seismic events in a deep longwall coal mine. *Int. J. Rock Mech. Min. Sci.*, **46** (2), 408-420.

Amitrano D., Grasso J.R. & Senfaute, G. (2005). Seismic precursory patterns before a cliff collapse and critical-point phenomena. *Geophys. Res. Lett.*, **32** (8), L08314.

Amitrano D., Gaffet S., Malet J.-P. & Maquaire O. (2007). Understanding mudslides through micro-seismic monitoring: The Super-Sauze (South French Alps) case study. *B. Soc. Geol. Fr.*, **178** (2), 149-157.

Amitrano D., Arattano M., Chiarle M., Mortara G., Occhiena C., Pirulli M. & Scavia C. (2010). Microseismic activity analysis for the study of the rupture mechanism in unstable rock masses. *Nat. Hazard Earth Syst. Sci.*, **10**, 831-841.

Artman B. (2006). Imaging passive seismic data. *Geophysics*, **71**, 177-187.

Asten M.W. (1978). Geological control of the three-component spectra of Rayleigh-wave microseisms. *Bull. Seism. Soc. Am.*, **68** (6), 1623-1636.

Asten M.W. & Henstridge J.D. (1984). Arrays estimators and the use of microseisms for reconnaissance of sedimentary basins. *Geophysics*, **49** (11), 1828-1837.

ASTM (2006). D854-06. Standard test methods for specific gravity of soil solids by water pycnometer. In: *ASTM Volume 04.08 Soil and Rock (I)*. ASTM International.

ASTM (2008). D5731-08. Standard test method for determination of the Point Load Strength Index of rock and application to rock strength classifications. In: *ASTM Volume 04.08 Soil and Rock (I)*. ASTM International.

Bakun W.H. & Joyner W.B. (1984). The M_L scale in Central California. *Bull. Seism. Soc. Am.*, **74**, 1827-1843.

Barton N. & Choubey V. (1977). The shear strength of rock joints in theory and practice. *Rock Mech.*, **10** (1-2), 1-54.

Barzaghi L. & Ferulano M.F. (2012). Borehole microseismic in deep live oil wells: an example. *Boll. Geofis. Teor. Appl.*, **53** (4), 509-522.

Bichler A., Bobrowsky P., Best M., Douma M., Hunter J., Calvert T. & Burns R. (2004). Three-dimensional mapping of a landslide using a multi-geophysical approach: the Quesnel Forks landslide. *Landslides*, **1** (1), 29-40.

Bigi S. & Costa Pisani P. (2002). Structural setting of the Cicolano-M. Calvo area (Central Apennines, Italy). *Boll. Soc. Geol. It.*, Spec **1**, 141-149.

Blevins R.D. (2001). *Formulas for natural frequencies and mode shape*. Krieger Publishing.

Borcherdt R.D. (1970). Effects of local geology on ground motion near San Francisco Bay. *Bull. Seism. Soc. Am.*, **60**, 29-61.

Borcherdt R.D. (1994). Estimates of site-dependent response spectra for design (methodology and justification). *Earthq. Spectra*, **10**, 617-653.

Boni C.F., Bono P. & Capelli G. (1986). Schema idrogeologico dell'Italia Centrale. *Mem. Soc. Geol. It.*, **35**, 991-1012.

Boni C.F., Capelli G. & Petitta M. (1995). *Carta idrogeologica dell'alta e media Valle del F. Velino*. Elaborazione cartografica e stampa System Cart.

Bonnefoy-Claudet S., Cotton F. & Bard P.-Y. (2006). The nature of noise wavefield and its applications for site effects studies: a literature review. *Earth-Sci. Rev.*, **79** (3), 205-227.

Bogoslovsky V.A. & Ogilvy A.A. (1977). Geophysical methods for the investigation of landslides. *Geophysics*, **42** (3), 562–571.

Bottelin P., Jongmans D., Baillet L., Lebourg T., Hantz D., Lévy C., Le Roux O., Cadet H., Lorier L., Rouiller J.-D., Turpin J. & Darras L. (2013a). Spectral analysis of prone-to-fall rock compartments using ambient vibrations. *J. Environ. Eng. Geophys.*, **18** (4), 205-217.

Bottelin P., Lévy C., Baillet L., Jongmans D. & Gueguen P. (2013b). Modal and thermal analysis of Les Arches unstable rock column (Vercors massif, French Alps). *Geophys. J. Int.*, **194** (2), 849-858.

Bottelin P., Jongmans D., Daudon D., Mathy A., Helmstetter A., Bonilla-Sierra V., Cadet H., Amitrano D., Richefeu V., Lorier L., Baillet L., Villard P. & Donzé F. (2014).

Seismic and mechanical studies of the artificially triggered rockfall at Mount Néron (French Alps, December 2011). *Nat. Hazards Earth Syst. Sci.*, 14 (12), 3175-3193.

Bottelin P., Baillet L., Larose E., Jongmans D., Hantz D., Brenguier O., Cadet H. & Helmstetter A. (2017). Monitoring rock reinforcement works with ambient vibrations: La Bourne case study (Vercors, France). *Eng. Geol.*, **226**, 136-145.

Bourdeau C. & Havenith H.-B. (2008). Site effects modelling applied to the slope affected by the Suusamyr earthquake (Kyrgyzstan, 1992). *Eng. Geol.*, **97** (3), 126-145.

Bozzano F., Martino S., Naso G., Prestininzi A., Romeo R.W. & Scarascia Mugnozza G. (2004). The large Salcito landslide triggered by the 2002 Molise, Italy, earthquake. *Earthq. Spectra*, **20** (S1), S95-S105.

Bozzano F., Bretschneider A. & Martino S. (2008a). Stress-strain history from the geological evolution of the Orvieto and Radicofani cliff slopes (Italy). *Landslides*, **5** (4), 351-366.

Bozzano F., Cardarelli E., Cercato M., Lenti L., Martino S., Paciello A. & Scarascia Mugnozza G. (2008b). Engineering-geology model of the seismically-induced Cerda landslide (Sicily, Italy). *Boll. Geofis. Teor. Appl.*, **49** (2), 205-225.

Bozzano F., Lenti L., Martino S., Paciello A. & Scarascia Mugnozza G. (2011). Evidences of landslide earthquake triggering due to self-excitation process. *Int. J. Earth Sci.*, **100** (4), 861-879.

Bozzano F., Martino S., Montagna A., & Prestininzi A. (2012). Back analysis of a rock landslide to infer rheological parameters. *Eng. Geol.*, **131**, 45-56.

Brabb E.E. (1984). Innovative approaches to landslide hazard and risk mapping. In: *IV international symposium on landslides*, vol. 1, pp. 307-324.

Bullen K.E. & Bolt B.A. (1985). *An introduction to the theory of seismology*. Cambridge University Press.

Burjánek J., Gassner-Stamm G., Poggi V., Moore J.R. & Fäh D. (2010). Ambient vibration analysis of an unstable mountain slope. *Geophys. J. Int.*, **180** (2), 820-828.

Burjánek J., Moore J.R., Yugsi Molina F.X. & Fäh D. (2012). Instrumental evidence of normal mode rock slope vibration. *Geophys. J. Int.*, **188** (2), 559-569.

Burtin A., Bollinger L., Cattin R., Vergne J. & Nábělek J.L. (2009). Spatiotemporal sequence of Himalayan debris flow from analysis of high-frequency seismic noise. *J. Geophys. Res.*, **114** (F4), F04009.

Cai M., Kaiser P.K. & Martin C.D. (2001). Quantification of rock mass damage in underground excavations from microseismic event monitoring. *Int. J. Rock Mech. Min. Sci.*, **38** (8), 1135-1145.

Cao A.Y., Dou L.M., Wang C.B., Yao X.X., Dong J.Y. & Gu Y. (2016). Microseismic precursory characteristics of rock burst hazard in mining areas near a large residual coal pillar: a case study from Xuzhuang Coal Mine, Xuzhou, China. *Rock Mech. Rock Eng.*, **49** (11), 4407-4422.

Capon J. (1969). High-resolution frequency-wavenumber spectrum analysis. *Proceedings of the IEEE*, **57** (8), 1408-1418.

Casini S., Martino S., Petitta M. & Prestininzi A. (2006). A physical analogue model to analyses interactions between tensile stresses and dissolution in carbonate slopes. *Hydrogeol. J.*, **14**, 1387-1402.

Ciotoli G., Di Filippo M., Nisio S. & Romagnoli C. (2001). La Piana di S. Vittorino: dati preliminari sugli studi geologici, strutturali, geomorfologici, geofisici e geochimici. *Mem. Soc. Geol. It.*, **56**, 297-308.

Chambers J.E., Wilkinson P.B., Kuras O., Ford J.R., Gunn D.A., Meldrum P.I., Pennington C.V.L., Weller A.L., Hobbs P.N.R. & Ogilvy R.D. (2011). Three-dimensional geophysical anatomy of an active landslide in Lias Group mudrocks, Cleveland Basin, UK. *Geomorphology*, **125** (4), 472-484.

Cheng G., Ma T., Tang C., Liu H. & Wang S. (2017). A zoning model for coal mining-induced strata movement based on microseismic monitoring. *Int. J. Rock Mech. Min. Sci.*, **94**, 123-138.

Clinton J.F., Case Bradford S., Heaton T.H. & Favela J. (2006). The observed wander of the natural frequencies in a structure. *Bull. Seism. Soc. Am.*, **96** (1), 237-257.

Colombero C., Baillet L., Comina C., Jongmans D. & Vinciguerra S. (2017). Characterization of the 3-D fracture setting of an unstable rock mass: From surface and seismic investigations to numerical modelling. *J. Geophys. Res.*, **122**, 6346-6366.

Contrucci I., Klein E., Bigarre P., Lizeur A., Lomax A. & Bennani M. (2010). Management of post-mining large-scale ground failures: blast swarms field experiment for calibration of permanent microseismic early-warning systems. *Pure Appl. Geophys.*, **167** (1-2), 43-62.

Cornell C.A. (1968). Engineering seismic risk analysis. *Bull. Seism. Soc. Am.*, **58** (5), 1583-1606.

Cruden D.M. (1991). A simple definition of a landslide. *Bulletin of the International Association of Engineering Geology*, **43**, 27-29.

Dai F.C., Lee C.F. & Ngai Y.Y. (2002). Landslide risk assessment and management: an overview. *Eng. Geol.*, **64** (1), 65-87.

Dammeier F., Moore J.R., Haslinger F. & Loew S. (2011). Characterization of alpine rockslides using statistical analysis of seismic signals. *J. Geophys. Res.*, **116** (F40), F04024.

Danneels G., Bourdeau C., Torgoev I. & Havenith H.-B. (2008). Geophysical investigation and dynamic modelling of unstable slopes: case-study of Kainama (Kyrgyzstan). *Geophys. J. Int.*, **175** (1), 17-34.

Deere D.U. & Miller R.P. (1966). *Engineering classification and index properties for intact rock*. Illinois Univ. At Urbana Dept. Of Civil Engineering.

Del Gaudio V. (2017). Instantaneous polarization analysis of ambient noise recordings in site response investigations. *Geophys. J. Int.*, **210** (1), 443-464.

Del Gaudio V. & Wasowski J. (2007). Directivity of slope dynamic response to seismic shaking. *Geophys. Res. Lett.*, **34**, L12301.

Del Gaudio V., Wasowski J., Pierri P., Mascia U. & Calcagnile G. (2000). Gravimetric study of a retrogressive landslide in southern Italy. *Surv. Geophys.*, **21** (4), 391-406.

Del Gaudio V., Coccia S., Wasowski J., Gallipoli M.R. & Mucciarelli M. (2008). Detection of directivity in seismic site response from microtremor spectral analysis. *Nat. Hazards Earth Syst. Sci.*, **8**, 751-762.

Del Gaudio V., Muscillo S. & Wasowski J. (2014). What we can learn about slope response to earthquakes from ambient noise analysis: an overview. *Eng. Geol.*, **182**, 182-200.

Delgado J., Garrido J., Lenti L., Lopez-Casado C., Martino S. & Sierra F.J. (2015). Unconventional pseudostatic stability analysis of the Diezma landslide (Granada, Spain) based on a high-resolution engineering geological model. *Eng. Geol.*, **184**, 81-95.

Della Seta M., Martino S. & Scarascia Mugnozza G. (2013). Quaternary sea-level change and slope instability in coastal areas: Insights from the Vasto Landslide (Adriatic coast, central Italy). *Geomorphology*, **201**, 468-478.

Delle Rose M. (2012). Some insights about the relation among seismic activity, tectonic structures and rockslide kinematics at the Vajont Dam Site. In: *Atti del 31° Convegno Nazionale Gruppo Nazionale di Geofisica della Terra Solida (31GNGTS). Tema 1: Geodinamica*, Potenza (Italia), 20-22 Novembre 2012, vol. 1, pp. 44-50.

Deparis J., Jongmans J., Cotton F., Bailler L., Thouvenot F. & Hantz D. (2008). Analysis of rock-fall and rock-fall avalanche seismograms in the French Alps. *Bull. Seism. Soc. Am.*, **98** (2), 1781-1796.

Dewez T.J.B., Rohmer J., Regard V. & Cnudde C. (2013). Probabilistic coastal cliff collapse hazard from repeated terrestrial laser surveys: Case study from Mesnil Val (Normandy, northern France). *J. Coast. Res.*, Spec. Issue, **65**, 702-707.

Di Grazia G., Langer H., Ursino A., Scarfi L. & Gresta S. (2001). On the estimate of earthquake magnitude at a local seismic network. *Ann. Geophys.*, **44**, 579-591.

Dickson M.E., Ogawa H., Kench P.S. & Hutchinson A. (2013). Seacliff retreat and shore platform widening: Steady-state equilibrium?. *Earth Surf. Proc. Landforms*, **38**, 1046-1048.

Dilley M., Chen S. & Lerner-Lam A. (2005). *Natural Disaster Hotspots: A Global Risk Analysis*. The World Bank and Columbia University.

Doebling S.W., Farrar C.R., Prime M.B. & Shevitz D.W. (1996). *Damage identification and health monitoring of structural and mechanical systems from changes in their vibration: a literature review. Technical Report LA-13070-MS.* Los Alamos National Laboratory.

Douglas A. (2007). Forensic seismology revisited. *Surv. Geophys.*, **28**, 1-31.

Douze E.J. (1964). Rayleigh waves in short-period seismic noise. *Bull. Seism. Soc. Am.*, **54** (4), 1197-1212.

Douze E.J. (1967). Short-period seismic noise. *Bull. Seism. Soc. Am.*, **57** (1), 55-81.

Driad-Lebeau L., Lahaie F., Al Heib M., Josien J.P., Bigarre P. & Noirel J.F. (2005). Seismic and geotechnical investigations following a rockburst in a complex French mining district. *Int. J. Coal Geol.*, **64** (1), 66-78.

Edwards B., Kraft T., Cauzzi C., Kästli P. & Wiemer S. (2015). Seismic monitoring and analysis of deep geothermal projects in St Gallen and Basel, Switzerland. *Geophys. J. Int.*, **201** (2), 1022-1039.

Epifanio B., Zezere J.L. & Neves M. (2013). Identification of hazardous zones combining cliff retreat rates with landslide susceptibility assessment. *J. Coast. Res.*, **65**, 1681-1686.

Esposito C., Martino S. & Scarascia Mugnozza G. (2007). Mountain slope deformations along thrust fronts in jointed limestone: an equivalent continuum modelling approach. *Geomorphology*, **90**, 55-72.

Fanti R., Gigli G., Lombardi L., Tapete D. & Canuti P. (2013). Terrestrial laser scanning for rockfall stability analysis in the cultural heritage site of Pitigliano (Italy). *Landslides*, **10** (4), 409-420.

Farrugia D., Paolucci E., D'Amico S. & Galea P. (2016). Inversion of surface wave data for subsurface shear wave velocity profiles characterized by a thick buried low-velocity layer. *Geophys. J. Int.*, **206**, 1221-1231.

Farrugia D., Galea P., D'Amico S. & Paolucci E. (2017). Sensitivity of ground motion parameters to local shear-wave velocity models: The case of buried low-velocity layers. *Soil Dyn. Earthq. Eng.*, **100**, 196-205.

Feignier B. & Young R.P. (1992). Moment tensor inversion of induced microseisnmic events: Evidence of non-shear failures in the $-4< M<-2$ moment magnitude range. *Geophys. Res. Lett.*, **19** (14), 1503-1506.

Fiorucci M., Iannucci R., Lenti L., Martino S., Paciello A., Prestininzi A. & Rivellino S. (2015). Seismic monitoring of the gravity-induced deformation involving the Peschiera Spring slope (Italy) for the management of a main infrastructure. In: *Proceedings of 6th International Conference on Earthquake Geotechnical Engineering (6ICEGE)*, Christchurch (New Zealand), 1-4 November 2015, paper 130.

Fiorucci M., Iannucci R., Martino S., Prestininzi A., Rivellino S., Lenti L. & Paciello A. (2016a). Integrated seismic monitoring system in a major aqueduct infrastructure. In: *Landslides and Engineered Slopes. Experience, Theory and Practice*. Eds Aversa S., Cascini L., Picarelli L. & Scavia C., pp. 917-924, CRC Press.

Fiorucci M., Iannucci R., Martino S. & Paciello A. (2016b). Detection of nanoseismic events related to slope instabilities in the quarry district of Coreno Ausonio (Italy). *Italian Journal of Engineering Geology and Environment*, **2**, 51-63.

Fiorucci M., Iannucci R., Lenti L., Martino S., Paciello A., Prestininzi A. & Rivellino S. (2017). Nanoseismic monitoring of gravity-induced slope instabilities for the risk management of an aqueduct infrastructure in Central Apennines (Italy). *Nat. Hazards*, **86** (Suppl. 2), 345-362.

Friedel S., Thielen A. & Springman S.M. (2006). Investigation of a slope endangered by rainfall-induced landslides using 3D resistivity tomography and geotechnical testing. *J. Appl. Geophys.*, **60** (2), 100-114.

Galea P. (2007). Seismic history of the Maltese islands and considerations on seismic risk. *Ann. Geophys.*, **50** (6), 725-740.

Galea P., D'Amico S. & Farrugia D. (2014). Dynamic characteristics of an active coastal spreading area using ambient noise measurements-Anchor Bay, Malta. *Geophys. J. Int.*, **199**, 1166-1175.

Galve J.P., Cevasco A., Brandolini P., Piacentini D., Azañón J. M., Notti D. & Soldati M. (2016). Cost-based analysis of mitigation measures for shallow-landslide risk reduction strategies. *Eng. Geol.*, **213**, 142-157.

Gibowicz S.J., Young R.P., Talebi S. & Rawlence D.J. (1991). Source parameters of seismic events at the Underground Research Laboratory in Manitoba, Canada: Scaling relations for events with moment magnitude smaller than −2. *Bull. Seism. Soc. Am.*, **81** (4), 1157-1182.

Gigli G., Frodella W., Mugnai F., Tapete D., Cigna F., Fanti R., Intrieri E. & Lombardi L. (2012). Instability mechanisms affecting cultural heritage sites in the Maltese Archipelago. *Nat. Hazards Earth Syst. Sci.*, **12**, 1883-1903.

Glade T., Stark P. & Dikau R. (2005). Determination of potential landslide shear plane depth using seismic refraction - case study in Rheinhessen, Germany. *Bull. Eng. Geol. Environ.*, **64** (2), 151-158.

Got J.-L., Mourot P. & Grangeon J. (2010). Pre-failure behaviour of an unstable limestone cliff from displacement and seismic data. *Nat. Hazards Earth Syst. Sci.*, **10**, 819-829.

Goudie A. (2004). *Encyclopedia of Geomorphology*. Routledge.

Gutenberg B. (1958). Microseisms. *Adv. Geophys.*, **5**, 53-92.

Gutenberg B. & Richter C.F. (1954). *Seismicity of the Earth and associated phenomena*. Princeton University Press.

Guzzetti F., Carrara A., Cardinali M. & Reichenbach P. (1999). Landslide hazard evaluation: a review of current techniques and their application in a multi-scale study, Central Italy. *Geomorphology*, **31** (1-4), 181-216.

Guzzetti F., Stark C.P. & Salvati P. (2005). Evaluation of Flood and Landslide Risk to the Population of Italy. *Environ. Manage.*, **36** (1), 15-36.

Hack R. (2000). Geophysics for slope stability. *Surv. Geophys.*, **21**, 423-448.

Hafemeister D. (2007). Progress in CTBT monitoring since its 1999 Senate defeat. *Science and Global Security*, **15** (3), 151-183.

Häge M. & Joswig M. (2009a). Spatiotemporal distribution of aftershocks of the 2004 December 5 M_L=5.4 Waldkirch (Germany) earthquake. *Geophys. J. Int.*, **178**, 1523-1532.

Häge M. & Joswig M. (2009b). Spatiotemporal characterization of interswarm period seismicity in the focal area Nový Kostel (West Bohemia/Vogtland) by a short-term microseismic study. *Geophys. J. Int.*, **179**, 1071-1079.

Häge M. & Joswig M. (2009c). Mapping local microseismicity using short-term tripartite small array installations. Case study: Coy region (SE Spain). *Tectonophys.*, **471**, 225-231.

Häge M., Blascheck P. & Joswig M. (2013). EGS hydraulic stimulation monitoring by surface arrays - location accuracy and completeness magnitude: the Basel Deep Heat Mining Project case study. *J. Seismol.*, **17**, 51-61.

Hagerty M.T., Schwartz S.Y., Garces M.A. & Protti M. (2000). Analysis of seismic and acoustic observations at Arenal Volcano, Costa Rica, 1995–1997. *J. Volcanol. Geoth. Res.*, **101** (1), 27-65.

Hampton M.A., Griggs G.B., Edil T.B., Guy D.E., Kelley J.T., Komar P.D., Mickelson D.M. & Shipman H.M. (2004). Processes that Govern the Formation and Evolution of Coastal Cliffs. In: *Formation, Evolution, and Stability of Coastal Cliffs-Status and Trends*. Eds Hampton M.A. & Griggs G.B., pp. 1-4, USGS - Professional Paper 1693.

Haque U., Blum P., da Silva P.F., Andersen P., Pilz J., Chalov S.R., Malet J.-P., Auflič M.J., Andres N., Poyiadji E., Lamas P.C., Zhang W., Pesevski I., Pétursson H.G., Kurt T., Dobrev N., Davalillo J.C.G., Halkia M., Ferri S., Gaprindashvili G., Engström J. & Keellings D. (2016). Fatal landslides in Europe. *Landslides*, **13**, 1545-1554.

Havenith H.-B., Jongmans D., Abdrakmatov K., Trefois P., Delvaux D. & Torgoev A. (2000). Geophysical investigations on seismically induced surface effects, case study of a landslide in the Suusamyr valley, Kyrgyzstan. *Surv. Geophys.*, **21**, 349-369.

Havenith H.-B., Jongmans D., Faccioli E., Abdrakhmatov K. & Bard P.-Y. (2002). Site effect analysis around the seismically induced Ananevo rockslide, Kyrgyzstan. *Bull. Seism. Soc. Am.*, **92** (8), 3190-3209.

Havenith H.-B., Strom A., Jongmans D., Abdrakhmatov A., Delvaux D. & Tréfois P. (2003a). Seismic triggering of landslides, Part A: Field evidence from the Northern Tien Shan. *Nat. Hazards Earth Syst. Sci.*, **3** (1/2), 135-149.

Havenith H.-B., Vanini M., Jongmans D. & Faccioli E. (2003b). Initiation of earthquake-induced slope failure: influence of topographical and other site specific amplification effects. *J. Seismol.*, **7** (3), 397-412.

Helmstetter A. & Garambois S. (2010). Seismic monitoring of Séchilienne rockslide (French Alps): Analysis of seismic signals and their correlation with rainfalls. *J. Geophys. Res.*, 115 (F3), F03016.

Hibert C., Grandjean G., Bitri A., Travelletti J. & Malet J.-P. (2012). Characterizing landslides through geophysical data fusion: Example of the La Valette landslide (France). *Eng. Geol.*, **128**, 23-29.

Hibert C., Ekström G. & Stark C.P. (2014). Dynamics of the Bingham Canyon Mine landslides from seismic signal analysis. *Geophys. Res. Lett.*, **41** (13), 4535-4541.

Hibert C., Stark C.P. & Ekström G. (2015). Dynamics of the Oso-Steelhead landslide from broadband seismic analysis. *Nat. Hazards Earth Syst. Sci.*, **15** (6), 1265-1273.

Hibert C., Ekström G. & Stark C.P. (2017a). The relationship between bulk-mass momentum and short-period seismic radiation in catastrophic landslides. *J. Geophys. Res.*, **122** (5), 1201-1215.

Hibert, C., Malet, J.-P., Bourrier F., Provost F., Berger F., Bornemann P., Tardif P. & Mermin E. (2017b). Single-block rockfall dynamics inferred from seismic signal analysis. *Earth Surf. Dynam.*, **5** (2), 283-292.

Hoek E. & Bray J.W. (1981). *Rock slope engineering*. Institution of Mining and Metallurgy.

Horike M. (1985). Inversion of phase velocity of long-period microtremors to the S-wave-velocity structure down to the basement in urbanized areas. *J. Phys. Earth*, **33**, 59-96.

Hudyma M. & Potvin Y.H. (2010). An engineering approach to seismic risk management in hardrock mines. *Rock Mech. Rock Eng.*, **43**, 891-906.

Hungr O. (1997). Some methods of landslide hazard intensity mapping. In: *Proceedings, Landslide Risk Workshop*. Eds Fell R. & Cruden D.M., pp. 215-226, Balkema.

Hutchinson J.N. (1988). General Report: Morphological and geotechnical parameters of landslides in relation to geology and hydrogeology. In: *Proceedings of Fifth International Symposium on Landslides*. Ed. Bonnard C., vol. 1, pp. 3-35, Balkema.

Hutchinson J.N. (1968) Mass movement. In: *Geomorphology. Encyclopedia of Earth Science*. Ed. Fairbridge R.W., pp 688-696, Springer.

Hutchinson J.N., Bromhead E.N. & Chandler M.P. (1991). Investigations of landslides at St. Catherine's Point, Isle of Wight. In: *Slope stability engineering: developments and applications*. Ed. Chandler M.P., pp. 169-178, Thomas Telford Publishing.

Hyde H.P.T. (1955). *Geology of the Maltese Islands*. Lux Press.

Iannucci R., D'Amico S., Farrugia D., Galea P., Martino S. & Paciello A. (2015). Seismic measurements in unstable sea cliff areas. *Atti del 34° Convegno Nazionale Gruppo Nazionale di Geofisica della Terra Solida (34GNGTS). Tema 3: Geofisica Applicata*, Trieste (Italia), 17-19 Novembre 2015, vol. 3, pp. 56-63.

Iannucci R., Martino S., Paciello A. & D'Amico S. (2016). Preliminary evidences of slope instabilities through seismic measurements at Cala Rossa bay (Italy). *Riassunti estesi del 35° Convegno GNGTS (Gruppo Nazionale di Geofisica della Terra Solida)*, Lecce (Italia), 22-24 Novembre 2016, pp. 363-368.

Iannucci R., Martino S., Paciello A. & D'Amico S. (2017). Rock mass characterization coupled with seismic noise measurements to analyze the unstable cliff slope of the Selmun Promontory (Malta). *Procedia Engineering*, **191**, 263-269.

Imposa S., Grassi S., Fazio F., Rannisi G. & Cino P. (2017). Geophysical surveys to study a landslide body (northeastern Sicily). *Nat. Hazards*, **86**, S327-S343.

ISRM (1978). Suggested methods for the quantitative description of discontinuities in rock masses. *Int. J. Rock Mech. Min. Sci. Geomech. Abstr.*, **15**, 319-368.

ISRM (1979). Suggested method for determining water content, porosity, density, absorption and related properties and swelling and slake durability index properties. *Int. J. Rock Mech. Min. Sci. Geomech. Abstr.*, **16**, 141-156.

Jaedicke C., Van Den Eeckhaut M., Nadim F., Hervás J., Kalsnes B., Vangelsten B.V., Smith J.T., Tofani V., Ciurean R., Winter M.G., Sverdrup-Thygeson K., Syre E. & Smebye H. (2014). Identification of landslide hazard and risk 'hotspots' in Europe. *B. Eng. Geol. Environ.*, **73**, 325-339.

Jongmans D. & Garambois S. (2007). Geophysical investigation of landslides: a review. *Bulletin de la Société géologique de France*, **178** (2), 101-112.

Joswig M. (1990). Pattern recognition for earthquake detection. *Bull. Seism. Soc. Am.*, **80** (1), 170-186.

Joswig M. (1993). Single-trace detection and array-wide coincidence association of local earthquakes and explosions. *Comput. Geosci.*, **19**, 207-221.

Joswig M. (1995). Automated classification of local earthquake data in the BUG small array. *Geophys. J. Int.*, **120**, 262-286.

Joswig M. (2008). Nanoseismic monitoring fills the gap between microseismic networks and passive seismic. *First Break*, **26**, 121-128.

Kanamori H. & Given J.W. (1982). Analysis of long-period seismic waves excited by the May 18, 1980, eruption of Mount St. Helens—a terrestrial monopole?. *J. Geophys. Res.*, **87** (B7), 5422-5432.

Kim J.T. & Stubbs N. (2003). Crack detection in beam-type structures using frequency data. *J. Sound Vibrat.*, **259** (1), 145-160.

Klose M., Maurischat P. & Damm B. (2015). Landslide impacts in Germany: a historical and socioeconomic perspective. *Landslides*, **13** (1), 183-199.

Kochnev V.A., Goz I.V., Polyakov V.S., Murtayev I.S., Savin V.G., Zommer B.K. & Bryksin I.V. (2007). Imaging hydraulic fracture zones from surface passive seismic data. *First Break*, **25**, 77-80.

Konno K. & Ohmachi T. (1998). Ground-motion characteristics estimated from spectral ratio between horizontal and vertical components of microtremor. *Bull. Seism. Soc. Am.*, **88**, 228-241.

Korup O., Densmore A.L. & Schlunegger F. (2010). The role of landslides in mountain range evolution. *Geomorphology*, **120** (1), 77-90.

Lacoss R.T., Kelly E.J. & Nafi T.M. (1969). Estimation of seismic noise structure using arrays. *Geophysics*, **34** (1), 21-38.

Lahr J.C. (1989). *Hypoellipse/version 2.0: a computer program for determining local earthquake hypocentral parameters, magnitude, and first motion patterns.* US. Geol. Surv.

Lawn B.R. (1993). *Fracture of brittle solids*. Cambridge University Press.

Lawrence W.S. & Williams T.R. (1976). Seismic signals associated with avalanches. *J. Glaciol.*, **17** (77), 521-526.

Lee W.H.K. & Stewart S.W. (1981). *Principles and applications of microearthquake networks.* Academic Press.

Lenti L., Martino S., Paciello A., Prestininzi A. & Rivellino S. (2012). Microseismicity within a karstified rock mass due to cracks and collapses triggered by earthquakes and gravitational deformations. *Nat. Hazards*, **64**, 359-379.

Lenti L., Martino S., Paciello A., Prestininzi A. & Rivellino S. (2015). Recorded displacements in a landslide slope due to regional and teleseismic earthquakes. *Geophys. J. Int.*, **201**, 1335-1345.

Lévy C., Baillet L., Jongmans D., Mourot P. & Hantz D. (2010). Dynamic response of the Chamousset rock column (Western Alps, France). *J. Geophys. Res.*, **115** (F4), F04043.

Lévy C., Jongmans D. & Baillet L. (2011). Analysis of seismic signals recorded on a prone-to-fall rock column (Vercors massif, French Alps). *Geophys. J. Int.*, **186**, 296-310.

Li T.M.C., Ferguson J.F., Herrin E. & Durham H.B. (1984). High-frequency seismic noise at Lajitas, Texas. *Bull. Seism. Soc. Am.*, **74** (5), 2015-2033.

Li T., Cai M.F. & Cai M. (2007). A review of mining-induced seismicity in China. *Int. J. Rock Mech. Min. Sci.*, **44** (8), 1149-1171.

Liu J.P., Feng X.T., Li Y.H. & Sheng Y. (2013). Studies on temporal and spatial variation of microseismic activities in a deep metal mine. *Int. J. Rock Mech. Min. Sci.*, **60**, 171-179.

Lockner D. (1993). The role of acoustic emission in the study of rock fracture. *Int. J. Rock Mech. Min. Sci. Geomech. Abstr.*, **30** (7), 883-899.

Lollino G. & Audisio C. (2006). UNESCO World Heritage sites in Italy affected by geological problems, specifically landslide and flood hazard. *Landslides*, **3** (4), 311-321.

Lu C.P., Dou L.M., Zhang N., Xue J.H., Wang X.N., Liu H. & Zhang J.W. (2013). Microseismic frequency-spectrum evolutionary rule of rockburst triggered by roof fall. *Int. J. Rock Mech. Min. Sci.*, **64**, 6-16.

Maffei A., Martino S. & Prestininzi A. (2005). From the geological to the numerical model in the analysis of the gravity-induced slope deformations: an example from the Central Apennines (Italy). *Eng. Geol.*, **78**, 215-236.

Mainsant G., Larose E., Brönnimann C., Jongmans D., Michoud C. & Jaboyedoff M. (2012). Ambient seismic noise monitoring of a clay landslide: Toward failure prediction. *J. Geophys. Res*, **117** (F1), F01030.

Mantovani M., Devoto S., Forte E., Mocnik A., Pasuto A., Piacentini D. & Soldati M. (2013). A multidisciplinary approach for rock spreading and block sliding investigation in the north-western coast of Malta. *Landslides*, **10** (5), 611-622.

Martino S., Prestininzi A. & Scarascia Mugnozza G. (2004). Geological-evolutionary model of a gravity-induced slope deformation in the carbonate central Apennines (Italy). *Q. J. Eng. Geol. Hydrogeol.*, **37** (1), 31-47.

Martino S. & Mazzanti P. (2014). Integrating geomechanical surveys and remote sensing for sea cliff slope stability analysis: the Mt. Pucci case study (Italy). *Nat. Hazards Earth Syst. Sci.*, **14**, 831-848.

Martino S., Lenti L., Delgado J., Garrido J. & Lopez-Casado C. (2016). Application of a characteristic periods-based (CPB) approach to estimate earthquake-induced displacements of landslides through dynamic numerical modelling. *Geophys. J. Int.*, **206** (1), 85-102.

Martino S., Bozzano F., Caporossi P., D'Angiò D., Della Seta M., Esposito C., Fantini A., Fiorucci M., Giannini L.M., Iannucci R., Marmoni G.M., Mazzanti P., Missori

C., Moretto S., Rivellino S., Romeo R.W., Sarandrea P., Schilirò L., Troiani F. & Varone C. (2017). Ground effects triggered by the 24th August 2016, M_W 6.0 Amatrice (Italy) earthquake: surveys and inventorying to update the CEDIT catalogue. *Geografia Fisica e Dinamica Quaternaria*, **40**, 77-95.

Mateos R.M., Herrera G., García-Davalillo J.C, Grandjean G., Poyiadji E., Maftei R., Filipciuc T.-C., Auflič M.J., Jez J., Podolszki L., Trigila A., Comerci V., Raetzo H., Kociu A., Przyłucka M., Kułak M., Laskowicz I., Sheehy M., Kopackova V., Frei M., Kuhn D., Dehls J.F., Hermanns R.L., Koulermou N., Smith C.A., Engdahl M., Pagespetit P.B., González M., Banks V., Dashwood C., Reeves H., Cigna F., Liščák P., Mikulėnas V., Demir V., Raha M., Quental L., Oliveira D., Dias R. & Sandić C. (2017). Integration of geohazards into urban and land-use planning. Towards a landslide directive. The EuroGeoSurveys Questionnaire. In: *Advancing Culture of Living with Landslides. Volume 2 Advances in Landslide Science*. Eds Mikos M., Tiwari B., Yin Y. & Sassa K., pp. 1067-1072, Springer.

Maurer H., Spillmann T., Heincke B., Hauck C., Loew S., Springman S.M. & Green A.G. (2010). Geophysical characterization of slope instabilities. *First Break*, **28** (8), 53-61.

McCann D.M. & Forster A. (1990). Reconnaissance geophysical methods in landslide investigations. *Eng. Geol.*, **29**, 59-78.

McGarr A. (1992). Moment tensors of ten Witwatersrand mine tremors. *Pure Appl. Geophys.*, **139** (3-4), 781-800.

Méric O., Garambois S., Jongmans D., Wathelet M., Chatelain J.L. & Vengeon J.M. (2005). Application of geophysical methods for the investigation of the large gravitational mass movement of Séchilienne, France. *Can. Geotech. J.*, **42** (4), 1105-1115.

Michel C., Guéguen P., El Arem S., Mazars J. & Kotronis P. (2010). Full scale dynamic response of a RC building under weak seismic motions using earthquake recordings, ambient vibrations and modelling. *Earthq. Eng. Struct. Dyn.*, **39**, 419-441.

Moore J.R., Gischig V., Burjánek J., Loew S. & Fäh D. (2011). Site effects in unstable rock slopes: dynamic behavior of the Randa instability (Switzerland). *Bull. Seism. Soc. Am.*, **101** (6), 3110-3116.

Moore J.R., Thorne M.S., Koper K.D., Wood J.R., Goddard K., Burlacu R., Doyle S., Stanfield E. & White B. (2016). Anthropogenic sources stimulate resonance of a natural rock bridge. *Geophys. Res. Lett.*, **43** (18), 9669-9676.

Montaldo V., Meletti C., Martinelli F., Stucchi M. & Locati M. (2007) On-line seismic hazard data for the new Italian building code. *J. Earthq. Eng.*, **11** (supp.1), 119-132.

Montoya-Montes I., Rodríguez-Santalla I., Sánchez-García M.J., Alcántara-Carrió J., Martín-Velázquez S., Gómez-Ortiz D. & Martín-Crespo T. (2012). Mapping of landslide susceptibility of coastal cliffs: The Mont-Roig del Camp case study. *Geol. Acta*, **10**, 439-455.

Nakamura Y. (1989). A method for dynamic characteristics estimation of subsurface using microtremor on the ground surface. *Quarterly Report of Railway Technical Research Institute (RTRI)*, **30** (1), 25-33.

Nogoshi M. & Igarashi T. (1970). On the propagation characteristics of microtremors. *J. Seism. Soc. Japan*, **23**, 264-280. (in Japanese with English abstract)

Nogoshi M. & Igarashi T. (1971). On the amplitude characteristics of microtremors. *J. Seism. Soc. Japan*, **24**, 24-40. (in Japanese with English abstract)

Oil Exploration Directorate (1993). *Geological map of the Maltese Islands. Sheet 1: Malta. Scale 1:25.000*. Office of the Prime Minister.

Panzera F., D'Amico S., Lotteri A., Galea P. & Lombardo G. 2012. Seismic site response of unstable steep slope using noise measurements: the case study of Xemxija Bay area, Malta. *Nat. Hazards Earth Syst. Sci.*, **12** (11), 3421-3431.

Panzera F., D'Amico S., Galea P., Lombardo G., Gallipoli M.R. & Pace S. (2013). Geophysical measurements for site response investigation: preliminary results on the island of Malta. *Boll. Geofis. Teor. Appl.*, **54**, 111-128.

Panzera F., Pischiutta M., Lombardo G., Monaco C. & Rovelli A. (2014). Wavefield polarization in fault zones of the Western flank of Mt. Etna: Observations and fracture orientation modelling. *Pure Appl. Geophys.*, **171** (11), 3083-3097.

Pazzi V., Tanteri L., Bicocchi G, D'Ambrosio M., Caselli A. & Fanti R. (2017). H/V measurements as an effective tool for the reliable detection of landslide slip surfaces: Case studies of Castagnola (La Spezia, Italy) and Roccalbegna (Grosseto, Italy). *Phys. Chem. Earth*, **98**, 136-153.

Pedley M. (2011). The Calabrian Stage, Pleistocene highstand in Malta: a new marker for unravelling the Late Neogene and Quaternary history of the islands. *J. Geol. Soc. Lond.*, **168** (4), 913-926.

Pedley H.M., House M.R. & Waugh B. (1976). The geology of Malta and Gozo. *Proc. Geol. Assoc.*, **87**, 325-341.

Pedley H.M., House M.R. & Waugh B. (1978). The geology of the Pelagian block: the Maltese islands. In: *The Ocean Basins and Margins*. Eds Nairn A.E.M., Kanes W.H. & Stehli F.G., pp. 417-433, Plenum Press.

Pedley M., Clarke M. & Galea P. (2002). *Limestone Isles in a Crystal Sea: The Geology of the Maltese Islands*. Publishers Enterprises Group Ltd.

Petley D. (2012). Global patterns of loss of life from landslides. *Geology*, **40**, 927-930.

Pennetta M. & Russo E.L. (2011). Hazard factors in high rocky coasts of Capri Island (Gulf of Naples, Italy). *J. Coast. Res.*, **61**, 428-434.

Phillips W.S., Pearson D.C., Edwards C.L. & Stump B.W. (1997). Microseismicity induced by a controlled, mine collapse at white pine, Michigan. *Int. J. Rock Mech. Min. Sci.*, **34**, 314, paper 246.

Pischiutta M., Villani F., D'Amico S., Vassallo M., Cara F., Di Naccio D., Farrugia D., Di Giulio G., Amoroso S., Cantore P., Mercuri A., Famiani D., Galea P., Akinci A. & Rovelli A. (2017). Results from shallow geophysical investigations in the northwestern sector of the island of Malta. *Phys. Chem. Earth*, **98**, 41-48.

Ramamurthy T. (2004). A geo-engineering classification for rocks and rock masses. *Int. J. Rock Mech. Min. Sci.*, **41**, 89-101.

Renalier F., Jongmans D., Campillo M. & Bard P.-Y. (2010). Shear wave velocity imaging of the Avignonet landslide (France) using ambient noise cross correlation. *J. Geophys. Res.*, **115** (F3), F03032.

Richter C.F. (1958). *Elementary seismology*. Freeman.

Rodríguez-Peces M.J., Azañón J.M., García-Mayordomo J., Yesares J., Troncoso E. & Tsige M. (2011). The Diezma landslide (A-92 motorway, Southern Spain): history and potential for future reactivation. *Bull. Eng. Geol. Environ.*, **70**, 681-689.

Rosser N.J., Brain M.J., Petley D.N., Lim M. & Norman E.C. (2013). Coastline retreat via progressive failure of rocky coastal cliffs. *Geology*, **41** (8), 939-942.

Sass O., Bell R. & Glade T. (2008). Comparison of GPR, 2D-resistivity and traditional techniques for the subsurface exploration of the Öschingen landslide, Swabian Alb (Germany). *Geomorphology*, **93** (1), 89-103.

Savage W.Z. & Varnes D.J. (1987). Mechanism of gravitational spreading of steep-sided ridges ("sacking"). *Bull. Int. As. Eng. Geol.*, **35**, 31-36.

Senfaute G., Duperret A. & Lawrence J.A. (2009). Micro-seismic precursory cracks prior to rock-fall on coastal chalk cliffs: a case study at Mesnil-Val, Normandie, NW France. *Nat. Hazards Earth Syst. Sci.*, **9**, 1625-1641.

SESAME (2004). *Guidelines for the implementation of the H/V spectral ratio technique on ambient vibrations: measurements, processing and interpretation*. Deliverable D23.12 European Commission - Research General Directorate Project No. EVG1-CT-2000-00026 SESAME.

Sick B., Walter M. & Joswig M. (2014). Visual event screening of continuous seismic data by supersonograms. *Pure Appl. Geophys.*, **171**, 549-559.

Sitharam T.G., Sridevi J. & Shimizu N. (2001). Practical equivalent continuum characterization of jointed rock masses. *Int. J. Rock Mech. Min. Sci.*, **38**, 437-448.

Spillmann T., Maurer H., Green A.G., Heincke B., Willenberg H. & Husen S. (2007). Microseismic investigation of an unstable mountain slope in the Swiss Alps. *J. Geophys. Res.*, **112** (B7), B07301.

Spudich P., Hellweg M. & Lee W.H.K. (1996). Directional topographic site response at Tarzana observed in aftershocks of the 1994 Northridge, California, earthquake: implications for mainshock motions. *Bull. Seism. Soc. Am.*, **86** (1B), S193-S208.

Starr A.M., Moore J.R. & Thorne M.S. (2015). Ambient resonance of Mesa Arch, Canyonlands National Park, Utah. *Geophys. Res. Lett.*, **42** (16), 6696-6702.

Suriñach E., Vilajosana I., Khazaradze G., Biescas B., Furdada G. & Vilaplana J.M. (2005). Seismic detection and characterization of landslides and other mass movements. *Nat. Hazards Earth Syst. Sci.*, **5** (6), 791-798.

Szwedzicki T. (2003). Rock mass behaviour prior to failure. *Int. J. Rock Mech. Min. Sci.*, **40**, 573-584.

Tang C., Li L., Xu N. & Ma K. (2015). Microseismic monitoring and numerical simulation on the stability of high-steep rock slopes in hydropower engineering. *Journal of Rock Mechanics and Geotechnical Engineering*, **7**, 493-508.

Tonnellier A., Helmstetter A., Malet J.-P., Schmittbuhl J., Corsini A. & Joswig M. (2013). Seismic monitoring of soft-rock landslides: the Super-Sauze and Valoria case studies. *Geophys. J. Int.*, **193** (3), 1515-1536.

Toksöz M.N. & Lacoss R.T. (1968). Microseisms: mode structure and sources. *Science*, **159**, 872-873.

Torgoev A., Lamair L., Torgoev I. & Havenith H.-B. (2013). A Review of Recent Case Studies of Landslides Investigated in the Tien Shan Using Microseismic and Other Geophysical Methods. In: *Earthquake-Induced Landslides*. Eds Ugai K., Yagi H. & Wakai A., pp. 285-294, Springer.

Valentin J., Capron A., Jongmans D., Baillet L., Bottelin P., Donze F., Larose E. & Mangeney A. (2017). The dynamic response of prone-to-fall columns to ambient vibrations: comparison between measurements and numerical modelling. *Geophys. J. Int.*, **208** (2), 1058-1076.

Van Den Eeckhaut M., Hervas J., Jaedicke C., Malet J.-P., Montanarella L. & Nadim F. (2012). Statistical modelling of Europe-wide landslide susceptibility using limited landslide inventory data. *Landslides*, **9**, 357-369.

Varnes D.J. (1978). Slope movement types and processes. In: *Landslides Analysis and Control, Special Report 176*. Eds Schuster R.L. & Krizek R.J., pp. 11-33, National Academy of Science.

Varnes D.J. & IAEG (1984). *Landslide hazard zonation: a review of principles and practice*. United Nations Scientific and Cultural Organization.

Vella A., Galea P. & D'Amico S. (2013). Site frequency response characterisation of the Maltese islands based on ambient noise H/V ratios. *Eng. Geol.*, **163**, 89-100.

Vidale J.E. (1986). Complex polarisation analysis of particle motion. *Bull. Seism. Soc. Am.*, **76**, 1393-1405.

Wasowski J. & Del Gaudio V. (2000). Evaluating seismically induced mass movement hazard in Caramanico Terme (Italy). *Eng. Geol.*, **58** (3), 291-311.

Walter M. & Joswig M. (2008). Seismic monitoring of fracture processes generated by a creeping landslide in the Vorarlberg Alps. *First Break*, **26**, 131-136.

Walter M. & Joswig M. (2009). Seismic characterization of slope dynamics caused by softrock-landslides: The Super-Sauze case study. In: *Proceedings of the International Conference on Landslide Processes: from geomorpholgic mapping to*

dynamic modelling. Eds Malet J.-P., Remaître A. & Boogard T.A., pp. 215-220. CERG Editions.

Walter M., Niethammer U., Rothmund S. & Joswig M. (2009). Joint analysis of the Super-Sauze (French Alps) mudslide by nanoseismic monitoring and UAV-based remote sensing. *First Break*, **27**, 75-82.

Walter M., Walser M. & Joswig M. (2011). Mapping rainfall-triggered slidequakes and seismic landslide-volume estimation at Heumoes slope. *Vadose Zone J.*, **10**, 487-495.

Walter M., Schwaderer U. & Joswig M. (2012a). Seismic monitoring of precursory fracture signals from a destructive rockfall in the Vorarlberg Alps, Austria. *Nat. Hazards Earth Syst. Sci.*, **12**, 3545-3555.

Walter M., Arnhardt C. & Joswig M. (2012b). Seismic monitoring of rockfalls, slide quakes and fissure development at the Super-Sauze mudslide, French Alps. *Eng. Geol.*, **128**, 12-22.

Walter M., Gomberg J., Schulz W., Bodin P. & Joswig M. (2013). Slidequake generation versus viscous creep at softrock-landslides: synopsis of three different scenarios at Slumgullion landslide, Heumoes slope and Super-Sauze mudslide. *J. Environ. Eng. Geophys.*, **18** (4), 269-280.

Wang H. & Ge M. (2007). Acoustic emission/microseismic source location analysis for a limestone mine exhibiting high horizontal stresses. *Int. J. Rock Mech. Min. Sci.*, **45**, 720-728.

Wong I.G., Humphrey J.R., Adams J.A. & Silva W.J. (1989). Observations of mine seismicity in the eastern Wasatch Plateau, Utah, USA: A possible case of implosional failure. *Pure Appl. Geophys.*, **129** (3), 369-405.

Wust-Bloch G.H. (2010). Characterizing and locating very weak (-2.2 ≥ ML ≥ -3.4) induced seismicity in unstable sandstone cliffs by nanoseismic monitoring. *Pure Appl. Geophys.*, **167**, 153-167.

Wust-Bloch G.H. & Joswig M. (2006). Pre-collapse identification of sinkholes in unconsolidated media at Dead Sea area by 'nanoseismic monitoring' (graphical jackknife location of weak sources by few, low-SNR records). *Geophys. J. Int.*, **167**, 1220-1232.

Xu N.W., Tang C.A., Li L.C., Zhou Z., Sha C., Liang Z.Z. & Yang J.Y. (2011). Microseismic monitoring and stability analysis of the left bank slope in Jinping first stage hydropower station in southwestern China. *Int. J. Rock Mech. Min. Sci.*, **48** (6), 950-963.

Xu N.W., Dai F., Liang Z.Z., Zhou Z., Sha C. & Tang C.A. (2014). The dynamic evaluation of rock slope stability considering the effects of microseismic damage. *Rock Mech. Rock Eng.*, **47** (2), 621-642.

Xu N.W., Li T.B., Dai F., Li B., Zhu Y.G. & Yang D.S. (2015). Microseismic monitoring and stability evaluation for the large scale underground caverns at the Houziyan hydropower station in Southwest China. *Eng. Geol.*, **188**, 48-67.

Yalcinkaya E., Alp H., Ozel O., Gorgun E., Martino S., Lenti L., Bourdeau C., Bigarre P. & Coccia S. (2016). Near-surface geophysical methods for investigating the Buyukcekmece landslide in Istanbul, Turkey. *J. Appl. Geophys.*, **134**, 23-35.

Yamanaka H., Takemura M., Ishida H. & Niwa M. (1994). Characteristics of long-period microtremors and their applicability in exploration of deep sedimentary layers. *Bull. Seismol. Soc. Am.*, **84** (6), 1831-1841.

Young A.P. & Ashford S.A. (2008). Instability investigation of cantilevered seacliffs. *Earth Surf. Process. Landforms*, **33**, 1661-1677.

Zischinsky U. (1969). Uber Sackungen. *Rock Mech.*, **1**, 30-52.

Zang A., Stephansson O., Stenberg L., Plenkers K., Specht S., Milkereit C., Schill E., Kwiatek G., Dresen G., Zimmermann G., Dahm D. & Weber M. (2017). Hydraulic fracture monitoring in hard rock at 410 m depth with an advanced fluid-injection protocol and extensive sensor array. *Geophys. J. Int.*, **208** (2), 790-813.

Zucca J.J. (1998). Forensic seismology supports the Comprehensive Test Ban Treaty. In: *Science & Technology Review*, pp. 4-11, Lawrence Livermore National Laboratory.

Zucca J.J., Carrigan C., Goldstein P., Jarpe S., Sweeney J., Pickles W.L. & Wright B. (1996). Signatures of testing: on-site inspection technologies. In: *Monitoring a Comprehensive Test Ban Treaty*. Eds Husebye E.S. & Dainty A.M., pp. 123-134, Kluwer.